Equilibrium and Structural Characterization of M(III) - OPC2A and its Mixed Ligand Complexes: Prospective Use in Medical Imaging and Therapy

Thesis for the Degree of Doctor of Philosophy (Ph.D.)

Bayar Abdulghafoor Wahab Dahman

Supervisor: Dr. Imre Tóth

professor emeritus

UNIVERSITY OF DEBRECEN

Doctoral Council for Natural Sciences and Engineering

Doctoral School of Chemistry

Debrecen, 2025

Hereby I declare that I prepared this thesis within the Doctoral Council for Natural Sciences and Engineering, Doctoral Program in Coordination Chemistry (K/2), University of Debrecen in order to obtain a Ph.D. Degree in Natural Sciences/ Engineering at Debrecen University.
The results published in the thesis are not reported in any other PhD thesis.

Debrecen, 2025.11.25

signature of the candidate

Hereby I confirm that Bayar Dahman candidate conducted his studies with my supervision within the Doctoral Program in Coordination Chemistry (K/2) between 2021 and 2025. The independent studies and research work of the candidate significantly contributed to the results published in the thesis.

I also declare that the results published in the thesis are not reported in any other thesis.

I support the acceptance of the thesis.

Debrecen, 2025. 11.25

signature of the supervisor

Equilibrium and Structural Characterization of M(III) - OPC2A and its Mixed Ligand Complexes: Prospective Use in Medical Imaging and Therapy

Dissertation submitted in partial fulfilment of the requirements for the doctoral (Ph.D.) degree in Chemistry. (Coordination Chemistry)

Written by Bayar Abdulghafoor Wahab Dahman certified chemist

Prepared within the framework of the Doctoral Program in Coordination Chemistry (K/2), University of Debrecen.

Dissertation supervisor: Dr. Imre Tóth

The official opponents of the dissertation:

Dr.

Dr.

The evaluation board:

chairperson: Dr.

members: Dr.

Dr.

Dr.

Dr.

The date and venue of the dissertation defense: 2026. .

Acknowledgement

I would like to express my deepest gratitude and heartfelt appreciation to my supervisor, **Prof. Imre Tóth**, for his unwavering support, guidance, and encouragement throughout the entire course of my Ph.D. journey. His fatherly attitude, patience, and constant availability provided not only academic direction but also personal reassurance during challenging times.

It has truly been an honor to learn under his mentorship I have gained far more than just scientific knowledge. His integrity, dedication, and humanity have left a lasting impression on me, and I feel that no words can adequately express how thankful I am for everything he has done.

I am also sincerely thankful to **Prof. Zsolt Baranyai** for his constructive input and support, and to **Prof. Gyula Tircsó** for his scientific collaboration and for fostering a warm research environment. I appreciate the cooperation and friendship of his research group members.
Special thanks go to **Ms. Katalin Takács** for her kind assistance in the lab, and to **Dr. Tibor Csupász** for his support specially during synthesis part.

I am grateful to **Dr. Attila Bényei** for his help in solving crystal structures.

A special thank you goes to **Prof. István Bányai** for his valuable guidance on kinetic and dynamic NMR. And **Mr. László Zékány** for his valuable guidance and evaluation of potentiometric titration data.

I would like to thank **Dániel Szücs** for performing the radiolabeling of ^{44}Sc and for evaluating the stability of its complex.

I am grateful to **Prof. Mauro Botta** and his group at the Università del Piemonte Orientale, especially **Lorenzo Risolo** and **Marco Ricci** for their collaboration and hospitality during my stay in Italy.

Thanks also to all members of the **department of Physical Chemistry at the University of Debrecen** for their support.

This research was supported by **NKFIH grants K-134694 (Gy.T.) and K-131989 (I.B)**, the Scientific Publication Support Program of the University of Debrecen, the **Stipendium Hungaricum Scholarship**, and a **visiting grant from the Università del Piemonte Orientale**, for which I am sincerely grateful.

Finally, I owe my heartfelt thanks to my beloved family, my parents, wife, siblings, and my son for their unwavering love and support.

Table of Contents:

Formulas of the ligands mentioned in the thesis

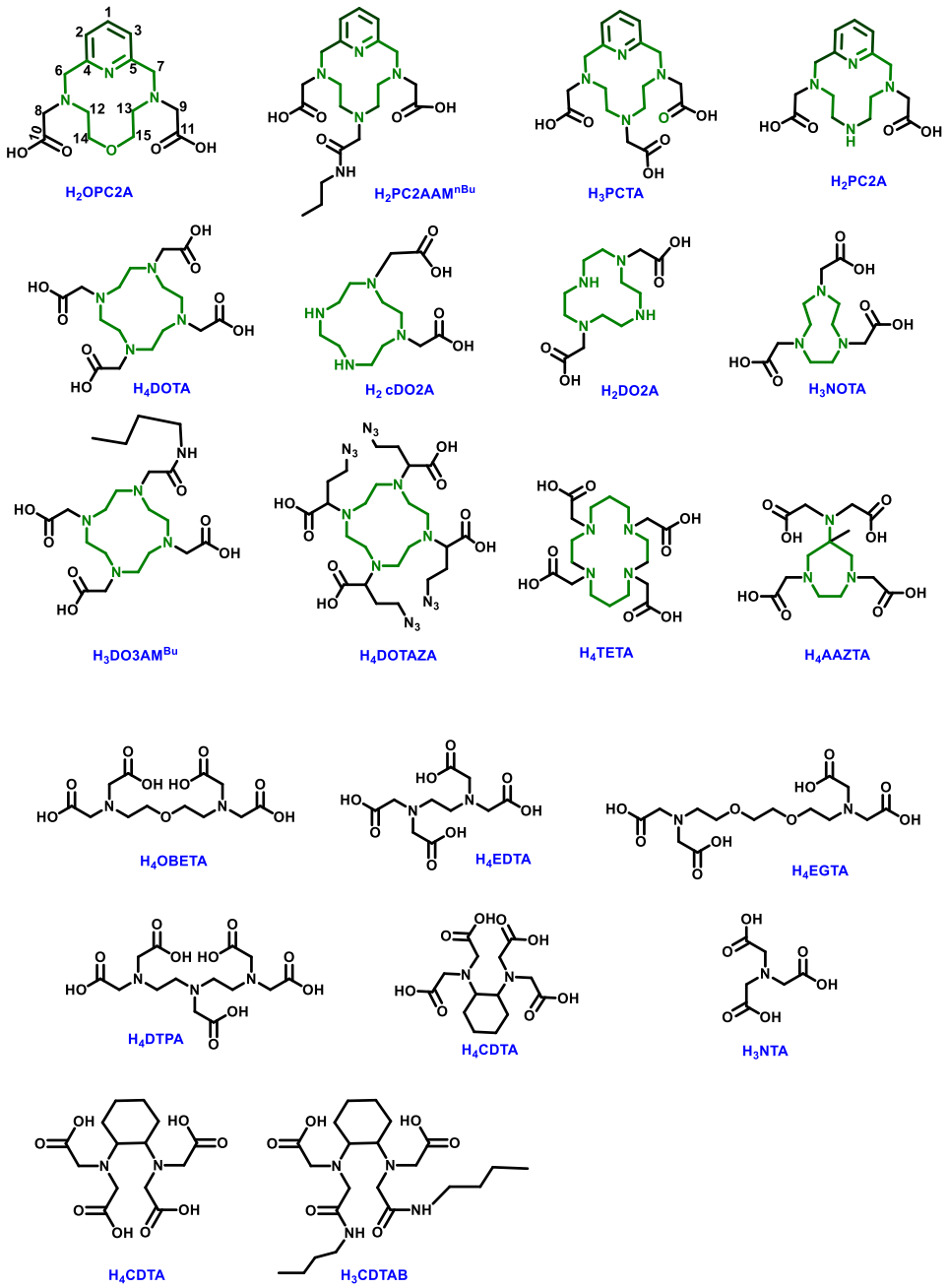

Scheme 1. Formula of ligands mentioned in the thesis

Abbreviations

MRI	Magnetic resonance imaging
SPECT	Single photon emission computed tomography
PET	Positron emission tomography
APCs	Amino polycarboxylates
BFCs	Bifunctional chelates
LET	Linear Energy Transfer
AE	Auger Electron
NTA	Nitrilotriacetic acid
NOTA	1,4,7-triazacyclononane-1,4,7-triacetic acid
AAZTA	6-amino-6-methylperhydro-1,4-diazepinetetraacetic acid
H_5DTPA	Diethylenetriaminepentaacetic acid
H_4EDTA	Ethylenediaminetetraacetic acid
H_4CDTA	1,2-Diaminocyclohexane-N,N,N′,N′-tetraacetic acid
DOTAZA	1,4,7,10-Tetraazacyclododecane-1,4,7,10-tetraazidoethylacetic Acid
H_3NOTA	1,4,7-triazacyclononane-1,4,7-triacetic acid
H_2PC2A	1,4,7-triazacyclononane-1,4-diacetic acid
H_3PCTA	3,6,9,15-tetraazabicyclo [9.3.1] pentadeca-1(15),11,13-triene-3,6,9-triacetic acid
H_3DO3AM^{Bu}	2,2',2''-(10-(2-(butylamino)-2-oxoethyl)-1,4,7,10 tetraazacyclodo decane-1,4,7-triyl)triacetic acid
FDG	^{18}F-Fluorodeoxyglucose
CDTAB	1,2-diaminocyclohexane- N,N,N',N'-tetraacetic acid - N,N'-bis(butylamide)
H_2cDO2A	1,4,7,10-tetracyclododecane-1,4-diacetic acid
HSAB	Hard and Soft Acids and Bases
C.N	Coordination number
HSA	Human serum albumin

1. Introduction

Chemistry plays a vital role in pharmaceutical research, particularly in the synthesis of specialized compounds and the characterization of their chemical properties, which are essential steps before moving on to biological, preclinical, and clinical studies. Coordination chemistry, in particular, contributes significantly through the study of metal complexes, which are widely applied in medical imaging and other diagnostic techniques.[1] Although the physics behind the different imaging modalities (like Magnetic Resonance Imaging–MRI, Positron Emission Tomography–PET, Single–Photon Emission Computed Tomography–SPECT, X–ray) are vastly diverse, the chemistry shows substantial similarities: high stability and selectivity, fast formation (mainly for short lived radioisotopes) and slow decomplexation kinetics (inertness), together with effectiveness, low toxicity, reasonable price etc. are required.[2,3] Moreover, research of novel metallic radionuclides that can be used for medical treatment and diagnostics is crucial in nuclear medicine. See Table 1. For example, in the context of imaging, radioisotopes need to emit gamma rays (γ) with appropriate energy for single photon emission computed tomography (SPECT), while the isotopes are positron emitters (β^+, generating two γ photons) for (PET). In therapeutic applications, it is necessary for the radioisotopes to undergo decay by emitting either beta (β^-) or alpha (α) particles.[4,5] This provides an opportunity for diagnosis, to monitor drug administration and treatment effectiveness. Recently, the concept of theranostics merges: diagnosis and therapy that use similar compounds (isotopologs) containing either diagnostic or therapeutic isotopes. (In chemistry, isotopologues (also spelled isotopologs) are molecules that differ only in their isotopic composition.)[6] Many identical

nuclide pairs have been nominated for this application, for instance (^{90}Y-^{86}Y, ^{67}Cu-(^{46}Cu,^{61}Cu-,Cu^{62}), and ^{47}Sc-^{44}Sc). The organic ligand might be bifunctional, by means of binding (chelating) the metal ions and having an anchor group suitable to form a covalent bond with a biological vector responsible for selective transport of the molecule to the targeted tissue. Among the isotopes, such as ^{99m}Tc, ^{68}Ga, ^{90}Y, ^{111}In, ^{153}Sm, and ^{177}Lu, emerged recently, the most classical theranostic pair is based on iodine-isotopes, which are used for PET (^{124}I) or SPECT (^{123}I) in addition to using ^{131}I for beta-radionuclide therapy.[7] Recently, radioisotope ^{18}F, as well as other non-metallic elements including ^{13}N, ^{15}O are routinely utilized.[8] Metal complexes may play a role as carriers of anionic radiotracers. Al(III)-ligand complexes can be labeled by ^{18}F providing a fast and effective method.[9–11]

Table 1. Some examples of radioisotopes used in various modalities with decay mode characteristics with their potential application.[5]

Radiometal	Decay Mode	Use
^{68}Ga ^{18}F	Positron emission (β^+ decay)	PET imaging
^{64}Cu	Positron/Beta decay	PET imaging and therapy
^{99m}Tc	Gamma rays	SPECT
^{111}In	Gamma rays	
^{223}Ra	Alpha particles	Therapy
^{177}Lu	Beta decay (β^-)	
^{90}Y	Beta decay (β^-)	
^{10}B	Neutron capture	
^{43}Sc, $^{44-47}$Sc ^{131}I, $^{123-124}$I	Positron/ Gamma rays- Beta decay (β^-)	Theragnostic

2. Literature review

This chapter deals with selected basic inorganic/coordination chemistry of the metallic elements in aqueous solution: electronic structure, oxidation state, redox properties, size and coordination number of metal ions, "hard-soft" characterization, hydration and hydrolysis, solvent exchange rate in water, complexes with APCs and halides anions, mixed ligand [M(APC)X] (X = OH^-, or halide, F^-, Cl^-, I^-) complexes, NMR isotopes and parameters, radio-isotopes, medical applications. Related literature of the ligands is also reviewed, mostly macrocyclic amino polycarboxylates (MC-APCs) to bind metal ions used in medical imaging/therapy.

2.1. Chemistry of Scandium (Z = 21)

Scandium is the lightest element (atomic weight 44.95591 g/mol) of the Group 3 in the Periodic Table. Scandium possesses an electron configuration with [Ar] $4s^2$ $3d^1$. Sc(III) predominantly exists in the +3 - oxidation state, especially in aqueous solutions. Sc(III) is characterized by its high acidity and strong inclination to form complexes.[12] Scandium exhibits certain chemical properties similar to rare earth elements, lanthanides. This element also shares chemical characteristics with aluminum and gallium, because of its relatively small ionic radius.[13] The similarity is attributed to the similar size of Sc(III) ion compared to those of Al(III) and Ga(III).[14] Although Sc(III) is larger in ionic size compared to Al(III) (0.745 Å against 0.535 Å), $Sc(III)_{aq}$ undergoes hydrolysis to a much greater extent. The explanation for this is the existence of d orbitals in scandium, despite the absence of electrons in its d orbital. Both scandium hydroxide and scandium oxide phases observed for scandium(III) consisting of $Sc(OH)_{3(s)}$, which is presumed to exist in both amorphous and crystalline states.[15,16] The hydrolysis starts at pH > 3,

$Sc(OH)^{2+}$, $Sc_2(OH)_2^{4+}$ and $Sc_3(OH)_5^{4+}$ are formed.[17] The hydrated ions of Sc(III) are classified as hard acids according to Pearson's classification.[18] Scandium is known for its wide range of coordination numbers, typically ranging from 3 to 9, with a hexa-coordination number being the most common.[19] The hydration number of scandium in aqueous solution of $Sc(III)_{aq}$, is known as $Sc(H_2O)_8^{3+}$. Based on the structure of the chelators, Sc(III) might be 7 and 8 coordinated even with water molecule(s) in the inner sphere of Sc(III) ion. The hydration of the Sc(III) ion in aqueous solution and in crystalline hydrates were studied by XAFS spectroscopy, large-angle x-ray scattering and crystallography.[20] The water exchange rate is fast and follows associative (A) mechanism. Hydrated Sc(III) halides, $ScX_3 \cdot 6H_2O$ (X = Cl, Br) can be easily prepared by dissolving scandium oxide (Sc_2O_3) in the appropriate acid, while anhydrous ScX_3 resulted by drying with P_2O_5. The fluoride is an exception, as it undergoes hydrolysis upon heating and cannot be dehydrated.[21] Sc(III) forming complexes with well-known ligands, such as APCs. Macrocyclic ligands that possess preorganized cyclic structures tend to form stable and inert complexes from both thermodynamic and kinetic perspectives.[22] The thermodynamic stability of APCs ligands such as DOTA, NOTA (macrocyclic), EDTA, and DTPA (open-chain) with Sc(III) was published.[23–25] Majkowska et al. studied new ligands for labeling biomolecules with ^{47}Sc in radiotherapy, while with ^{44}Sc for diagnostic imaging. It was found that DOTA and NOTA exhibited notable labeling effectiveness. NMR spectroscopy was employed to investigate the stability and kinetic inertness of complexes. ^{47}Sc might be used as an alternative for ^{177}Lu radionuclide therapy.[26] Scandium is naturally present with only one stable isotope, ^{45}Sc. ^{45}Sc (I = 7/2, it is quadrupolar), and it is considered one of the best NMR-active nuclei with 100% natural

abundance, and relative receptivity to ^{1}H is 0.302. The resonance frequency is 24.29 MHz at 2.35 Tesla, i.e. 100 MHz for ^{1}H).[27,28] Scandium has several radioisotopes, ^{43}Sc, ^{44}Sc, ^{44m}Sc, and ^{47}Sc which are highly recommended for using in medical field. Due to the comparable and shared chemical characteristics of ^{44}Sc with ^{68}Ga, along with differences in physical properties, the possibilities of utilizing the ^{44}Sc radionuclide have been broadened. The research group led by F. Rösch in Germany recommended ^{44}Sc as an attractive replacement for ^{68}Ga in diagnostic applications.[29] DOTA, DTPA and AAZTA have been studied as Sc(III)-binder ligands.[8,30] Sc(III)-fluoro complexes are extremely stable, $\log K_1$ = 6.19, $\log K_2$ = 5.28, $\log K_3$ = 4.08.[31]

One of the most used compounds in PET is ^{18}F-fluorodeoxyglucose (FDG). The ^{18}F-radioisotope possesses favorable characteristics for PET, with a half-life of 109 minutes and positron energy (E = 635 keV).[30,32] A new concept has been raised [9] for ^{18}F labeling based on Al(III)-F^{-}- organic ligand complexes. This new radiotracer is carrying F^{-}, allowing ^{18}F to be selectively delivered to the target tissue, if the organic ligand is a suitable bifunctional ligand. Recently, similar technology has been suggested to carry both ^{44}Sc/^{47}Sc and ^{18}F for theragnostic application via Sc(III)-complexes with-triaza-MC ligands.[10]

The ^{44}Sc isotope can be produced in the cyclotron by the $^{44}Ca(p, n)^{44}Sc$ nuclear reaction,[33,34] or from the ^{44}Ti/^{44}Sc radionuclide generator system.[35] Proteins and their fragments generally have a longer distribution time, and it is therefore preferable to label them with ^{44}Sc, as this radionuclide allows longer monitoring time required for PET imaging.[36] The beta-emitting ^{47}Sc isotope and the ^{44}Sc form a theranostic pair, that is

excellently suited for cancer theranostic.[7,10] For some important radioisotopes of Sc(III) radiometals with their applications see Table 2.

Table 2. Important radioisotopes of Sc, Al, Ga, In, Tl, F, and I with decay characteristics, half-life times, and their applications[5,37]

Element	Radionuclide	Decay	$t_{1/2}$ (hr.)	Application
Sc	^{43}Sc	β^+ decay	3.89	PET
	^{44}Sc	$\varepsilon + \beta^+$ decay	3.97	PET
	^{47}Sc	$\varepsilon + \beta^-$ decay	80.4	Therapy & SPECT
Al	^{26}Al	β^+ decay		PET
Ga	^{66}Ga	$\varepsilon + \beta^+$ decay	9.49	PET
	^{67}Ga	Auger, ɣ	78.2	Therapy & SPECT
	^{68}Ga	$\varepsilon + \beta^+$ decay	1.13	PET
In	^{110}In	$\varepsilon + \beta^+$ decay	1.15	PET
	^{111}In	ε + ɣ	67.3	SPECT
Tl	^{201}Tl	ε	73.01	SPECT & Therapy
F	^{18}F	β^+ decay	1.82	PET
I	^{120}I	$\varepsilon + \beta^+$ decay	1.36	PET
	^{122}I	$\varepsilon + \beta^+$ decay	0.06	PET
	^{123}I	ε	13.2	SPECT
	^{124}I	$\varepsilon + \beta^+$ decay	1003.22	PET
	^{125}I	ε	83.4	SPECT
	^{131}I	ɣ + β^- decay	192.6	Therapy

2.2. Chemistry of Gallium (Z = 31)

Gallium is a metallic element in Group 13 of the Periodic Table. Ga has the electron configuration [Ar]3d^{10}4s^{2}4p^1. Ga can exist in multiple oxidation states, namely (I), (II), and (III), but the only stable form in an aqueous solution is the +3-oxidation state Ga(III), the reduction potential Ga(III)/Ga = –0.56 V. The effective ionic radius of Ga(III) is 0.62 Å at C.N. = 6. The C.N. of gallium in complexes varies from 3 to 6, depending on the nature of the attached ligands. Ga(III) has hard acid properties and prefers to coordinate with hard donor atoms such as negative oxygen and nitrogen.[5,38–40] The hydrated form, $[Ga(H_2O)_6]^{3+}$, is stable as a free ion only under acidic conditions, with a pK_1= 2.56. Among the mononuclear hydroxo complexes ($Ga(OH)^{2+}$, $Ga(OH)_2^{+}$, $Ga(OH)_3$ and $Ga(OH)_4^{-}$) there is a polynuclear species, $[Ga_{13}O_4(OH)_{24}(OH_2)_{12}]^{7+}$ identified both in the solid state and in solution.[41] Due to the amphoteric behavior of gallium, $[Ga(OH)_3]$ can be dissolved in alkaline solutions around pH = 7.4 forming gallate, $[Ga(OH)_4]^{-}$.[39,42] Showing similarity to Al(III), the water exchange rate of $[Ga(H_2O)_6]^{3+}$ is quite slow (4.0 x 10^2 s^{-1}), while $[Ga(OH)(H_2O)_5]^{2+}$ is much less inert (2 x 10^5 s^{-1}).[41] Ga(III) forms quite stable complexes with fluoride especially in the solid state,[43] and weak complexes with other halides in solution.[17,44] Ga(III) forms stable complexes with “classic” APCs as EDTA.[45] Ga(III) ions are coordinated by six donor atoms (N_2O_4) in distorted octahedral coordination geometries. The ^{1}H and ^{13}C NMR spectra show that acetate groups undergo rapid interchanges between the axial and equatorial positions in solution.[46,47] A renewed interest in coordination chemistry of gallium with organic chelators is steamed by the PET application of ^{68}Ga. The bifunctional chelators (having both metal-binding entity and covalently attached bio-vector) are structurally quite

diverse, a recent review makes eight categories: DOTA and 1,4,7-triazacyclononane, the acyclic HBED, pyridinecarboxylates, siderophore -es, tris(hydroxypyridinones) and DTPA; and the mesocyclic diazepines.[48] There are two naturally stable isotopes of gallium, ^{69}Ga (60.1% , I = 3/2) and ^{71}Ga (39.9%, I = 3/2). Both are quadrupolar NMR-active nuclei and produce broad signals. However, ^{71}Ga has a lower quadrupolar moment, resulting in narrower signal and higher receptivity (0.0517 relative to ^{1}H, the resonance frequency is 30.50 MHz at 2.35 Tesla, i.e. 100 MHz for ^{1}H).[49,50] There are 29 radioisotopes of Ga ranging from ^{57}Ga to ^{87}Ga; especially ^{67}Ga and ^{68}Ga are widely used for medical purposes. The ^{68}Ge/^{68}Ga generator has shown enormous potential for molecular imaging. ^{68}Ga-tracers, with their high positron branching of 89% and ability to produce radiopharmaceuticals in a kit-type manner, are especially suited for regular use in nuclear medicine. Nevertheless, the relatively limited half-life of ^{68}Ga, namely 67.71 minutes, might restrict the possible utilization of ^{68}Ga-labeled radio diagnostics and for therapeutic aims.[51] ^{67}Ga has a half-life of 3.25 days. It has frequently been utilized in nuclear medicine to detect the location of malignant tumors.[52] The use of the ^{68}Ga positron emitter provides superior quality images. For some important radioisotopes of Ga(III) radiometals with their applications see Table 2.

2.3. Chemistry of Indium (Z = 49)

Indium is a metallic element in Group 13 of the Periodic Table. It has an electron configuration of [Kr]4d^{10}5s^{2}5p^{1}. Indium has two oxidation states (III) and (I), reduction potentials are: In(III)/In(I) –0.44 V; In(III)/In(s) –0.34 V.[53] In(I) is readily oxidized to In(III) in aqueous solution. Like gallium, indium generally exhibits a +3-oxidation state in aqueous solution, indium has a relatively greater atomic radius of 0.62, 0.80 and

0.92 Å, for coordination number 4, 6 and 8, respectively. Unlike Al(III) and Ga(III), $In(H_2O)_6^{3+}$ has a faster rate of water exchange, k_{ex} = 4 x 10^4 s^{-1}. According to the HSAB concept, indium is categorized as intermediate acid because it tends to form stable bonds with donor atoms of intermediate and soft character, such as negatively charged sulfur and neutral nitrogen. Ligands with a coordination number of 6 or 7 form stable complexes with cavity sizes that match indium.[18,38,44] Since In(III) is d^{10} metal ion, its coordination geometry is determined by the steric needs of the ligands, and there is no any ligand field or crystal field stabilization energy.[5] Compared to Al(III) and Ga(III), In(III) could form more stable complexes with chloride. However, in terms of the stability of mononuclear hydroxide complexes, In(III) lies between these two trivalent ions. Above pH = 2-3, hydrolysis becomes noticeable in perchlorate solutions. There is a dominating $[In_4(OH)_6(OH_2)_{12}]^{6+}$ tetrameric species in nitrate solution.[54] The hydrolysis is suppressed at higher chloride concentrations, it is not observed until the pH reaches 4. In contrast to Al(III) and Ga(III), In(III) forms its hydrolysis products quickly.[17] In(III) forms mixed organic ligand-fluoro complexes.[55] Examples of coordination complexes of indium fluorides with neutral donor ligands are few, but include the layered polymer $[InF_3(4,4'\text{-bipy})]$, having bridging fluorides as In-F-In.[56] Direct reaction of $InF_3 \cdot 3H_2O$ with 2,2'-bipy or 1,10-phen (L-L) forms the distorted octahedral species $[InF_3(L\text{-}L)(H_2O)]$.[57] Recently, $M_2[InF_3(C_2O_4)H_2O]$ (M = K^+, Rb^+ cation) was structurally characterized**,** the indium atom in the complex anion was surrounded by four F^- atoms, two of which were bridging.[58]

Polyaminopolycarboxylates form stable complexes with indium. The recent interest can obviously be attributed to the complexes of ^{111}In used

as SPECT tracer, see below. Both open chain ligand as DTPA or cyclic one as DOTA and their bifunctional versions are widely used in labeling with ^{111}In.[59,60]

Indium has two naturally occurring isotopes, ^{115}In (95.72%, I = 9/2) and ^{113}In (4.28%, I = 9/2).[61,62] Both are quadrupolar NMR-active nuclei and produce broad signals. However, ^{115}In has a lower quadrupolar moment, resulting in somewhat narrower signal and higher receptivity (0.338 relative to ^{1}H NMR, the resonance frequency is 21.91MHz at 2.35 Tesla, i.e. 100 MHz for ^{1}H).[63] High resolution NMR spectra can only be detected for symmetric species, like $In(H_2O)_6^{3+}$ used as chemical shift standard. Recently, relatively narrow ^{115}In NMR signal of InPOP (polyoxo-palladate) having cubic InO_8 entity has been recorded.[64] Radioisotopes of indium are mainly used for single photon emission computed tomography (SPECT). Moreover, indium radioisotopes emit positrons and Auger electrons, which are utilized for therapy.[37] ^{111}In is the most medicinally valuable radioisotope of indium, even though $^{114,113}In$ were previously used for medical purposes. ^{111}In possesses a half-life of 67.3 hours, making it an appropriate radiolabel for vectors that exhibit longer pharmacokinetic characteristics. While a gamma camera can take pictures of it, the quality of the pictures isn't great, because it has multiple photopeak's at 171 keV and 245 keV. The decay processes of ^{111}In include the release of Auger electrons, which have low energy and travel very small distances (less than the diameter of a single cell). In imaging applications, this effect adds to the undesired cellular radiation dosage.[5,65] ^{114m}In is another isotope of indium with a half-life of (1188 hr.). Together with ^{111}In, it forms a therapeutic companion pair. At the same time, ^{114m}In emits 190 keV photons, which are suitable for gamma detection. It is produced mainly by

either proton or deuteron irradiation of cadmium targets through the following reactions: ^{114}Cd(1p,1n) ^{114m}In, ^{116}Cd(1p,3n)^{114m}In and ^{114}Cd(1d,2n) ^{114m}In.[37] For some important radioisotopes of In(III) radiometals with their applications see Table 2.

2.4. Chemistry of Thallium (Z = 81)

Thallium is the heaviest stable element in Group 13 of the Periodic Table. This metal possesses an electron configuration with [Xe] $4f^{14}5d^{10}6s^2$ $6p^1$. Tl is predominantly found in two oxidation states (I) and (III). Both forms are widely recognized, and oxidation potential details suggest that the (I) state is usually the stable form in aqueous systems open to air. (It is worth noting that Tl(I) is more stable than the monovalent oxidation states of the other three metallic elements of group 13, Al, Ga, and In.) The standard reduction potentials at 25 ˚C (1M H^+) are: Tl(I)/Tl = −0.336 V, Tl(III)/Tl = +0.72 V, and Tl(III)/Tl(I) = +1.25 V. The ionic radii are: 1.49 Å for Tl(I) and 1.05 Å for Tl(III). The C.N. of Tl(I) is less well-defined, it resembles K^+, while C.N. of Tl(III) is often 6 with octahedral geometry, but it could go up to 7 or 8, depending on the bulkiness and structure of the coordinated ligand(s). The $Tl(H_2O)_6^{3+}$ has octahedral structure both in the solid state and in solution. The aqua ligands of the $Tl(H_2O)_6^{3+}$ ion are quite labile; the pseudo first-order rate constant for the exchange of water is 5×10^7 s^{-1}. The $Tl(H_2O)_6^{3+}$ ion is very acidic, the acid constants pK_1 and pK_2 are 0.5 and 1.2, respectively.[17] In other words, $Tl(OH)^{2+}$ and $Tl(OH)_2^+$ are among of the most stable metal–hydroxo species. However, in contrast to Al(III), Ga(III), and In(III), no polynuclear species of type $M_x(OH)_y^{(+3x-y)}$ are known for Tl(III). On the contrary, Tl(I) exhibits hydrolytic stability in water.[66] Tl(III) is distinguished in Group 13 as the unique “soft acid”

unlike Al(III), Ga(III) and In(III). Tl(I) can be categorized as “borderline acid”.[18]

Thallium(III) has the ability to form a robust complex with polyamino polycarboxylate ligand derivatives, whether they are open or macrocyclic ligands. For instance, Tl(III) has the ability to form a strong complex with linear ligands such as EDTA.[45,67] The reported stability constant is log*K*= 37.8. (Only cobalt(III) possesses a unique ability to make more stable complexes with EDTA compared to thallium(III)). Tl(III) forms robust complex with DOTA,[68] the stability constant of $[Tl(DOTA)]^-$ is likely very large, but no reliable value has been published. The $[Tl(EDTA)]^-$ (formed with the 6-dentate ligand) forms remarkably stable mixed ligand complexes (C.N. = 7) with halogenides, (Cl^-, Br^-, I^-) and pseudo halogenides (SCN^-, CN^-), $[Tl(EDTA)X]^-$. The stability increases from hard to soft as $Cl^- < Br^- < I^-$. $[Tl(DOTA)]^-$ (formed with the 8-dentate ligand) cannot accommodate halogenides. However, several Tl(III)-DOTA-derivatives with lower than 4 pendant arms can coordinate iodide.[69,70] These complexes can be considered as iodide carrying agent and might be used for labelling with radio-iodine isotopes.

Tl is found in nature as a combination of two stable isotopes, namely ^{205}Tl (70.5%) and ^{203}Tl (29.5%). The atomic mass of natural thallium is 204.38 g/mol. (Note: The ratio of these isotopes can vary by around 2% depending on the isotope composition present in different natural resources, such as oceans, rivers, seawater and sedimentary rocks.[71] Both ^{205}Tl and ^{203}Tl have I = 1/2 nuclear spin, they are high sensitivity NMR active nuclei. ^{205}Tl is more sensitive (receptivity relative to ^1H NMR is 0.142) and yields less broad signal than ^{203}Tl. The resonance frequency (57.68 MHz at 2.35 Tesla, i.e. 100 MHz for ^1H) is outside the range of most NMR probes, only

very few laboratories can record $^{203/205}$Tl NMR spectra using selective Tl-probe. Thallium has 42 isotopes with atomic mass ranging from 176 to 217, most of them have very short half-life. ^{203}Tl and ^{205}Tl are the stable isotopes (considered to be observationally stable). ^{204}Tl is the most stable radioisotope with a half-life of 3.78 years. ^{207}Tl, with a half-life of 4.77 minutes, has the longest half-life of naturally occurring Tl radioisotopes. ^{201}Tl is a synthetic radioisotope, and it has been used in medical imaging, especially for myocardial perfusion scintigraphy as Tl(I)Cl. Although ^{99m}Tc has largely replaced ^{201}Tl in such clinical routine, ^{201}Tl is an emerging isotope for "targeted Auger electron-emitting therapy". To get thermodynamically stable and kinetically inert chelates, the ^{201}Tl isotopes must be used as Tl(III). Substantial research activity has been devoted to find suitable ligand (including APCs as EDTA, DTPA and DOTA).[72,73] Very recently, bifunctional open chain chelators having picolinate pendants have been tested for carrying ^{201}Tl as Tl(III). Good serum stability is found compared to DOTA and DTPA, but the redox stability against bio reduction (Tl(III) to Tl(I) resulting in loss of stability and selectivity) still remains a temptation.[74] ^{201}Tl has a half-life of 73 hours and decays by electron capture, emitting X-rays (~70–80 keV), and photons of 135 and 167 keV in 10% total abundance.[75] Production can involve neutron activation of stable thallium in a nuclear reactor or in a cyclotron via the ^{203}Tl(p,3n)^{201}Pb reaction, with ^{201}Pb decaying naturally to ^{201}Tl. ^{201}Tl is considered a radiopharmaceutical used in nuclear cardiac stress testing because of its favorable imaging characteristics and relatively low radiation dose to the patient.

^{201}Tl with 73 h half lifetime is considered a potentially very useful therapeutic radionuclide for molecular radiotherapy (MRT) applications,

because it emits 37 Auger and other high LET secondary electrons per decay as compared to 25 and 12 emitted by ^{125}I and ^{161}Tb, respectively. Like other AE emitters, ^{201}Tl also emits X-ray and gamma rays, allowing SPECT imaging. This dual-purpose feature paves the way for accurate dosimetry and theranostics. Previously, ^{201}Tl was a widely accepted SPECT agent for myocardial perfusion imaging, though ^{99m}Tc-based agents, such as tetrofosmin and sestamibi, have since taken on businesses.[73,74] Some important radioisotopes of Tl(III) radiometals with their applications, see Table 2.

Aim of the study

The objective of this work is to study the equilibrium, structural and kinetic (formation and decomposition) properties of macrocyclic H_2OPC2A ligand complexes with selected M(III) metal ions, such as scandium(III), gallium(III), indium(III) and thallium(III). The $[M(OPC2A)]^+$ complexes are considered as potential halide binders forming [M(OPC2A)X] mixed complexes (X = F in case of M = Sc, Ga and In; X = I in case of M = Tl). These metal complexes, especially their radio-labelled isotopologs may have promising applications in biomedical fields, including both diagnostics (PET, SPECT), therapy (β^-) or theragnostic.

The OPC2A is a DOTA analog 12-membered macrocyclic (MC) see Scheme 1, having one of the three N-donors in a pyridine ring, and an ether O-atom trans to this N, and only two carboxylate pendants. According to our working hypothesis, this rigidified MC with reduced denticity (6) allows the $[M(OPC2A)]^+$ for easier binding of additional ions or water molecule to the central metal ion, while the stability remains acceptable, the inertness might be very good, as it has been proven for the $[Mn(OPC2A)(H_2O)]$.[76] These findings motivate us for the synthesis and investigation of this ligand and its complexes with selected M(III) metal ions of Group 13 of the periodic table together with the Sc(III). The common properties of these three main-group metal ions with d^{10} and the transition metal Sc(III) with d^0 electronic configuration are, that these central metal ions have no useful UV-Vis spectra and all are diamagnetic (EPR silent), therefore the equilibrium of complex formation must be followed by other way, i.e. by potentiometry, or UV-Vis and/or $^1H/^{13}C$ NMR spectra of the ligand, and using metal NMR. Fortunately, ^{45}Sc, ^{71}Ga,

^{115}In and ^{205}Tl NMR spectroscopy can readily be used, while high resolution MS and X-ray crystallography may contribute to the structural information.

The aims of the sub-projects:

- Determination of the thermodynamic stability of parent $[M(OPC2A)]^+$ complexes by multinuclear NMR and UV-Vis spectroscopy
- Study of the formation and dissociation kinetics of $[M(OPC2A)]^+$ complexes by UV-vis spectroscopy
- Equilibrium and kinetic study of mixed fluoride complexes, [M(OPC2A)F], by ^{19}F NMR spectroscopy and study of $[Sc(PC2AAM^{nBu})(F)]$ mixed complex for comparison
- Structural study of selected crystals by X-ray diffraction
- Selection and recommendation of some suitable systems for radiolabeling

3. Experimental part

3.1. Preparation of metal stock solutions (M = Sc(III), Ga(III), In(III) and TI(III))

All chemicals and solvents used in this study were obtained from commercial sources and used without further purification. Stock solutions of the metal ions ($Tl(NO_3)_3 \cdot 6H_2O$, $In(NO_3)_3 \cdot 6H_2O$, $Ga(NO_3)_3 \cdot 6H_2O$, and $ScCl_3 \cdot 6H_2O$) were prepared by dissolving the solid salts in distilled water containing a known amount of acid (HNO_3 or HCl) to suppress hydrolysis. The concentrations of these stock solutions were determined by complexometric titration.

Thallium(III) concentration of $Tl(NO_3)_3$ solution was determined by direct titration method in acid medium. The known volume of $Tl(NO_3)_3$ solution was diluted with nitric acid and then titrated with standardized EDTA using Xylenol Orange as indicator. The pH was adjusted with ammonium acetate buffer to 3.5-4.5. The color changed from purple to yellow at the end point. This direct titration with EDTA was also used for indium(III). The pH was adjusted to the best range for complexation, to pH 5-6 and Xylenol Orange was used as the indicator. A sharp color change indicated the titration endpoint.

The back titration method was used for gallium(III). Known excess of standardized EDTA was added to the $Ga(NO_3)_3$ solution at slightly acidic region between pH = 5-6, kept by hexamethyl tetraamine as buffer solution, after that the excess of EDTA was measured back with the standardized $ZnSO_4$ in the presence of Xylenol Orange indicator. The concentration of Sc(III) solution was determined as follows: First, a sample of $ScCl_3 \cdot 6H_2O$ was dissolved in 0.01 M HCl; then, it was titrated

with the standardized EDTA in the presence of Xylenol Orange as an indicator. The titration took place within a pH range of 2.3-2.4. At the very end of the titration, color changes from red to yellow color. The acid content of the solution was determined by pH-potentiometric titration, where DTPA was used for titration with the $ScCl_3$ solution.[77]

3.2. Preparation of OPC2A ligand

The OPC2A ligand was prepared following the synthetic procedures described in the literature,[76] see Scheme 2. The synthesis began with the preparation of 2,6-bis(chloromethyl)pyridine (2) from 2,6-pyridinedime thanol (1). Simultaneously, bis(2-chloroethyl) ether (3) was converted into bis(2-aminoethyl) ether (4) via a Gabriel synthesis using potassium phthalimide. The amino groups in compound (4) were protected by tosyl groups to afford the protected diamine, which was then used to prepare compound (5), followed by a cyclization reaction yielding the tosylated macrocycle (6). The tosylated O-pyclene was then detosylated in a microwave reactor with the assistance of concentrated sulfuric acid to produce O-pyclene (7) from the tosylated precursor. Side arms were introduced onto the macrocycle by alkylation of compound (7) with ethyl bromoacetate, yielding compound (8). Base-mediated deprotection of compound (8) gave the desired OPC2A ligand after adjusting the pH of product (9) to obtain product (10). The OPC2A ligand was purified using preparative HPLC (Luna 10u-prep C18(2), and its purity was determined using ESI-MS and NMR spectroscopy. Trifluoroacetic acid was used as eluent (c_{TFA} = 5 mM), and it was found as Na-salt in the stock solution of H_2OPC2A as detected by ^{13}C and ^{19}F NMR.

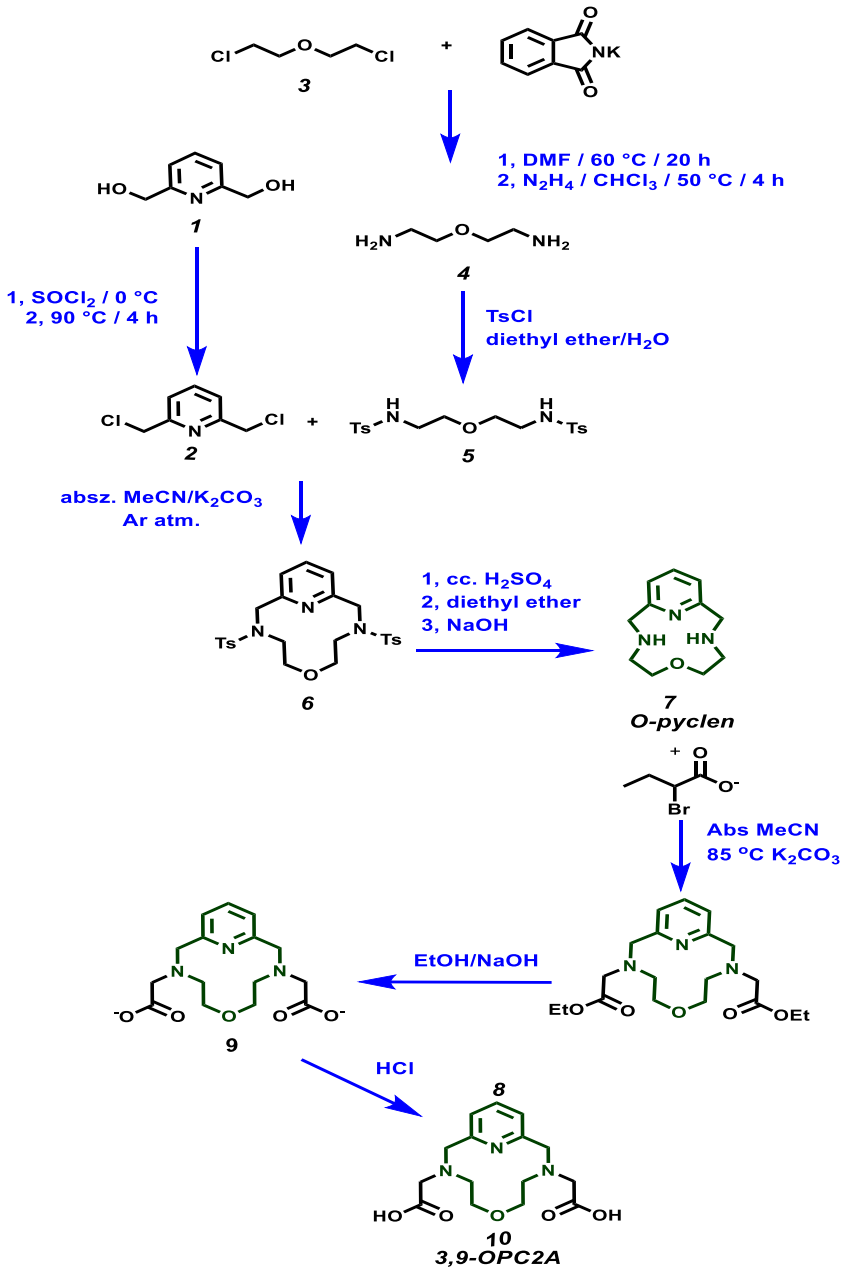

Scheme 2. Preparation of 6-Oxa-3,9,15-triazabicyclo (9.3.1) pentadeca-1(15),11,13-triene-3,9-diacetic acid (3,9-OPC2A) ligand.

Structural Assignment of OPC2A and Its M(III) Complexes $[Sc(OPC2A)]^+$, [Sc(OPC2A)F], $[Ga(OPC2A)]^+$, $[In(OPC2A)]^+$ via ^1H NMR, ^{13}C NMR and ESI-MS Techniques

OPC2A with formula $C_{15}H_{21}N_3O_5$ ^1H NMR (500 MHz, D_2O) δ 7.94 (t, J = 7.8 Hz, 1H), 7.44 (d, J = 7.9 Hz, 2H), 5.04 – 4.73 (m, 4H), 4.06 (s, 4H), 3.81 (s, 2H), 3.59 (t, J = 4.8 Hz, 4H), 3.07 (s, 2H). ^{13}C NMR - δ (ppm). 57.09, 59.07, 59.38, 64.11(4 × 2C, -CH_2), 122.20(2C, aromatics), 139.88 (1C, aromatics), 149.77(2C, Cq, aromatics), 169.89(2C, Cq, C=O). ESI-MS positive mode m/z calculated for $[C_{15}H_{21}N_3O_5 + H]^+$ 324.1554 and found 324.1554. and m/z calculated for $[C_{15}H_{21}N_3O_5 + Na]^+$ 346.1377; and found 346.1373. c_{OPC2A} = 0.3 mM. See Appendix Figure A.1.

$[Sc(OPC2A)]^+$ with formula $C_{15}H_{19}N_3O_5Sc$ ^1H NMR (500 MHz, D_2O) see Appendix Figure A. 2 δ 8.01 (t, *J* = 7.9 Hz, 1H), 7.48 (d, *J* = 7.8 Hz, 2H), 4.57–4.49 (m, 2H), 4.23 (d, *J* = 17.0 Hz, 2H), 3.83–3.75 (m, 4H), 3.70 (d, *J* = 16.9 Hz, 2H), 3.34 (td, *J* = 13.0, 5.0 Hz, 2H), 3.04 (dd, *J* = 13.9, 3.4, 1.4 Hz, 2H), 2.65–2.57 (m,2H). ^{13}C NMR (126 MHz, D_2O) Appendix Figure A.3, δ17 , 0.05(2C, Cq, C=O), 149.81(2C, Cq, aromatics) 139.85 (1C, aromatics), 122.25(2C, aromatics), 64.13, 59.33, 59.17, 56.90 (4×2C, -CH_2-) 122.20, 139.88, 149.77, 169.89. ESI-MS positive mode m/z calculated for $[C_{15}H_{19}N_3O_5Sc]^+$ 366.0878 and found 366.880. $c_{Sc(OPC2A)}$ = 0.3 mM.

[Sc(OPC2A)F] with formula $C_{15}H_{19}N_3O_5ScF$: ^1H NMR (500 MHz, D_2O) see Appendix Figure A.7. δ 7.95 (d, *J* = 7.8 Hz, 1H), 7.39 (d, *J* = 7.8 Hz, 2H), 4.34 – 4.11 (m, 4H), 4.01 (t, *J* = 10.9 Hz, 2H), 3.70 (d, *J* = 17.4 Hz, 2H), 3.57 (d, *J* = 10.2 Hz, 2H), 3.47 (d, *J* = 17.5 Hz, 2H), 2.88 (s, 2H), 2.72 (d, *J* = 13.8 Hz, 2H).^{13}C NMR (126 MHz, D_2O) see Appendix Figure A.8. δ 180.42 (2C, Cq, C=O), 157.17(2C, Cq, aromatics), 141.90 (1C,

aromatics), 122.36 (2C, aromatics), 71.74, 63.49, 63.14, 58.27(4× 2C, -CH_2-). ESI-MS positive mode m/z calculated for $[C_{15}H_{19}N_3O_5Sc]^+$ 366.0878 and found 366.880. $c_{Sc(OPC2A)}$ = 0.3 mM. ESI-MS positive mode m/z calculated for $[C_{15}H_{19}FN_3NaO_5Sc]^+$ 408.0760 and found 408.0762. $c_{Sc(OPC2A)F}$ = 0.3 mM.

[Ga(OPC2A)]$^+$ with formula $C_{15}H_{19}N_3O_5Ga$ ^{1}H NMR (500 MHz, D_2O) see Appendix Figure A. 12. δ 7.95 (d, J = 7.8 Hz, 1H), 7.39 (d, J = 7.8 Hz, 2H), 4.34 – 4.11 (m, 4H), 4.01 (t, J = 10.9 Hz, 2H), 3.70 (d, J = 17.4 Hz, 2H), 3.57 (d, J = 10.2 Hz, 2H), 3.47 (d, J = 17.5 Hz, 2H), 2.88 (s, 2H), 2.72 (d, J = 13.8 Hz, 2H).13C NMR (126 MHz, D_2O) see Appendix Figure A.13. δ 176.71 (2C, Cq, C=O), 152.39 (2C, Cq, aromatics), 144.18 (1C, aromatics), 122.99 (2C, aromatics), 64.37, 60.65, 58.05, 57.15 (4× 2C, -CH_2-). ESI-MS positive mode m/z calculated for $[C_{15}H_{19}FN_3NaO_5Ga]^+$ 432.0496 and found 432.0491, $c_{[Ga(OPC2A)]+}$ = 0.5 mM. ESI-MS positive mode m/z calculated for $[C_{15}H_{19}N_3O_5In]^+$ 436.0308 and found 436.0358 $c_{[In(OPC2A)]+}$ = 0.5 mM. and ESI-MS positive mode m/z calculated for $[C_{15}H_{20}N_3O_6In+Na]^+$: 476.0253 and found 476.0283 calculated with formula $C_{15}H_{20}N_3O_6InNa$.

3.3. NMR-Measurements

A Bruker AM 360 (8.45 T), a Bruker DRX 400 MHz (9.4 T), and a Bruker Avance III 500 MHz (11.75 T) DRX NMR spectrometers, equipped with Bruker Variable Temperature Unit (BVT), Bruker Cooling Unit (BCU) and a BB inverse *z* gradient probe (5 mm) were used. The temperature of the probe was maintained at 298 ± 0.1 K using a Bruker VT-1000 temperature controller. The frequencies used for ^{1}H, ^{13}C, ^{45}Sc, ^{71}Ga, ^{111}In, ^{205}Tl and ^{19}F are indicated in the captions of the figures. The ^{1}H and ^{13}C chemical shifts were calibrated to the tetramethyl silane (TMS) standard,

while ^{19}F was referenced to the CCl_3F (TFA was used as a secondary standard set to –75.0 ppm referring to CCl_3F as 0 ppm). Metal NMRs (Sc, Ga, In, and Tl) were calibrated to 0 ppm using aqueous solutions (1–5 mM) of MX_3 prepared in 0.1 M acid. Samples were prepared in H_2O and 10 % D_2O was added to all samples for deuterium-lock. Some samples for ^1H NMR were dissolved in D_2O as indicated in the figure captions. The ^1H-^1H (COSY), ^1H-^{13}C (HSQC) and ^1H-^{13}C (HMBC) correlation spectra were collected by using gradient pulses in the *z* direction with the standard Bruker pulse programs.

3.3.1. DANTE- Selective Magnetization Transfer

The chemical exchange between the [Sc(OPC2A)F] ternary complex and F^- anion was investigated with selective magnetization transfer experiments by using a DANTE pulse train in the temperature range of 273–333 K.[78] In each series of experiments, the ^{19}F NMR signal of the [Sc(OPC2A)F] ternary complex or the free F^- was inverted by a composite 180° pulse and then both ^{19}F NMR signals were observed using a τ - time delayed 90° pulse. The exchange phenomenon is described by the Bloch equations:

$$\frac{d[M-M_\infty]}{dt} = R[M - M_\infty] \quad (1)$$

where the z-magnetization is M at time t and M_∞ at time $t = \infty$, whereas R is the sum of the k_{ij} rate constant and $1/(T_1)_i$ (where $i \neq j$ and $(T_1)_i$ is the spin-lattice relaxation time for the site i). The differential equation describing the distribution of the negative magnetization between the [Sc(OPC2A)F] ternary complex and F^- anion, can be expressed by the following equation:

$$\frac{\mathrm{d}[M_{\mathrm{ScLF}}-M_{\mathrm{ScLF},\infty}]}{\mathrm{d}t} = -\left(\left(\frac{1}{T_{1,\mathrm{ScLF}}}\right) + k_{\mathrm{ScLF}}^{obs}\right)\left[M_{\mathrm{ScLF}} - M_{\mathrm{ScLF},\infty}\right] + k_{\mathrm{F}}^{obs}\left[M_{\mathrm{F}} - M_{\mathrm{F},\infty}\right] \quad (2)$$

$$\frac{\mathrm{d}[M_{\mathrm{F}}-M_{\mathrm{F},\infty}]}{\mathrm{d}t} = -\left(\left(\frac{1}{T_{1,\mathrm{F}}}\right) + k_{\mathrm{F}}^{obs}\right)\left[M_{\mathrm{F}} - M_{\mathrm{F},\infty}\right] + k_{\mathrm{ScLF}}^{obs}\left[M_{\mathrm{ScLF}} - M_{\mathrm{ScLF},\infty}\right] \quad (3)$$

where M_{ScLF}, M_{F} are the value of magnetization at time t, and $M_{\mathrm{ScLF},\infty}$, $M_{\mathrm{F}\infty}$ at time $t = \infty$. The k_{ScLF}^{obs}, k_{F}^{obs} and $T_{1,\mathrm{ScLF}}$ values have been calculated by the simultaneous fitting of the peak area of the ^{19}F NMR signal of the [Sc(OPC2A)F] ternary complex and F^- anion τ delay time data pairs to eq 2 and 3. The longitudinal relaxation time of F^- anion ($T_{1,F}$) was determined with the "inversion recovery" method (180°–τ–90°) by using 16 different τ values with typical 90° pulse width of 18 μs, 8 scans. The measurements were performed with a 9 mM NaF solution at pH = 5.4. The $T_{1,F}$ values, determined in the separate experiments, were fixed during the fitting procedure. The pulse imperfections were corrected by treating the initial and equilibrium magnetizations as adjustable parameters in the least-squares refinements. Calculations were performed with the computer program *Micromath Scientist*, version 2.0 (Salt Lake City, UT, USA).

3.3.2. Deduction of the rate constants from line broadening data

The mutual exchange reaction in the $[Sc(OPC2A)F]^-$–$*F^-$ system is:

$$[Sc(OPC2A)F] + *F \rightleftharpoons [Sc(OPC2A)*F] + F^- \quad (4)$$

For the sake of simplicity, we introduce the following notations. [Sc(OPC2A)F] = [ScLF] and F^- = F. We suppose that ^{19}F NMR is measured and only this two fluorine containing species are present. The NMR experiment usually starts with a π/2 pulse which creates two

coherent transverse magnetizations M_{ScLF} and M_{F}. The ^{19}F NMR spectrum consists of two peaks with different chemical shifts and line width ($\nu_{1/2}$). After the pulse the relaxation starts. During a given time, the phase of the peak changes because of three reasons. First, the magnetic interaction with the elementary magnets presents in the environment. Second, the inhomogeneity of the B_0 field. The $\nu_{1/2}$ of the NMR peak is described with the following equation for these two effects:

$$\nu_{1/2} = \frac{1}{\pi T_2^*} \tag{5}$$

Where T_2^* is the relaxation time constant. In our case we have $\nu_{1/2\ \mathrm{ScLF}}$ and $\nu_{1/2\ \mathrm{F}}$ characterized by $T_{2,\ \mathrm{ScLF}}^*$ and $T_{2\ ,\mathrm{F}}^*$ for the two peaks. Third, the loss of coherence can happen on other way. One F^- ion goes to the [ScLF] complex, and one leaves for the free state. Their phase is random and decreases the coherence of the phase at both states. It is characterized by first order rate constants k_{ScLF}^{obs} and k_{F}^{obs}. The loss of the coherence of the phase causes the decrease of the transverse magnetizations according to Bloch's suggestion:

$$\frac{\mathrm{d}M_{\mathrm{ScLF}}}{\mathrm{d}t} = -\left(\frac{1}{T_{2,\ \mathrm{ScLF}}^*} + k_{\mathrm{ScLF}}^{obs}\right) M_{\mathrm{ScLF}} \tag{6}$$

and

$$\frac{\mathrm{d}M_{\mathrm{F}}}{\mathrm{d}t} = -\left(\frac{1}{T_{2,\ \mathrm{F}}^*} + k_{\mathrm{ScLF}}^{obs}\right) M_{\mathrm{ScLF}} \tag{7}$$

We can define the line broadening, *LB* as a consequence of the chemical exchange:

$$LB_{\mathrm{ScLF}} = \nu_{1/2,\ \mathrm{ScLF}} - \frac{1}{T_{2,\ \mathrm{ScLF}}\pi} = \frac{k_{\mathrm{ScLF}}^{obs}}{\pi} \tag{8}$$

$$LB_{\mathrm{F}} = \nu_{1/2,\ \mathrm{F}} - \frac{1}{T_{2,\ \mathrm{F}}\pi} = \frac{k^{obs}_{\mathrm{ScLF}}}{\pi} \qquad (9)$$

Therefore

$$LB_{\mathrm{ScLF}}\pi = k^{obs}_{\mathrm{ScLF}} \qquad LB_{\mathrm{F}}\pi = k^{obs}_{\mathrm{F}} \qquad (10)$$

The part of transverse relaxation origins from the chemical exchange can be written as:

$$\frac{\mathrm{d[ScLF]}}{\mathrm{d}t} = -k^{obs}_{\mathrm{ScLF}}[\mathrm{ScLF}] \qquad \text{and} \qquad \frac{\mathrm{d[F]}}{\mathrm{d}t} = -k^{obs}_{\mathrm{F}}[\mathrm{F}] \qquad (11)$$

because the intensity of magnetization is proportional to concentration. The general conclusion is that if we can determine the *LB* then the pseudo first order rate constant of the exchange reactions can be calculated.

The $\nu_{1/2\ \mathrm{ScLF}}$ is a very composite value. First, it is an (unresolved) octet from the scalar coupling of ^{45}Sc. All the peaks of the octet are broad because of the relaxation effect of the quadrupole nucleus of Sc. Further broadening also occurs from the F^- exchange described above. The result is a broad peak without any fine structure. (Theoretically, it can be modelled, but practically, it is very difficult to do taking into account of the experimental uncertainties. The only important information is that the $\nu_{1/2\ \mathrm{ScLF}}$ is independent on both the F^- ion and the H^+ ion concentrations. However, it has a temperature dependence indicating that the chemical exchange is part of this LW_{ScLF}. It means that k^{obs}_{ScLF} is not pseudo first order rate constant, but rather a real first order rate constant even if the value cannot be determined from line-shape. From eq 11 we can suggest that

$$\frac{\mathrm{d[ScLF]}}{\mathrm{d}t} = -k_{\mathrm{d}}[\mathrm{ScLF}] \qquad (12)$$

It is the rate constant of the dissociation of [ScLF]. The one way (we follow only the upper arrow of eq 4 of the F^- exchange process can follow the mechanism of eqs 13 and 14:

$$ScLF \xrightarrow{k_d} ScL^+ + F^- \quad (\text{slow}) \qquad (13)$$

$$ScL^+ + F^- \xrightarrow{k_f} ScLF \quad (\text{fast}) \qquad (14)$$

The rate determining step is the dissociation of [ScLF] followed by the fast formation of another [ScLF]. In this interpretation [ScL] is a very reactive intermediate in steady state concentration according to the following equations:

$$\frac{d[ScL]}{dt} = k_d[ScLF] - k_f[ScL][F] = 0 \qquad (15)$$

$$[ScL] = \frac{k_d[ScLF]}{k_F[F]} \qquad (16)$$

$$\frac{d[F]}{dt} = -k_f[ScL][F] = -k_f\frac{k_d[ScLF]}{k_F[F]}[F] =$$

$$-k_d\frac{[ScLF]}{[F]}[F] = -k^{obs}[F] \qquad (17)$$

The connection between k^{obs} in eq 17 and k_F^{obs} can be understood if we take into account that in eq 4 two F^- ion changes its phase while in eq 14 only one. Therefore $k^{obs} = \frac{1}{2}k_F^{obs}$. If we plot ½ $\pi^* LB_F = \frac{1}{2}k_F^{obs}$ against the [ScLF]/[F] eq 17 we should obtain k_d which is the rate constant of the rate determining step of F^- mutual exchange between [ScLF] and the F^- . It is important to note that this consideration is valid when the F^- ion is in large excess, and $[ScL]^+$ concentration is so low that it does not take part in the exchange process.

3.4. UV-visible spectrophotometry

The spectrophotometric measurements were performed with a JASCO V-760 UV-vis spectrophotometer (JASCO International Co., Ltd., Tokyo, Japan) at T = 298 K, using semimicro 1.0 cm cells. Kinetics of formation were measured in a 1.9–3.8 pH range, while the decomplexation experiments were carried out in acid solutions, c_{HCl} = 0.10–1.00 M using UV-vis spectra. Preprepared samples of 0.25 mM $[Sc(OPC2A)]^+$ were mixed with HCl solution adjusting the pH and the spectral change was followed at λ = 275 nm.

3.5. ESI-MS- Electrospray Ionization Mass Spectrometry

Experiments were carried out on a maXis II UHR ESI-QTOF mass spectrometer (Bruker, Bremen, Germany). The injector of an electrophoresis instrument was used to inject and transfer samples (7100 model, Santa Clara, California, US.) A triaxial CE-ESI interface (G1607B, Agilent) provided online hyphenation between the instruments.

3.6. pH- potentiometric titration

For the pH-potentiometric measurements we used a Metrohm 785 DMP Titrino titration device and a Metrohm-6.0233.100 combined glass electrode. The titrations were carried out in a volume of 5 cm^3 solutions. During the measurements, the system was stirred throughout, N_2-gas protected the sample against CO_2 contamination, and it was thermostated at 298.0 ± 0.2 K.

The titration of the OPC2A and preequilibrated M(OPC2A) complex with an ionic strength of 0.15 M NaCl or $NaNO_3$ was performed using a standardized sodium hydroxide (NaOH) solution. The concentration of the base was determined using a primary standard KH-phthalate solution. The

pH meter was calibrated using a KH-phthalate buffer (pH = 4.005) and a 0.010 M borax buffer solution (pH = 9.177). The method established by Irving et al. was used to determine the [H^+] concentration from pH values. The pH difference (ΔpH), i.e. the Irving coefficient (A) was used to correct the recorded pH values. It means that the calculated constants are stoichiometric constants. Additionally, the stoichiometric ion product (pK_w) was determined under the same conditions used to calculate the Irving coefficient (A).[79] Titrations were conducted over a pH range of 1.7 to 11.85, and the protonation constants and stability constants of the complex were calculated using the PSEQUAD software.[80]

3.7. Crystal structure analysis

Data for single-crystal X-ray diffraction were collected on the compound with the chemical formula $C_{15}H_{19.33}ClN_3O_5Tl \cdot C_{15}H_{19.67}ClN_3O_5Tl \cdot Cl_4Tl$, $C_{15}H_{17}ClN_3O_5Tl \cdot H_2O$. The crystals are triclinic with space group P1, with unit cell parameters a = 10.075(3) Å, b = 15.279(4) Å, c = 15.849(4) Å, α = 116.753(9)°, β = 90.097(9)°, γ = 109.203(9)°, and unit cell volume V = 2024.7(9) Å^3 at 293 K. There are two formula units per unit cell (Z = 2). The Bruker D8 VENTURE diffractometer data collection was performed with Mo Kα radiation (μ = 12.37 mm^{-1}) on a crystal measuring 0.30 × 0.23 × 0.11 mm. The multi-scan absorption correction was applied[81] with T min and T max set to 0.18 and 0.34, respectively. The data set comprised 19,490 reflections, of which 8137 were independent (R_{int} = 0.037), and 7099 were observed with $I > 2\sigma(I)$. The data set extended to a maximum value of (sin θ/λ) of 0.626 Å^{-1}. The structure was refined against F^2 with $R[F^2 > 2\sigma(F^2)] = 0.028$, $wR(F^2) = 0.077$, S = 1.07, using 8137 reflections, 504 parameters, and 2 restraints. Hydrogen atoms were treated by an independent and constrained refinement mixture. The final difference

Fourier map exhibited maximum and minimum electron densities of +1.41 and −1.01 eÅ^{-3}, respectively. The collection, solution, and refinement of the data were done by Bruker Instrument Service vV6.2.6, SAINT V8.40B (Bruker AXS LLC, 2019), XT (Version 2018/2) and SHELXL2019/1 (Sheldrick, 2019). Further manipulations of the structure and visualizations were performed with shelXle (C.B. Hübschle, rev 1365), WinGX, and publCIF.

4. Results and Discussion

4.1. Equilibrium studies of Sc(L)F

4.1.1 Determination of the protonation constants of OPC2A ligand

The protonation constants of macrocyclic OPC2A ligand have been studied by pH potentiometric titration. The protonation of ligands can be defined by eqs 18 and 19 (charges are omitted for simplicity.)

$$[H_{n-1}OPC2A] + H^{+} \rightleftharpoons [H_nOPC2A] \qquad (18)$$

$$K_n^H = \frac{[H_nOPC2A]}{[H_{n-1}OPC2A][H^+]} \qquad (19)$$

where n = 1,2, and 3. Note that: square brackets, **[]** (marking complex species in the text), have different meanings here, i.e. indicate equilibrium concentration (mol/dm^3) in eqs 19, 21, 23, 25, 30, 36, 39, 41 and 43 defining thermodynamic protonation and stability constants. The double brackets have been omitted for clarity. The logK_i^H values are summarized and compared with literature values of 3,9-OPC2A and *3,9*-PC2A in Table 3. They are in good agreement with the constants reported earlier.[76] The protonation steps (1 and 2) can be attributed to the N-donors at the 3 and

9 positions, and they are practically equal, log β_1 = 7.77 and log β_2 = 15.39, logK_2 = 7.66. (One must note: these constants describe the titration curve properly, although they are obviously not micro constants). The third protonation site is an acetate group, and logK_3 = 2.23.[82]

Table 3. Stepwise Protonation Constants of 3,9-OPC2A ligand and 3,9-PC2A (*I* = 0.15 M NaCl, *T* = 298 K, log β_2 = logK_1^H + logK_2^H)

	OPC2A	OPC2A[76]	*3,9*-PC2A[82]
log K_1^H	7.77 (1)	7.73	12.25
log K_2^H	7.51 (1)	7.66	5.97
log K_3^H	2.23 (1)	2.13	3.47
log K_4^H	—	—	1.99
log β_2	15.28	15.39	18.22

4.1.2 Determination of stability constants of $[Sc(OPC2A)]^+$ and [Sc(OPC2A)OH]

The acid-base properties of $[Sc(OPC2A)]^+$ have also been investigated by pH-potentiometry. Preprepared $[Sc(OPC2A)]^+$ ($c_{[Sc(OPC2A)]}$ = 2 mM) was titrated with NaOH in the pH-range of 2-10. The titration curve of $[Sc(OPC2A)]^+$ indicates a base consuming process at pH > 5.5 due to the formation of the mixed hydroxo [Sc(OPC2A)(OH)] complex according to eqs 20 and 21:

$$[Sc(OPC2A)(H_2O)]^+ \rightleftharpoons [Sc(OPC2A)(OH)] + H^+ \quad (20)$$

$$K_{[Sc(OPC2A)(OH)]} = \frac{[Sc(OPC2A)(OH)][H^+]}{[Sc(OPC2A)(H_2O)]} \quad (21)$$

The $\log K_{[Sc(OPC2A)(OH)]} = -7.00(4)$ can likely be associated with the deprotonation of an inner sphere water in the parent $[Sc(OPC2A)(H_2O)]^+$ complex. The formation of the protonated $[Sc(HOPC2A)]^{2+}$ was not detected in the studied pH range, in accordance with ^{45}Sc NMR and UV-vis experimental findings, see below.

Due to the expected quite high stability and slow formation rate, the equilibria could be studied in very acidic solutions using the "out-of-cell" method. Samples with different added acid content (c_{HCl} = 36.7–156.7 mM) have been prepared and kept at room temperature for 21 days until equilibration (the time needed to reach the equilibria was determined by NMR spectroscopy), Figure A.2 and Figure A.3. The equilibrium constant characterizing the formation of the $[Sc(OPC2A)]^+$ complex expressed by eqs 22 and 23 was calculated from the data obtained by ^{45}Sc NMR spectroscopy and spectrophotometry.

$$Sc^{3+} + (OPC2A)^{2-} \rightleftharpoons [Sc(OPC2A)]^+ \qquad (22)$$

$$K_{[Sc(OPC2A)]^+} = \frac{[Sc(OPC2A)^+]}{[(OPC2A)^{2-}][\,Sc^{3+}]} \qquad (23)$$

Both ^1H and ^{45}Sc NMR spectra show distinct signals for the free (uncomplexed) components Sc(III) and $H_3(OPC2A)^+$ and the parent complex $[Sc(OPC2A)]^+$, as shown in Figures 1. ^{45}Sc is a quadrupolar nucleus (I = 7/2) and for such complexes the line width of less symmetric species is often quite large, about 1 kHz. In our case, the intensity of the narrow signal of $[Sc(H_2O)_8]^{3+}$ at $\delta \approx 0$ ppm has been used to calculate the concentration of free Sc(III) by using the calibration curve. The broad ^{45}Sc NMR signal at 63 ppm corresponding to $[Sc(OPC2A)]^+$ has been detected, with the broadening being likely due to the C_2 symmetry of the complex.

The log$K_{[Sc(OPC2A)]}$ has been calculated by the PSEQUAD program using 5 and 6 data points (Table 5) obtained by ^{45}Sc NMR and spectrophotometry, see Figure 1 and Figure 2. Stability and deprotonation constant of $[Sc(OPC2A)]^+$ and the stability constant of the ternary [Sc(OPC2A)OH] complex are shown in Table 4.

Table 4. Thermodynamic Stability Constants of $[Sc(OPC2A)]^+$, and [Sc(OPC2A)(OH)] Complexes (I = 0.15 M NaCl, T = 298 K).

	$[Sc(OPC2A)]^+$	Methods
log$K_{[Sc(OPC2A)]}$	16.72 (4)	^{45}ScNMR, spectrophotometry
log$K_{[Sc(OPC2A)OH]}$	–7.00 (4)	pH potentiometry, ^{45}Sc NMR

Table 5. Data used to calculate the stability constant, log $K_{[Sc(OPC2A)]}$ with varying acid concentrations (0.03-0.15 M HCl) recorded by 121.3 MHz ^{45}Sc NMR (I = 0.15 M NaCl, $c_{Sc(III)}$ = 3 mM, c_{OPC2A} = 3.15 mM, T = 298 K) simultaneously with UV-Vis data using samples in the pH range (1.76-2.83) (I = 1 M NaCl, $c_{Sc(III)}$ = 0.25 mM, c_{OPC2A} = 0.25 mM, absorbance measured at 275 nm, l = 1 cm.

HCl $[H^+]_{tot}$	Equilibrium free [Sc(III)]	half width $\nu_{1/2}$ [Hz]	chemical shift (δ ppm)
0.0367	0.00064	86	1.39
0.0567	0.00124	51	1.02
0.0817	0.00176	45	0.95
0.1067	0.00228	41	0.75
0.1567	0.00266	31	0.49

pH	Absorbance (275 nm)
1.76	0.51705
1.95	0.62525
2.15	0.65702
2.26	0.74456
2.47	0.86446
2.83	0.93575

log$K_{[Sc(OPC2A)]}$ = 16.72(4)

Note* Free Sc(III) in fact is $[Sc(III)]_{tot} = [Sc(III)aq] + [*[Sc(H_2OPC2A)]^+]$ as indicated by the changing δ and $\nu_{1/2}$ values.

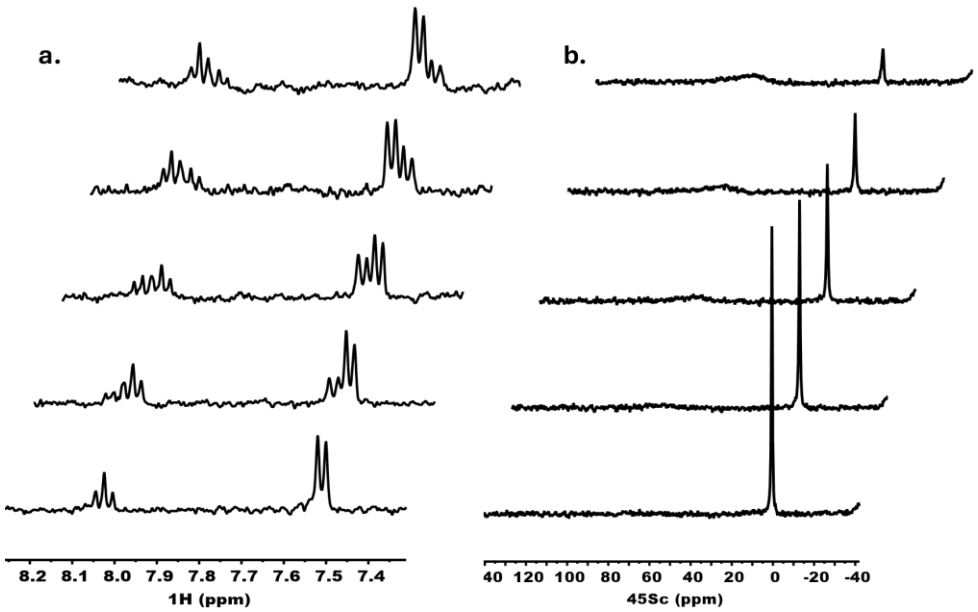

Figure 1. (**a)** 400 MHz ^{1}H-NMR spectra in the aromatic region (1, triplet; 2,3 doublets, see Scheme 1); (**b)** 97.3 MHz ^{45}Sc NMR spectra of Sc(III)-OPC2A^{2-}-H^{+} system (Sc(III) free peak $\delta \approx 0$ ppm, while the very broad signal of [Sc(OPCTA)]$^{+}$ is at $\delta = 63$ ppm). Experimental conditions: c_{Sc} = 3 mM, c_{OPC2A} = 3.15 mM, I = 0.15 M NaCl, T = 298 K; the acid concentrations are 36.7, 56.7, 82, 106.5, and 156.7 mM, from top to bottom.

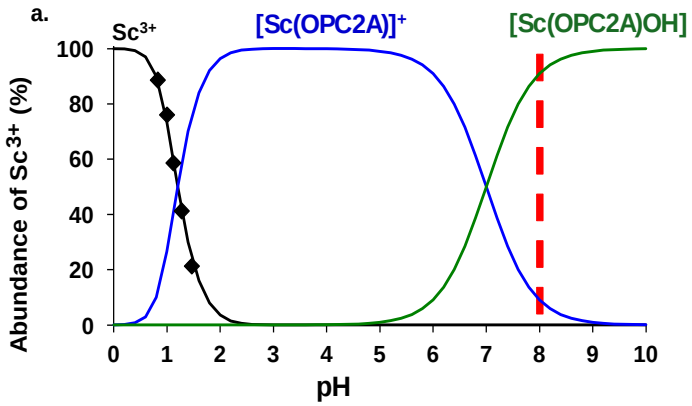

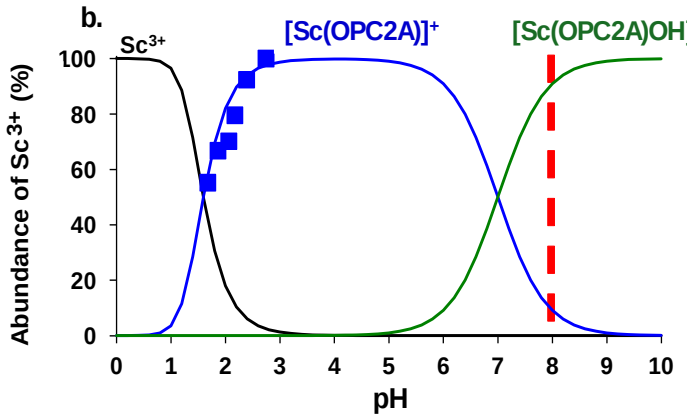

Figure 2. Species distribution diagram of the Sc^{3+}-$OPC2A^{2-}$-H^{+} system. Solid lines show calculated concentrations of free Sc^{3+}, and $[Sc(OPC2A)]^{+}$ parent complex ($\log K_{Sc(OPC2A)} = 16.72$, $\log K_{Sc(OPC2A)(OH)} = -7.00$), **(a)** black diamond (◆) symbols represent measured intensity of free Sc(III) by ^{45}Sc NMR ($c_{Sc} = 3.0$ mM, $c_{OPC2A} = 3.15$ mM, 0.15 M NaCl at T = 298 K). **(b)** blue square (■) symbols represent the measured concentration of $[Sc(OPC2A)]^{+}$ by UV-Vis spectrophotometry ($c_{Sc} = 0.25$ mM, $c_{OPC2A} = 0.25$ mM, $I = 0.15$ M NaCl at $T = 298$ K).

The $\log K_{[Sc(OPC2A)]} = 16.72(4)$ of $[Sc(OPC2A)]^{+}$ is substantially smaller than the stability constant of [Sc(PCTA)] ($\log K_{[Sc(PCTA)]} = 21.91$), as expected for a hexadentate ligand compared to the heptadentate one with considerably higher basicity (PCTA). One may mention that the stability constant of $[Sc(OPC2A)]^{+}$ is much smaller as compared to $\log K_{[Sc(EDTA)]} = 23.1$ of [Sc(EDTA)].[83] Both these chelators are hexadentate, and the overall basicity of the nitrogen atoms is nearly identical for the two ligands, although in the case of EDTA[84], the protonation of three acetate groups could be detected, whereas for OPC2A, only one such constant was observed making EDTA more basic. The main advantage of EDTA is likely the four carboxylate groups (compared to only two ones of OPC2A)

forming strong five-membered chelate rings contributing to the higher Sc(III) affinity of EDTA ligand.

Meanwhile, the Sc(III)-binding ability of the OPC2A ligand remains significant, particularly due to the formation of stable mixed hydroxo complexes. [Sc(OPC2A)(OH)] has been detected by pH-potentiometry (and its stability constant is also reported) and ^{45}Sc NMR, Figure 3. A new signal at 135 ppm is observed at pH > 9, and it has tentatively been attributed to $[Sc(OPC2A)(OH)_2]^-$ as discussed below. The $[Sc(OPC2A)]^+$ complex dominates at pH ≈ 5 with a δ value of 63 ppm, while [Sc(OPC2A)(OH)] shows a signal at δ = 83 ppm at pH ≈ 9. In the intermediate pH range of 6–8, these species do not give distinct signals, rather a broad time averaged peak is evidenced in the range of δ = 63–83 ppm. Chemical shift and half−width (line width at half intensity) of the species are summarized in Table 6. By contrast, at pH > 8.3, signals corresponding to [Sc(OPC2A)(OH)] and $[Sc(OPC2A)(OH)_2]^-$ species coexist an exhibit well-resolved ^{45}Sc NMR signal. The “fast exchange regime” observed between the parent complex and [Sc(OPC2A)(OH)] is likely due to their structural similarity. The parent complex presumably contains one coordinated water molecule $[Sc(OPC2A)(H_2O)]^+$ whose deprotonation yields [Sc(OPC2A)(OH)] without significant structural changes. In contrast, formation of $[Sc(OPC2A)(OH)_2]^-$ likely requires a more substantial structural rearrangement including substitution of donor atom(s) of the organic ligand by hydroxide ion(s). These changes result in a notable chemical shift to 135 ppm and the emergence of the “slow exchange regime”.

Table 6. 121.2 MHz ^{45}Sc-NMR Chemical Shift (δ) and Half Width ($v_{1/2}$) Data of [Sc(OPC2A)]$^+$ Parent Complex and Its Mixed Complexes. ($c_{[Sc(OPC2A)]}$ = 5 mM, T = 298 K, Estimated Uncertainties Are ± 2 ppm and ± 100 Hz, respectively.)

	[Sc(OPC2A)F]	[Sc(OPC2A)]$^+$	[Sc(OPC2A)(OH)]	[Sc(OPC2A)(OH)$_2$]$^-$
$\delta_{Sc,}$	49 ppm	63 ppm	83 ppm	135 ppm
$\nu_{1/2,}$	1700 Hz	2100 Hz	2000 Hz	700 Hz

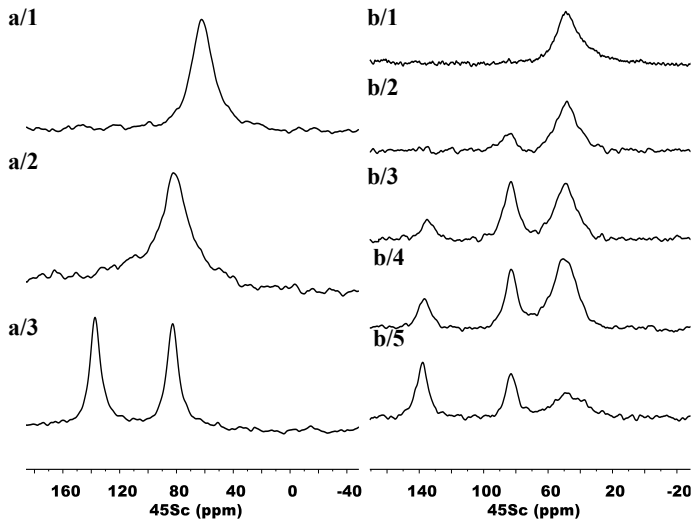

Figure 3. 121.2 MHz ^{45}Sc-NMR spectra recorded at different pH. **a/1**: [Sc(OPC2A)]$^+$ at pH = 4.15. **a/2**: time average signal of [Sc(OPC2A)]$^+$ / [Sc(OPC2A)(OH)] at pH = 7. **a/3**, [Sc(OPC2A)(OH)] and [Sc(OPC2A)(OH)$_2$]$^-$ at pH = 9.4, $c_{Sc(OPC2A)}$ = 5 mM. **b/1, 2, 3, 4,** and **5** show three peaks which belong to [Sc(OPC2A)F], [Sc(OPC2A)(OH)] and [Sc(OPC2A)(OH)$_2$]$^-$ at the pH = 5, 7, 8.3, 9, and 10 from top to bottom, $c_{[Sc(OPC2A)]}$ = 5 mM, c_F = 5 mM, T = 298 K, the chemical shifts are indicated in Table 6.

The ^{1}H NMR spectra of the Sc^{3+}-$OPC2A^{2-}$-H^{+} system are also in the "slow exchange regime" at 400 MHz (9.4 T), i.e., separate signals are observed for the free ligand and the $[Sc(OPC2A)]^{+}$ complex. The aliphatic region of the spectra is somewhat crowded, whereas the aromatic region is well resolved and simple, Figure 1. It shows a doublet corresponding to two *meta* positioned (2, 3) protons and a triplet signal of the proton *para* (1) to the N-atom of the pyridine ring in the ligand. The free ligand is clearly visible in the spectra recorded at high acid concentration, while the parent Sc(III) complex dominates at a lower acid content, in perfect agreement with the ^{45}Sc NMR results. The assignment of the ^{1}H NMR spectrum of the OPC2A ligand was reported in our earlier work,[76] while the ^{1}H-^{1}H and ^{1}H-^{13}C correlation spectra of $[Sc(OPC2A)]^{+}$, recorded at 500 MHz (11.75 T), are presented in Appendix Figure A.4 and Figure A.5.

Figure 4 shows the ^{1}H NMR spectra of the free ligand, the parent $[Sc(OPC2A)]^{+}$ complex and the [Sc(OPC2A)F] mixed fluoro complex. All three spectra exhibit sharp signals in the aromatic region (7.3–8.2 ppm), which are attributed to the pyridine ring in the ligand. The chemical shift values differ among the species, allowing for the straightforward identification of each component in mixtures containing multiple complexes. In the case of the free ligand and the mixed fluoro complex, broader signals are observed in the aliphatic region (2.5–5 ppm), suggesting intramolecular exchange processes (fluxionality). The assignments of $[Sc(OPC2A)]^{+}$ and [Sc(OPC2A)F] complexes using 1D and 2D NMR are presented in Figures A.3-A.11.

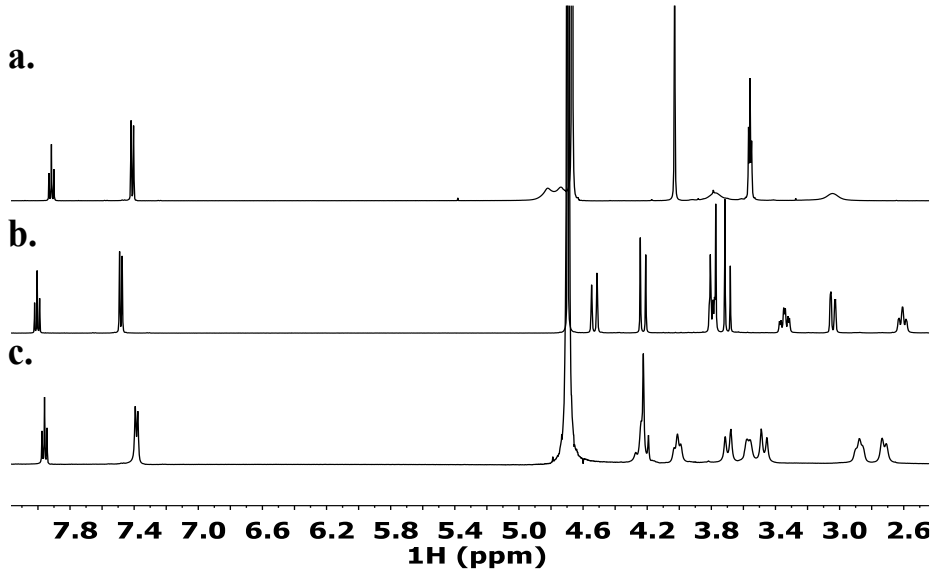

Figure 4. (a). 500 MHz ^{1}H-NMR spectra of H_2OPC2A ligand in D_2O pH = 5, **(b).** parent complex $[Sc(OPC2A)]^+$ pH = 4.75 and (**c).** ternary complex of [Sc(OPC2A)F] (c_{Sc} = 8.3 mM, c $_{OPC2A}$ = 8.3 mM, c_F = 8.3 mM, pH = 4.86, I = 0.15 M NaCl, T = 298 K).

4.1.3. Investigation of ScLF ternary complex

4.1.3.1. Investigation of [Sc(OPC2A)F] ternary complex

Considering the formation of the [Sc(OPC2A)(OH)] species from $[Sc(OPC2A)(H_2O)]^+$, the formation of the mixed fluoro complex can be predicted as follows, eqs 24 and 25:

$$[Sc(OPC2A)(H_2O)]^+ + F^- \rightleftharpoons [Sc(OPC2A)F] + H_2O \quad (24)$$

$$K_{[Sc(OPC2A)F]} = \frac{[Sc(OPC2A)F]}{[Sc(OPC2A)(H2O)^+][F^-]} \quad (25)$$

The $[Sc(OPC2A)]^+$ and [Sc(OPC2A)F] complexes were detected by ESI-MS in positive mode: m/z calculated for $[C_{15}H_{19}N_3O_5Sc]^+$ = 366.0878; found 366.088. m/z calculated for $[Sc(OPC2A)FNa]^+$, 408.0760; found

408.0762, $c_{[Sc(OPC2A)]} = c_F = 0.3$ mM, pH = 5.3, see Figure A 1. The equilibrium between $[Sc(OPC2A)]^+$ and F^- was studied by ^{19}F NMR. The mixed complex formed readily, giving an NMR signal at –39 ppm. The preliminary experiment using a sample containing equimolar concentrations ($c_{[Sc(OPC2A)]} = c_F = 5$ mM) of $[Sc(OPC2A)(H_2O)]^+$ and F^- at pH = 5 showed almost complete formation of the mixed complex, [Sc(OPC2A)F], suggesting a high stability.

In order to determine the stability constant, the competition reactions of [Sc(OPC2A)F] species with the hydroxide anion were followed by ^{19}F NMR spectroscopy. The reactions defined by eqs 24 and 25 represent competing equilibria in the pH range of 5-9. The pH-dependence of ^{19}F NMR spectra can be seen in Figure 14. The ratio of signal intensities corresponding to free and bound fluoride can be measured directly. The stability constant of the ternary fluoro complex is found to be $\log K_{[Sc(OPC2A)F]} = 4.54(8)$, using 5 mM samples without a buffer and $\log K_{[Sc(OPC2A)F]} = 4.21(2)$ using 3 mM samples in the presence of buffers. The anion of a buffer may compete with the ligand, leading to a decrease in the conditional stability of the mixed complex. A mixed acetate complex, Na[Sc(NOTA)Ac], has previously been reported in the solid state and also characterized in solution.[85] The stability constant of the mixed fluoro complex was calculated by using the PSEQUAD software. The validity of the model is demonstrated in Figure 5, showing the good agreement between the calculated distribution curves and the measured concentrations of the [Sc(OPC2A)F] and F^- species by ^{19}F NMR.

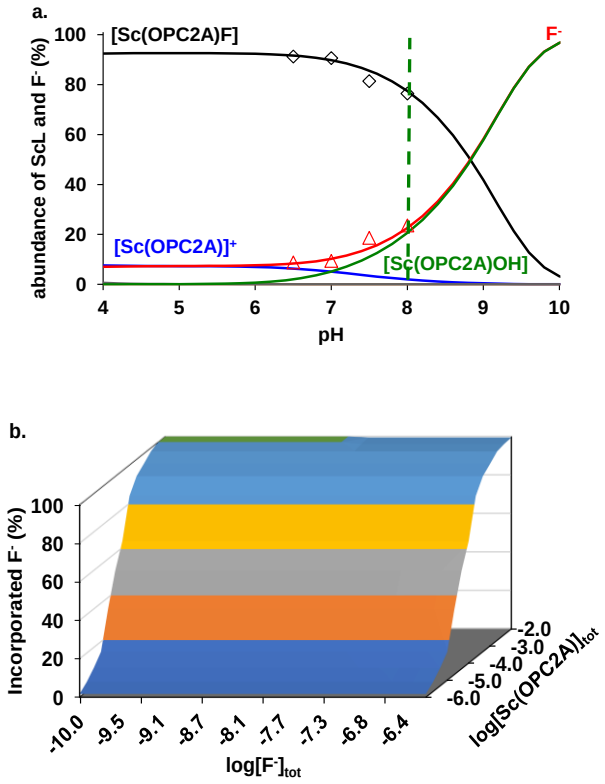

Figure 5 . a) Species distribution curves calculated (lines) and measured concentration (symbols) of [Sc(OPC2A)F] and free F^-, determined by ^{19}F NMR spectroscopy. ($c_{[Sc(OPC2A)]} = c_F$ = 5 mM, I = 0.15 M NaCl, T = 298 K), **b)** amount of the incorporated F^- ion by the [Sc(OPC2A)F] ternary complex as a function of $[F^-]$tot and $[Sc(OPC2A)]_{tot}$ at pH = 7.0.

The value of $\log K_{[Sc(OPC2A)F]}$ = 4.54(8) indicates a remarkably strong interaction. However, the stability of the mixed complex is not high enough to avoid the dissociation of fluoride in dilute solutions relevant to the radiochemical or PET-imaging conditions. Figure 5 shows that at $[Sc(OPC2A)^+]_{tot} = 10^{-6}$ M the dissociation of [Sc(OPC2A)F] is complete; $[Sc(OPC2A)^+]_{tot} = 10^{-3}$ M is needed for >95% incorporation of the F^- ion by [Sc(OPC2A)F] species. This limitation is further discussed in the

"Fluoride Exchange Kinetics of [Sc(OPC2A)F]" section. Similar mixed-ligand complexes have long been known for metal-APC systems. For example, $[Ln(EDTA)F]^{2-}$complexes have been detected across the entire lanthanide (Ln) series, with $\log K_{[Ln(EDTA)F]}$ values ranging 1.0–1.8 for La^{3+} to Lu^{3+}.[86] More recently, weak ternary fluoro species of Gd(III) and Y(III) based APCs (APC: EGTA and OBETA) have also been reported.[87] Unfortunately, several recent studies on [Sc(APC)F],[88] or [Ga(APC)F] complexes,[89] which use these species as ^{18}F-binding agents, do not provide thermodynamic stability data. A similar lack of such data is evidenced for [Al(APC)F] complexes proposed as fluoride carriers for PET imaging applications.[9,90] However, the $[Al(EDTA)F]^{2-}$ complex is known to be quite stable, $\log K_{[Al(EDTA)F]} = 4.63$, and it is also notably inert with respect to fluoride ligand exchange.[91,92] It is worth noting that $[Al(EDTA)F]^{2-}$ is formed from two anionic species, whereas [Sc(OPC2A)F] is formed from a cationic complex and the negatively charged fluoride ion, and yet the stability constants of these complexes are still very close.

4.1.3.2. Investigation of [Sc(PC2AAM^{nBu})X] ternary complex (where X= OH^- or F^-)

In addition, we used $PC2AAM^{nBu}$, a heptadentate ligand with an amide pendant arm and exhibiting higher basicity than the hexadentate OPC2A ligand, to study the ScLF system for comparison and to evaluate the effect of structural rigidity on ternary complex formation. A pH-potentiometric titration was performed to investigate the acid–base properties of the $[Sc(PC2AAM^{nBu})]^+$ complex. Within the investigated pH range of 1.52 to 12.0, the resulting titration curve using PSEQUAD software, showed no evidence of mixed hydroxo species such as $[Sc(PC2AAM^{nBu})(OH)]$. Attempts to detect $[HSc(PC2AAM^{nBu})]^{2+}$ were also unsuccessful.

One could be surprised, that the $[Sc(PC2AAM^{nBu})]^+$ complex (supposed to be 6 or 7 coordinated by the 6 or 7 dentate organic ligand, considering the weekly coordinating bulky amide group) does not contain a water molecule coordinated to Sc(III) at which deprotonation could occur, although $Sc(aq)^{3+}$ is known as 8 coordinated.[20] To confirm the absence of the mixed hydroxo species, we performed ^{45}Sc NMR measurements to further characterize the complex. In accordance with the pH-potentiometry, only one ^{45}Sc-NMR signal contributed to the $[Sc(PC2AAM^{nBu})]^+$ complex was detected at 92 ppm in the pH range of 3-9, i.e. ^{45}Sc-NMR spectra showed clearly that the formation of $[Sc(PC2AAM^{nBu})(OH)]$ was negligible until pH = 9, Figure 6. No change of ^{1}H NMR spectra of the same samples was found supporting the absence of mixed hydroxo complex in the system.

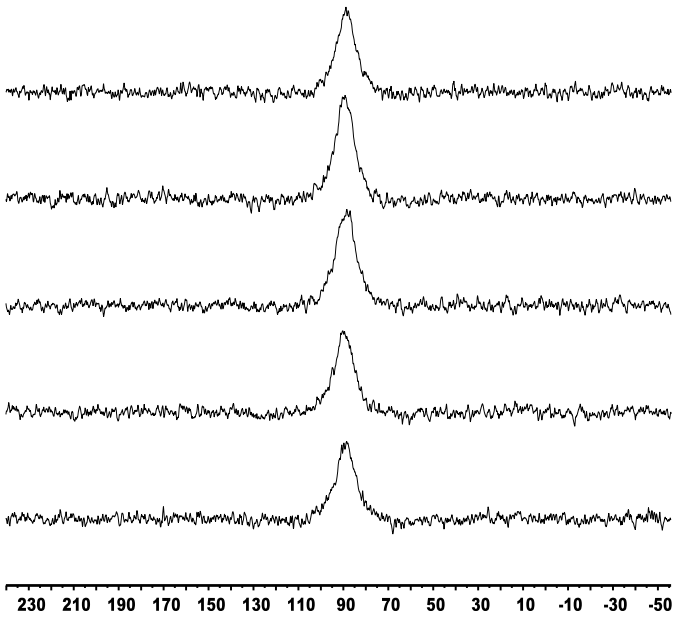

Figure 6. 97.199 MHz ^{45}Sc-NMR spectra of $[Sc(PC2AAM^{nBu})]^+$ at different pH (3.12, 5.5, 7.0, 8.0 and 9.0; from top to bottom; $c_{Sc} = c_L = 3$ mM, 0.15 M NaCl, 298 K).

Although the $[Sc(PC2AAM^{nBu})]^+$ cation seems to be „saturated", i.e. it does not form mixed hydroxo complex as it lacks coordinated water molecule, we have explored its interaction with fluoride ion using ^{19}F NMR spectroscopy. As it can be seen in Figure 7 a new signal appears at -31 ppm during the titration of a 5 mM solution of $[Sc(PC2AAM^{nBu})]^+$ at pH = 5.2. The formation of the ternary $[Sc(PC2AAM^{nBu})(F)]$ complex can be followed by ^1H-NMR, as two sets of signals ($\Delta\delta$ ~20 Hz) indicate slow exchange regime on the ^1H NMR time scale. Measuring the intensities of the free and bound fluoride signals, the stability constant, eq 27, of the $[Sc(PC2AAM^{nBu})(F)]$ complex can be calculated.

$$[Sc(PC2AAM^{nBu})]^+ + F^- \rightleftharpoons [Sc(PC2AAM^{nBu})(F)] \qquad (26)$$

$$K_{[Sc(PC2AAM^{nBu})(F)]} = \frac{[Sc(PC2AAM^{nBu})(F)]}{[Sc(PC2AAM^{nBu})^+][F^-]} \qquad (27)$$

The log $K_{[Sc(PC2AAM^{nBu})(F)]} = 2.5(1)$ indicates substantial strong interaction between the Sc(III) macrocyclic complex cation and the fluoride anion, and it is likely based on the replacement of one carboxylate (or amide) group of the ligand with fluoride. The ^{45}Sc NMR chemical shift of the reasonably (ca 100 Hz) broad signals of the parent and mixed fluoro complexes are 90±10 pm and 65±15 ppm.

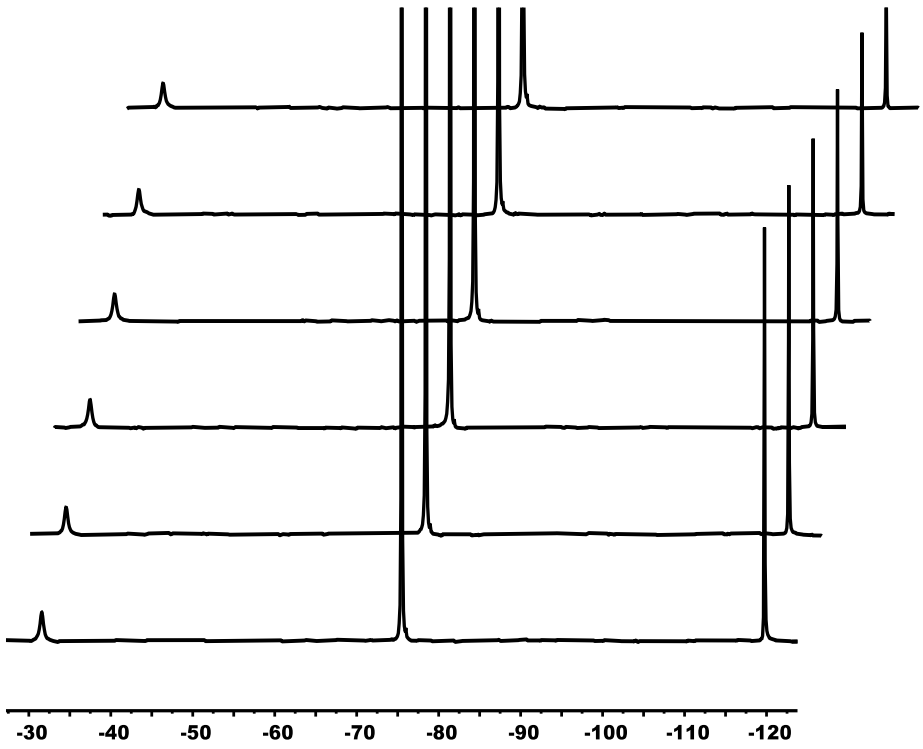

Figure 7. 376.4 MHz ^{19}F NMR spectra of 5 mM [Sc(PC2AAM^{nBu})(F)] at different concentration of added NaF (c_{NaF} = 10, 9, 8, 7,6 and 5 mM from the top to bottom). Chemical shift values: -31 ppm, [Sc(PC2AAM^{nBu})(F)] and -120 ppm, free F^-; -75 ppm (TFA impurity), pH = 5.2, *I* = 0.15 M NaCl, 298K.

4.2. Kinetic Studies

4.2.1. Formation of [Sc(OPC2A)]$^+$ Complex

The formation of metal ion–macrocyclic APC complexes is often slow, and the mechanism typically proceeds through the rapid equilibrium formation of a protonated intermediate. This long lived intermediate then undergoes consecutive deprotonation and structural rearrangement to yield the final product in the rate-determining step.[93,94] During the

equilibrium study, ″slow formation kinetics” of $[Sc(OPC2A)]^+$ has been evidenced by ^{45}Sc NMR at low pH. The OPC2A ligand has a strong absorption in the UV range, which can be assigned to the pyridine-ring in the ligand backbone. The complex formation of $[Sc(OPC2A)]^+$ can be followed by spectrophotometry, and the spectral changes are shown in Figure 8. Two isosbestic points are observed (at 225 and 260 nm), and the absorption band, or “shoulder”, at 275 nm is associated with the formation of the $[Sc(OPC2A)]^+$ complex. This wavelength is suitable for monitoring the time course of the reaction.

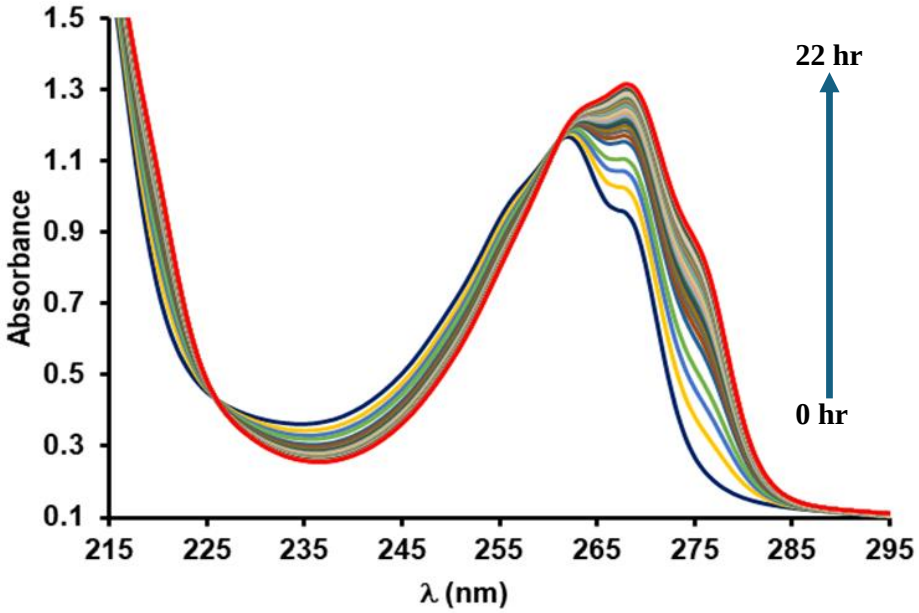

Figure 8. Spectral changes observed during the formation of $[Sc(OPC2A)]^+$. The blue line is the spectrum of the free ligand, while the red trace is the spectrum of $[Sc(OPC2A)]^+$. Intermediate spectra recorded in a cc. 22 h interval are shown by different colours ($c_{Sc} = c_{OPC2A} = 0.25$ mM, pH = 2.8, l = 1 cm).

The kinetic studies on the formation of $[Sc(OPC2A)]^+$ were performed in the presence of excess Sc(III) under pseudo-first-order conditions. The concentrations of Sc(III) were 5-50 times higher than those of the OPC2A ligand (c_{OPC2A} = 0.1 mM) and under these conditions the rate of complex formation can be expressed by eq 28:

$$\frac{d[Sc(OPC2A)^+]_t}{dt} = k_{obs}[OPC2A]_t \qquad (28)$$

where $[Sc(OPC2A)^+]_t$ was the concentration of the complex formed, $[OPC2A^{2-}]_t$ was the total concentration of the ligand at a given time point and k_{obs} was a pseudo-first-order rate constant, Figure 9. The formation reactions were studied by varying the metal ion concentration in the pH range of 1.9–3.8. Under these experimental conditions, hydrolysis of the Sc(III) ion may occur, resulting in the formation of $[Sc(OH)]^{2+}$, $[Sc(OH)_2]^+$, $[Sc(OH)_3]$, $[Sc(OH)_4]^-$, $[Sc_2(OH)_2]^{4+}$ and $[Sc_3(OH)_5]^{3+}$ species; i.e. OH^- ions might compete with the $OPC2A^{2-}$ for the Sc(III) ions. Since Sc(III) ion was applied in large excess, the concentration of free Sc(III) could be calculated using the known hydrolysis constants of Sc(III) ($\log\beta_{Sc(OH)} = -4.3$, $\log\beta_{Sc(OH)2} = -9.3$, $\log\beta_{Sc(OH)3} = -16.1$, $\log\beta_{Sc(OH)4} = -26.0$, $\log\beta_{Sc2(OH)2} = -6.0$, $\log\beta_{Sc3(OH)5} = -16.34$).[17] The concentration data of the samples are summarized in Table 5 (the absorbance vs. time traces were fitted by single exponential function returning the k_{obs}). The k_{obs} vs. [Sc(III)] data in Figure 9 show saturation profiles indicating the formation of the $*[Sc(H_2OPC2A)]^{3+}$ intermediate.

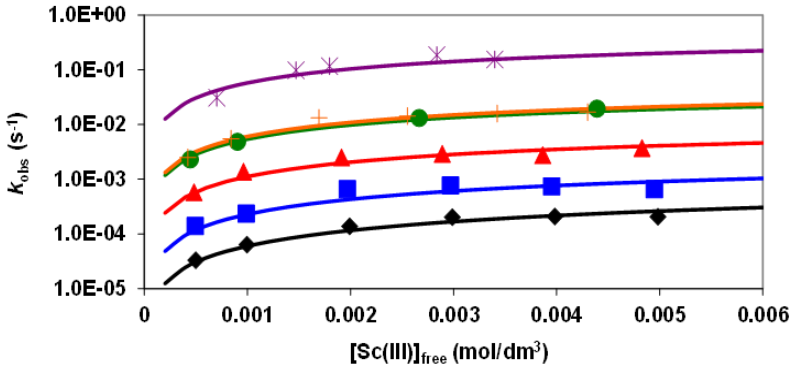

Figure 9. k_{obs} pseudo-first-order rate constants characterizing the formation of $[Sc(OPC2A)]^+$ as a function of $[Sc(III)]_{free}$ at various pH values. ([OPC2A] = 0.1 mM, $[ClCH_2CO_2H]$ = 10 mM, pH = 1.90 (♦), 2.40 (■), 2.90 (▲), 3.40 (●) 3.50 (+) and 3.85 (∗), 0.15 M NaCl, T = 298 K.)

The stability constant of this intermediate is defined by eqs 29 and 30:

$$Sc^{3+} + H_2OPC2A \rightleftharpoons {}^*[Sc(H_2OPC2A)]^{3+} \qquad (29)$$

$${}^*K_{[Sc(H_2OPC2A)^+]} = \frac{[{}^*Sc(H_2OPC2A)^{3+}]}{[Sc^{3+}][H_2OPC2A]} \qquad (30)$$

where $[{}^*Sc(H_2OPC2A)^{3+}]$ denotes the concentration of the intermediate and $[H_2OPC2A]$ is the concentration of the ligand. The ${}^*K_{[Sc(H2OPC2A)]}$ is relatively low, thus the k_{obs} values obtained even at high excess metal ion do not approach saturation. The rate-determining steps of the reaction are the deprotonation and rearrangement of the intermediate. This means the incorporation of the Sc(III) ion into the macrocyclic cage:

$$\frac{d[Sc(OPC2A)^+]_t}{dt} = k_{obs}[OPC2A^{2-}]_t = k_f[{}^*Sc(H_2OPC2A)^{3+}] \qquad (31)$$

where k_f is the rate constant characterizing the deprotonation and rearrangement of the intermediate to the $[Sc(OPC2A)]^+$ complex. By considering the protonation constants of OPC2A (Table 3) and the stability constant of $*[Sc(H_2OPC2A)]^{3+}$ intermediate, eqs 30 and 31, the pseudo-first order rate constant can be expressed by eq 32:

$$k_{obs} = \frac{k_f * K_{[Sc(H_2OPC2A)]} K_1^H K_2^H [Sc^{3+}][H^+]^2}{\alpha_H + * K_{[Sc(H_2OPC2A)]} K_1^H K_2^H [Sc^{3+}][H^+]^2} \qquad (32)$$

where $a_H = 1 + K_1^H[H^+] + K_1^H K_2^H[H^+]^2 + K_1^H K_2^H K_3^H[H^+]^3$. The stability constant of the $*[Sc(H_2OPC2A)]^{3+}$ intermediate and the k_f rate constants have been calculated by fitting the pseudo-first-order rate constants obtained at various pH and $[Sc(III)]_{free}$ values to eq 32. The obtained stability constant is reported in Table 7. The k_f rate constants for the formation of $[Sc(OPC2A)]^+$ complex is presented in Figure 10 as a function of $[OH^-]$. The kinetic data indicates that the k_f values increase with the increase of $[OH^-]$.

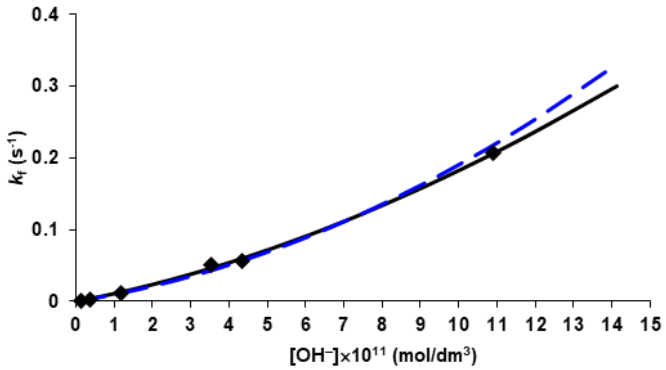

Figure 10. k_f pseudo-first-order rate constants characterizing the transformation of the $*[Sc(H_2OPC2A)]^{3+}$ intermediate as a function of $[OH^-]$ (0.15 M NaCl, T = 298 K). The solid black line and the filled symbols represent the calculated and the experimental k_f values,

respectively. The dashed blue line indicate the calculated k_f values obtained by assuming an alternative formation mechanism of $[Sc(OPC2A)]^+$.

Alternatively, the dependence of the k_f values on the OH^- (Figure 10) can also be interpreted by the H_2O (k_{H2O}) or OH^- assisted (k_{OH} and k_{OH}^2) deprotonation of the $*[Sc(H_2OPC2A)]^{3+}$ intermediate and rearrangement to the final $[Sc(OPC2A)]^+$ complex eq 33.

$$\frac{d[Sc(OPC2A)]}{dt} = k_f[{}^*Sc(H_2OPC2A)]_t = {}^{[Sc(H2OPC2A)]}k_{H_2O}[{}^*Sc(H_2OPC2A)] + {}^{[Sc(H2OPC2A)]}k_{OH}[{}^*Sc(H_2OPC2A)][OH^-] + {}^{[Sc(H2OPC2A)]}k_{OH^2}[{}^*Sc(H_2OPC2A)][OH^-]^2 \quad (33)$$

By considering the total concentration of intermediates $[*Sc(H_2OPC2A)]_t = [*Sc(H_2OPC2A)]$, and the ionic product of water (K_w), the k_f rate constant can be expressed by eq 34.

$$k_f = {}^{[Sc(H2OPC2A)]}k_{H_2O} + \frac{{}^{[Sc(H2OPC2A)]}k_{OH}K_W}{[H^+]} + {}^{[Sc(H2OPC2A)]}k_{OH^2}\left(\frac{K_W}{[H^+]}\right)^2 \quad (34)$$

eq. (34) was used for the fitting of the k_f values (blue dashed line in Figure 10) to determine the ${}^{[Sc(H2OPC2A)]}k_{H2O}$, ${}^{[Sc(H2OPC2A)]}k_{OH}$ and ${}^{[Sc(H2OPC2A)]}k_{OH}^2$ rate constants ${}^{[(Sc(H2OPC2A)]}k_{H2O} = (5 \pm 5) \times 10^{-4}$ s^{-1}; ${}^{[Sc(H2OPC2A)]}k_{OH} = (8 \pm 2) \times 10^8$ $M^{-1}s^{-1}$ and ${}^{[Sc(H2OPC2A)]}k_{OH}^2 = (1.0 \pm 0.1) \times 10^{19}$ $M^{-2}s^{-1}$). However, the fitting process results in an unrealistic ${}^{[Sc(H2OPC2A)]}k_{OH}^2$ value due to the inappropriate model of formation mechanism of the $[Sc(OPC2A)]^+$

complex. Based on this evidence, it can be assumed that the formation mechanism includes the deprotonation and rearrangement of the kinetically active monoprotonated *[Sc(HOPC2A)]$^{2+}$ intermediate to the final complex in the rate determining step.

According to the reaction mechanism proposed for the formation of [M(DOTA)]$^{-}$ complexes, [93,95] the mono- and di-protonated intermediates exist in equilibrium. The dependence of the k_f values on the [OH^{-}] can be interpreted by the formation of the kinetically active monoprotonated *[Sc(HOPC2A)]$^{2+}$ intermediate through the dissociation of the diprotonated *[Sc(H$_2$OPC2A)]$^{3+}$ intermediate in an equilibrium characterized with the ${}^{*}K^{H}_{[Sc(HOPC2A)]}K^{H}_{{}^{*}M(HL)}$ protonation constant, eq 36.

The rate-controlling step of complex formation involves the H_2O or OH^{-} assisted deprotonation and rearrangement of the monoprotonated *[Sc(HOPC2A)]$^{2+}$ intermediate to the final [Sc(OPC2A)]$^{+}$ complex, see Scheme 3.

$$*[Sc(HOPC2A)]^{2+} + H^{+} \rightleftharpoons *[Sc(H_2OPC2A)]^{3+} \qquad (35)$$

$${}^{*}K^{H}_{[Sc(HOPC2A)]} = \frac{[Sc(H_2OPC2A)^{3+}]}{[\ {}^{*}Sc(HOPC2A)^{2+}][H^{+}]} \qquad (36)$$

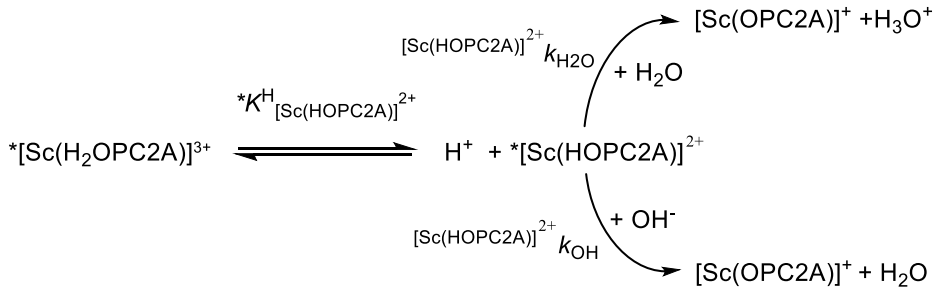

Scheme 3. Formation mechanism of the [Sc(OPC2A)]$^{+}$ complex.

According to the proposed reaction mechanism, the formation rate of the $[Sc(OPC2A)]^+$ complex can be given by eq 37:

$$\frac{d[Sc(OPC2A)^+]}{dt} = k_f[{}^*Sc(H_2OPC2A)^{3+}]_t = {}^{[Sc(HOPC2A)]2+}k_{H_2O}[{}^*Sc(OPC2A)^{2+}] + {}^{[Sc(HOPC2A)]2+}k_{OH}[{}^*Sc(HOPC2A)^{2+}][OH^-] \quad (37)$$

By considering the total concentration of intermediates $[{}^*Sc(H_2OPC2A)^{3+}]_t = [{}^*Sc(HOPC2A)^{2+}] + [{}^*Sc(H_2OPC2A)^{3+}]$, the definition of ${}^*K^H_{[Sc(HOPC2A)]}$ protonation constant eq 36 and the ionic product of water (K_w), the k_f rate constant can be expressed by eq 38

$$k_f = \frac{{}^{[Sc(HOPC2A)]+}k_{H_2O} + {}^{[Sc(HOPC2A)]+}k_{OH}K_W/[H^+]}{1 + {}^*K^H_{[Sc(HOPC2A)]+}[H^+]} \quad (38)$$

Eq 38 is used for the fitting of the k_f values, Figure 10, to determine the ${}^{[Sc(HOPC2A)]}k_{H2O}$ and ${}^{[Sc(HOPC2A)]}k_{OH}$ rate constants and the ${}^*K^H_{[Sc(HOPC2A)]}$ protonation constant. These constants are shown and compared with the related rate and equilibrium constants for the formation of $[Ce(DO2A)]^+$ and $[Yb(DO2A)]^+$ in Table 7.

Table 7. Rate (k_i) and Equilibrium Constants (K_i) Characterizing the Formation of $[Sc(OPC2A)]^+$ and $[Ln(DO2A)]^+$ Complexes (T = 298 K).

	$[Sc(OPC2A)]^+$	$[Ce(DO2A)]^+$ [96]	$[Yb(DO2A)]^+$ [96]
I	0.15 M NaCl	1.0 M KCl	
k_{H2O} (s^{-1})	1.0 ± 0.1	1.28	1.08
k_{OH} ($M^{-1}s^{-1}$)	$(1.0 \pm 0.3) \times 10^{10}$	2.8×10^5	2.5×10^5
$\log {}^*K^H_{M(HL)}$	4.8 (1)	$K^H_{M(HL)} \gg K_2^H/10$	
$\log K_{*M(H2L)}$	2.1 (1)	1.98	1.60

The comparison of the rate (k_i) and equilibrium constants (K_i) characterizing the formation of $[Sc(OPC2A)]^+$ and $[Ln(DO2A)]^+$ complexes reveals that the stability constants of the diprotonated intermediates ($\log K_{*[Sc(H_2OPC2A)]}$) are significantly lower than that of *[Ln(H_2DOTA)] intermediates ($\log K_{*[Ln(H_2L)]}$ = 4.2–4.5),[93] due to the coordination of the metal ions by only two carboxylate groups of $OPC2A^{2-}$. The k_{H2O} rate constants for the H_2O assisted deprotonation and rearrangement of the monoprotonated $*[Sc(HOPC2A)]^{2+}$ and $*[Ln(HDO2A)]^{2+}$ intermediates to the final $[Sc(OPC2A)]^+$ and $[Ln(DO2A)]^+$ complexes are very similar. Surprisingly, the OH^- catalyzed deprotonation and rearrangement of the monoprotonated $*[Sc(HOPC2A)]^{2+}$ intermediate (k_{OH}) is about 5 orders of magnitude higher than those of $*[Ln(HDO2A)]^{2+}$. Based on the k_{OH} value (Table 7), it seems that the OH^- assisted deprotonation of the $*[Sc(HOPC2A)]^{2+}$ intermediate takes place by diffusion control. Detailed kinetic studies on the formation reactions of $[Ga(DOTA)]^-$ reveal that the OH^- catalyzed deprotonation and the rearrangement of the *[Ga(HDOTA)] intermediate is also significantly faster than those of *[Ln(HDOTA)] showing the diffusion control of the reactions ($k_{OH} = 1.3 \times 10^{11}$ $M^{-1}s^{-1}$).[94] Considering the hydrolytic properties of Sc(III) and Ga(III) ions,[17] it might be assumed that the partial hydrolysis of Sc(III) and Ga(III) ions results in the formation of mixed ligand $*[Sc(HOPC2A)(OH)]^+$ and $*[Ga(HDOTA)(OH)]^-$ intermediates, which might deprotonate/ rearrange very rapidly in an intramolecular process.

4.2.2. Acid assisted dissociation of the $[Sc(OPC2A)]^+$ complex

The dissociation rate of $[Sc(OPC2A)]^+$ has been investigated to assess its inertness. The inertness, often termed to as ″kinetic stability" in the medical literature, is a key parameter for the safety and effectiveness of metal complexes intended for *in vivo* human applications. A suitably inert metal complex remains intact in the human body until it is fully excreted. The potential driving forces behind the decomposition include: *a)* essential metal ions present in biological fluids (Cu(II), Zn(II), Ca(II), Mg(II) etc.) which may induce metal-exchange (transmetalation) reactions; *b)* multidentate organic ligands that promote ligand exchange (transchelation) reactions; *c)* small anions (carbonate, phosphate, hydroxide etc.) that can act as catalyst or participate in the formation of sparingly soluble salts. The macrocyclic complexes are known to be more inert as compared to the complexes of open chain ligands. In many cases, the decomposition of MC-complexes proceeds via proton-assisted dissociation.[1]

Our experiments have been carried out by UV-vis spectrophotometry in strong acid solutions. Preprepared 0.25 mM samples of $[Sc(OPC2A)]^+$ have been mixed with HCl solution adjusting the c_{HCl} to 0.10 – 1.00 M and the spectral change have been followed at λ = 275 nm. An ionic medium of I = 1.5 M NaCl/HCl was used because of the high acid content required for this series of experiments. The pseudo-first-order rate constants (k_{obs}) were obtained by fitting a mono-exponential model to the primary kinetic traces of absorbance vs time. Representative experimental data along with the fitted curve used to determine the k_{obs} data are shown in Figure 11.

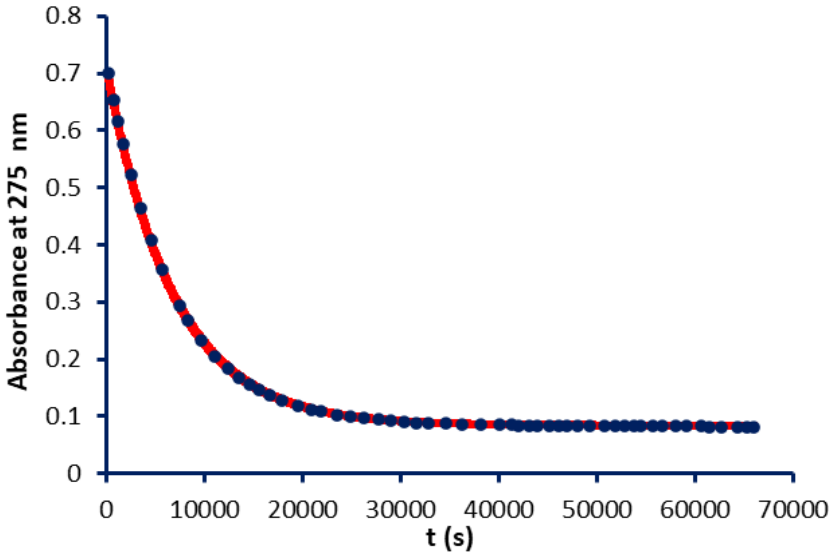

Figure 11 . Absorbance values of $[Sc(OPC2A)]^{+}$ as a function of time in 0.5 M HCl solution (c_{H+} = 0.5 M , c_{OPC2A} = 0.25 mM, c_{Sc} = 0.25M, I = 1M NaCl, l = 1cm, T = 298 K. (● symbol represents the experimental value while, the solid line — correspond to the fitted data, k_{obs}= 1.47×10^{-4} s^{-1}.)

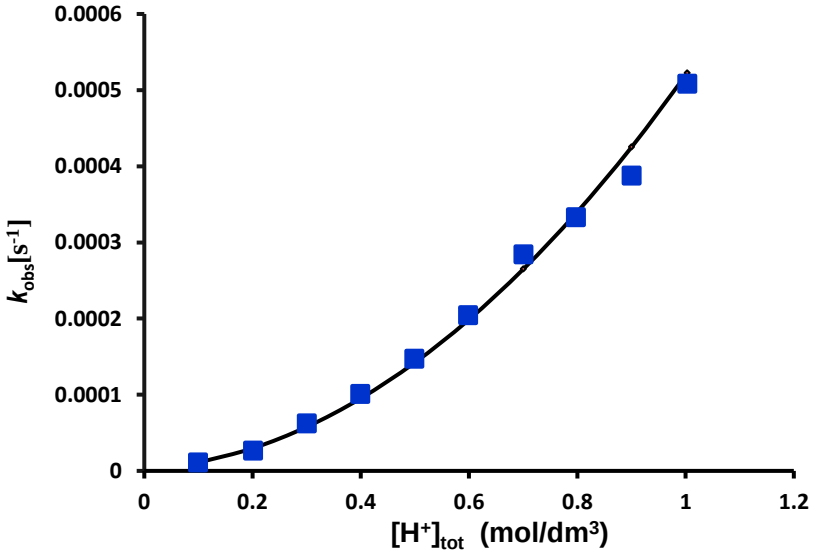

Figure 12. Pseudo-first-order rate constants (k_{obs}) plotted as a function of $[H^+]_{tot}$ for the dissociation of $[Sc(OPC2A)]^{+}$ (I = 1.5 M HCl/NaCl, $c_{[Sc(OPC2A)]}$ = 0.25 mM, and T = 298 K).

The k_{obs} vs. $[H^+]_{tot}$ curve is shown in Figure 12. The k_{obs} values increase with the first- and second-order function of $[H^+]$, which can be expressed as follows:

$$k_{obs} = k_0 + k_1[H^+] + k_2 [H^+]^2 \qquad (39)$$

where $k_0 = 0\ s^{-1}$, $k_1 = (6.2 \pm 0.5) \times 10^{-5}\ M^{-1}s^{-1}$ and $(4.6 \pm 0.2) \times 10^{-4}\ M^{-2}s^{-1}$. The $k_0 = 0\ s^{-1}$ does not mean the total absence of the spontaneous or water assisted dissociation, rather it indicates a negligible contribution to the dominating proton assisted dissociation. The contribution of reaction path with the k_2 rate constant to the decomplexation is dominant at high acid concentrations. These rate constant values (Table 8) indicate very good inertness compared to the $[Sc(AAZTA)]^-$ (k_1 = 0.1 $M^{-1}s^{-1}$), and it approaches the inertness of $[Sc(DOTA)]^-$ ($k_1 = 6 \times 10^{-6}\ M^{-1}s^{-1}$). One can calculate the dissociation half-life using the rate eq 39 for 1 M HCl ($t_{1/2}$ = ln2/k_{obs} = 0.693/ $5.22 \times 10^{-4}\ s^{-1}$ = 1329 s = 0.37 h. It is ca. 2.5 order of magnitude shorter compared to $[Sc(DOTA)]^-$,[8] $t_{1/2}$ = 44.9 h, but much longer than the $t_{1/2}$ = 6.9 s = 0.0019 hours of $[Sc(AAZTA)]^-$.[30]

Table 8. Dissociation Rate Constants and the Calculated Half-Lives of $[Sc(OPC2A)]^+$, $[Sc(DOTA)]^-$, and $[Sc(AAZTA)]^-$ in 1 M HCl.

	$[Sc(OPC2A)]^+$	$[Sc(AAZTA)]^-$ [30]	$[Sc(DOTA)]^-$ [8]
k^0 (s^{-1})	–	2×10^{-11}	–
k_1 ($M^{-1}s^{-1}$)	**$(6.23 \pm 0.5) \times 10^{-5}$**	0.1	6×10^{-6}
k_2 ($M^{-2}s^{-1}$)	**$(4.58 \pm 0.18) \times 10^{-4}$**	–	
$t_{1/2}$ (h) (in 1 M HCl)	**0.37**	0.0019	44.9

If we calculate the $t_{1/2}$ value at pH = 7.4 of the blood plasma based only on the acid catalyzed reactions, $k_{obs} = 2.48 \times 10^{-12}$ s ($t_{1/2} = \ln 2/k_{obs} = 0.693/2.48 \times 10^{-12} = 2.79 \times 10^{11}$ s = 7.75×10^{7} hours) we obtain ca. 8840 years. In order to screen the inertness experimentally at higher pH, i.e. in neutral or alkaline pH range, we have prepared samples by adding a 10-fold excess of nitrilotriacetate (NTA) ligand to the solution of $[Sc(OPC2A)]^{+}$. NTA forms quite stable $[Sc(NTA)_2]^{3-}$ complexes in the pH range of 4–10, providing a strong thermodynamic driving force for a ligand exchange reaction.[97] However, attempts to detect any exchange reaction by UV-vis spectrophotometry were unsuccessful, as no spectral changes were observed over 2 weeks. Similar lack of spectral change was observed even at pH = 11, where the hydroxo-complexes could also be formed in equilibrium. These findings support the outstanding inertness of $[Sc(OPC2A)]^{+}$ against decomposition at physiological pH (7.4), which is highly relevant for potential *in vivo* applications.

4.2.3. Fluoride exchange kinetics of [Sc(L)F] system

4.2.3.1. F^{-}exchange of [Sc(OPC2A)F]

In most medically oriented publications, ^{18}F-binding metal complexes are described as adducts formed between MF^{2+} species (e.g., AlF^{2+} or GaF^{2+}) and an organic ligand (often a cyclic APC). However, the interaction between the metal ion and fluoride is better understood as an equilibrium process in solution, which can be characterized by a stability constant: K_{MF} = [MF]/([M][F]) (the charges are omitted for the sake of clarity). The "hard–soft" classification of metal ions is based on their characteristic stabilities, with typical hard metal centers such as Al^{3+}, Sc^{3+}, and Zr^{4+} forming stable MF complexes with $\log K_{MF}$ = 6.5, 6.2, and 7.5 respectively.[98] In the presence of an organic ligand, the ternary species can

be regarded as an MLF mixed complex, whose stability is described by the constant K_{MLF} = [MLF]/([ML][F]). It is expected that logK_{MLF} – logK_{MF} < 0, meaning that the MF complex is generally more stable than the corresponding M(L)F species. In our case, the difference is –1.7, indicating that the stability of the mixed complex is approximately 1.7 orders of magnitude lower than that of the parent ScF^{2+} complex. This decrease in stability can be rationalized by considering the influence of the organic ligand, through both electronic and steric effects. The extent of this destabilization can vary depending on the ligand's denticity, donor atoms, and structural features. However, in general, it is unlikely that a mixed-ligand complex would be more stable than the parent MF complex. The best available literature data report logK_{MF} in the range of 5-7,[99] meaning that a maximum logK_{MLF} of around 4–5 can be realistically achieved. What are the implications of this limitation? At very low concentrations, typical for radiopharmaceuticals in body fluids (10^{-8}–10^{-10} M), such complexes would be expected to dissociate according to the principles of thermodynamics, leading to a loss of selectivity associated with the mixed complex. However, if decomposition does not occur, as observed for several ($Al^{18}F$)-ligand systems used in PET imaging,[11] the only plausible explanation is that the complexes exhibit significant inertness, preventing substantial dissociation during the time of PET- examination.

In the following section, we discuss our results on the ligand exchange dynamics of the [Sc(OPC2A)F] complex. Referring to the discussion above, given the high inertness of $[Sc(OPC2A)]^+$, we consider this species to be an intact entity. There are two F^- containing species, namely the free

F^- and the [Sc(OPC2A)F] mixed complex. ^{19}F NMR is able to detect the following mutual chemical exchange process:

$$[Sc(OPC2A)F] + *F^- \rightleftharpoons [Sc(OPC2A)*F] + F^- \qquad (40)$$

where* is used to differentiate the entering and leaving F^- anions. This particular reaction does not lead to any net change. In other words, the system is at equilibrium ($\Delta G = 0$), and the standard reaction free energy is also zero ($\Delta_r G^0 = 0$), since $\Delta_r G^0 = 0 = -RT\ln K$ and $K = 1$. The rates of this exchange reaction from left to right and *vice versa* are obviously identical. It is important to note that our considerations are strictly valid when the concentration of $[Sc(OPC2A)]^+$ is negligible. Typical ^{19}F NMR spectra are shown at different F^- concentrations in Figure 13.

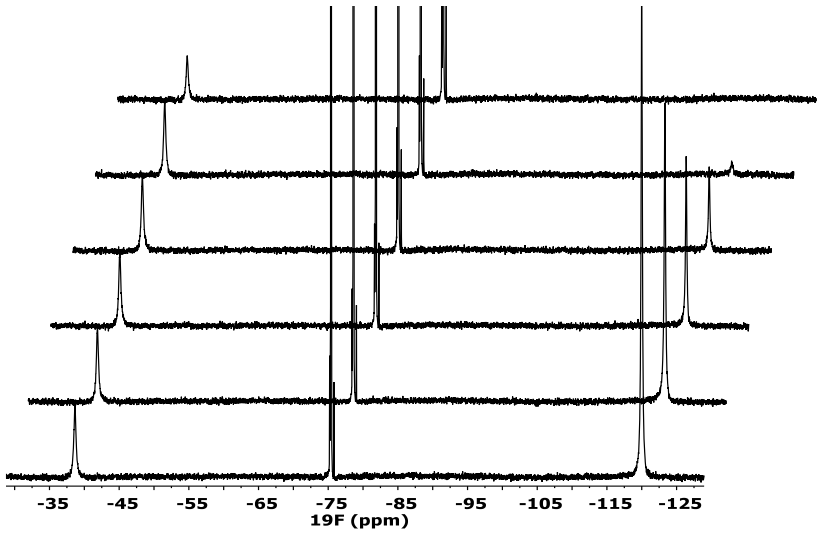

Figure 13 . 470.45 MHz ^{19}F NMR spectra (pH = 4.85, I = 0.15 M NaCl, T = 298 K) of a 5 mM solution of $[Sc(OPC2A)]^+$ at different concentration of added NaF (c_{NaF} = 2.5, 5, 7.5, 10, 20 and 30 mM) from top to bottom. Chemical shift values: –39 ppm, [Sc(OPC2A)F]; –120 ppm, free F^-; –75 ppm, TFA impurity.

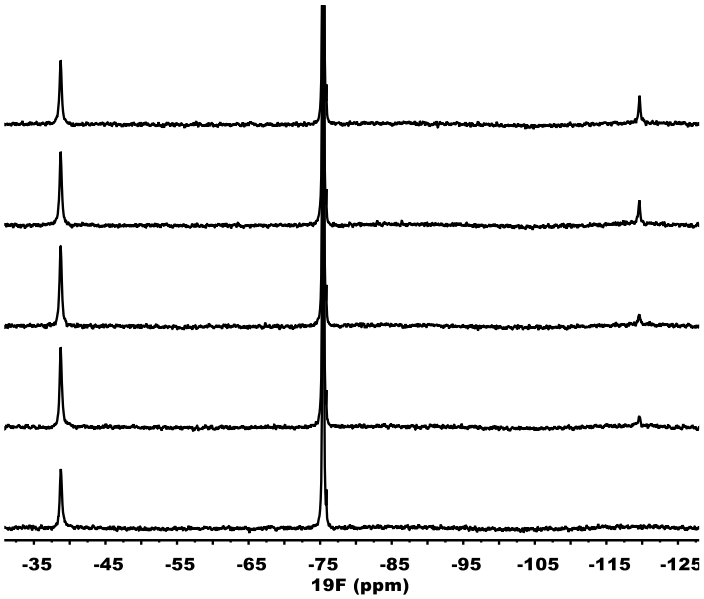

Figure 14 . Stacked plot of 470.45 MHz ^{19}F NMR spectra of 5 mM [Sc(OPC2A)]$^{+}$ and 5 mM NaF at different pH (6, 6.5, 7, 7.5, 8) from the bottom to the top. Chemical shift values: $\delta_{Sc\ (OPC2A)F}$ = -39 ppm, δ_{F^-} = -120 ppm, and δ_{TFA} = -75 ppm (impurity), I = 0.15 M NaCl, T = 298 K.

Taking a closer look at the spectra in Figure 13 one can see that both signals of [Sc(OPC2A)F] and F^- are substantially broader than that of TFA ($\nu_{1/2}$ = 1 Hz). The half width of F^- decreases from 220 Hz to 70 Hz from the top to bottom, while the half width of [Sc(OPC2A)F] remains constant, ca. 160 ± 10 Hz. Both are larger than the $\nu_{1/2}$ = 5 ± 1 Hz measured in a standard sample of NaF, at pH = 5. The NMR line width is determined by the transverse relaxation.

One source of this relaxation is the magnetic interactions with the environment; in the case of [Sc(OPC2A)F] it is mostly the result of the quadrupole coupling with the ^{45}Sc nucleus. The other source is the chemical exchange causing the faster loss of the coherent phase:

$$\nu_{1/2} \times \pi = \frac{1}{T_2^*} + k_{obs} \qquad (41)$$

The $\nu_{1/2}$ = 160 Hz broad peak of [Sc(OPC2A)F] is an (unresolved) octet ($^1J_{Sc\text{-}F}$), attributed to the spin-spin coupling between the ^{19}F (I = ½) and the quadrupolar ^{45}Sc (I =7/2). $^1J_{Sc\text{-}F}$ = 172 Hz has been published for the highly symmetric ScF_6^{3-} anion.[100,101] Therefore, instead of the expected multiplet structure of the ^{19}F NMR signal of [Sc(OPC2A)F], a single broad peak is observed, which reflects the first-order rate constant of magnetization exchange arising from chemical exchange, as described in eq. 40. However, these effects can rarely be separated. The broadening of the free F^- can obviously be attributed mainly to the chemical exchange, since the nonexchange line width can be measured experimentally (5 ± 1 Hz). However, the involvement of [Sc(OPC2A)F] in chemical exchange can be demonstrated by variable temperature measurements, as shown in Figure 15. The integrated intensity of the signals does not change with temperature, i.e., the equilibrium remains essentially constant. However, both peaks broaden as the temperature increases because the exchange rate becomes faster. The chemical shift values of the two sites, [Sc(OPC2A)F] and F^-, are almost constant and so we can conclude that the system is in a "two site, slow exchange regime".

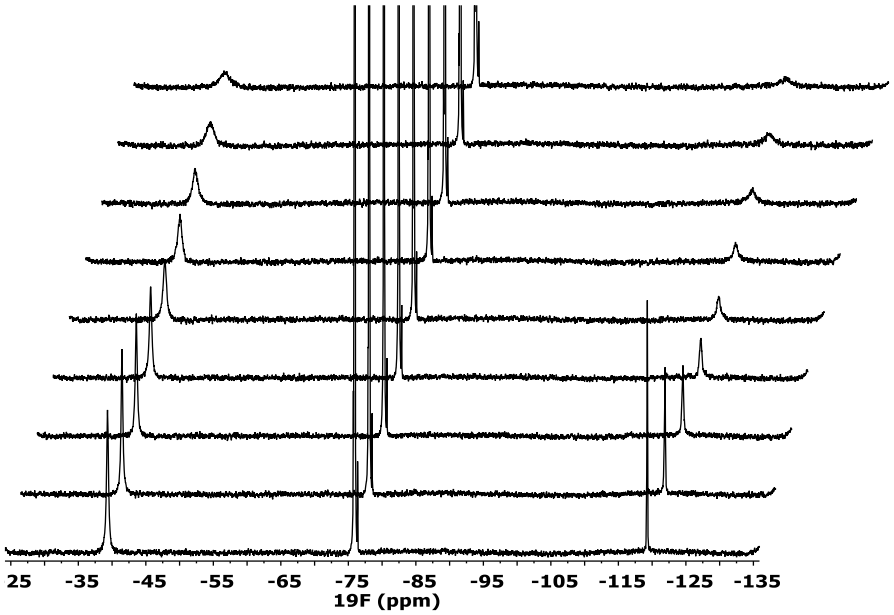

Figure 15. 470.45 MHz ^{19}F NMR variable temperature spectra of a 5 mM solution of [Sc(OPC2A)]$^{+}$ containing 7.5 mM NaF, at pH = 4.5. The temperature increases from the bottom (273 K) to the top (333 K).

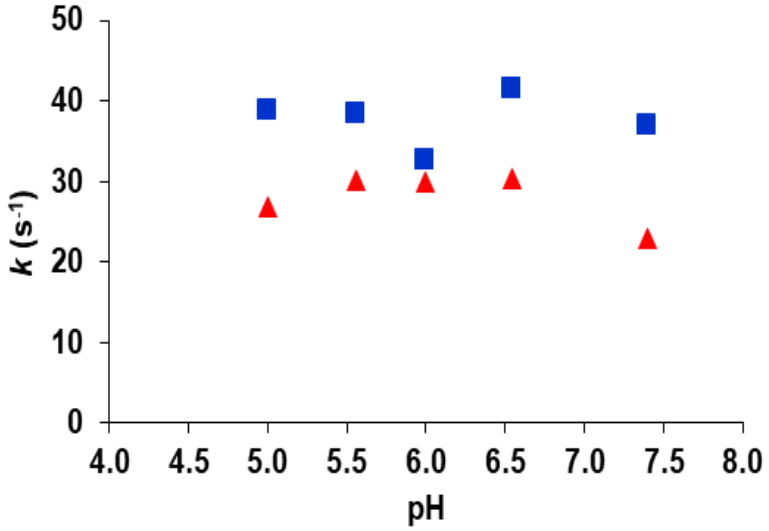

Figure 16. k_F^{obs}(■ blue squre) and k_{ScLF}^{obs} (▲red triangle) vs. pH measured by selective magnetization transfer ($c_{[Sc(OPC2A)]}$ = 5 mM, c_F = 10 mM, T = 298 K).

It should be noted, that the line width (or k_{ScLF}^{obs}) of [Sc(OPC2A)F] is not affected neither by the concentration of the excess fluoride nor by the hydroxide concentration, as Figure 13, Figure 14 and Figure 16 show. These findings clearly indicate that bimolecular reactions of [Sc(OPC2A)F] with fluoride or hydroxide are not active. The rate equations is fairly simple:

$$\text{rate} = \frac{-\text{d[Sc(OPC2A)F]}}{\text{dt}} = -k_d[\text{Sc(OPC2A)F}] \qquad (42)$$

where k_d is the rate constant of dissociation, i.e. the dissociation of [Sc(OPC2A)F] is the rate determining step. It is followed by the fast reaction between the intermediate parent complex and a fluoride ion.

$$[\text{Sc(OPC2A)F}] \xrightarrow{k_\text{d}} [\text{Sc(OPC2A)}]^+ + \text{F}^- \quad \text{(slow)} \qquad (43)$$

$$[\text{Sc(OPC2A)}]^+ + \text{F}^- \xrightarrow{k_\text{f}} [\text{Sc(OPC2A)F}] \quad \text{(fast)} \qquad (44)$$

The suggested mechanism appears reasonable, because the coordination sphere of the [Sc(OPC2A)F] complex is saturated, and the electrostatic interaction between the complex and the F^- ion is not enough strong to form an adduct serving as a reactive intermediate. Similar considerations were applied in our previous publication on the carbonate exchange kinetics of a coordinatively saturated complex, $UO_2(CO_3)_3^{4-}$, studied by line shape analysis using ^{13}C NMR.[102]

Variable temperature NMR, using techniques such as line shape analysis (T_2 time scale), or selective magnetization transfer experiments (T_1 time scale), is commonly employed to determine the activation parameters of the exchange processes. For intermolecular second order reactions, the application of the Eyring equation is well established, whereas its use for first-order reactions has certain limitations.[103,104]A detailed discussion of

collision theory is beyond the scope of this study; however, we will briefly mention the fundamental requirement for using a first-order rate constant (k in s^{-1}). It should not be k^{obs}, which is a concentration-dependent pseudo-constant often employed in reaction kinetics to derive the rate equation. The fluoride exchange in our system follows a simple rate equation, and the relation $k^{obs} = 2k_d$ holds true, where k_d is a true, concentration-independent first-order rate constant. The limitations of using line shape analysis have been addressed above. To circumvent these challenges, we conducted variable temperature selective magnetization transfer experiments.

Typical DANTE experiments, i.e. ^{19}F NMR spectra, are shown in Figure 17 and Figure 18. The signal intensity versus delay time curves, along with the fitted curves calculated for the two-site exchange system, are presented for all six different temperature values in Figure 19. The rate constants k_F^{obs}, k_{ScLF}^{obs} and the $T_{1\ ScLF}$ values were determined by simultaneously fitting the intensities of the ^{19}F NMR signals of the [Sc(OPC2A)F] ternary complex and the F^- anion. Fitting of the Abs. Int. values as a function of τ were performed with eqs. 2 and 3. The $T_{1,F}$ value was fixed to the experimentally measured value for the corresponding temperature.

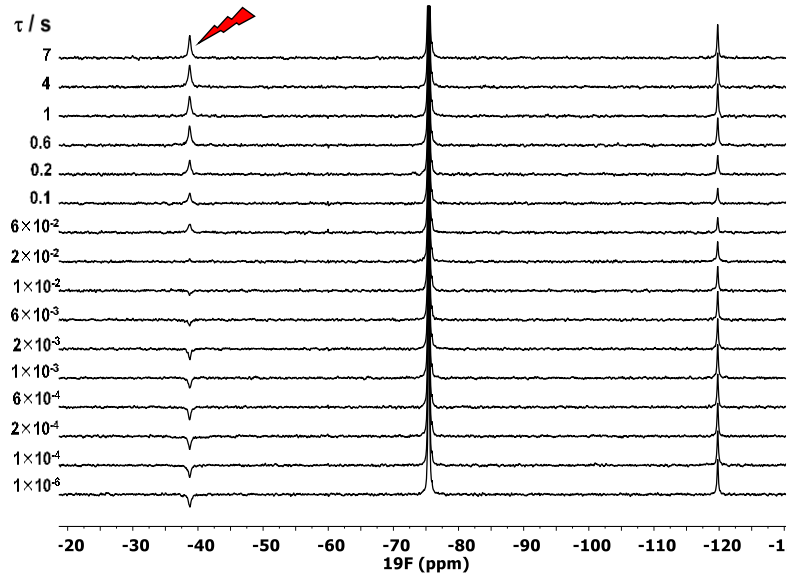

Figure 17. Selective magnetization transfer experiment by ^{19}F NMR. 5 mM [Sc(OPC2A)] and 9 mM NaF, pH = 5.4, T = 298 K. The bound $^{19}F^{-}$ signal was inverted.

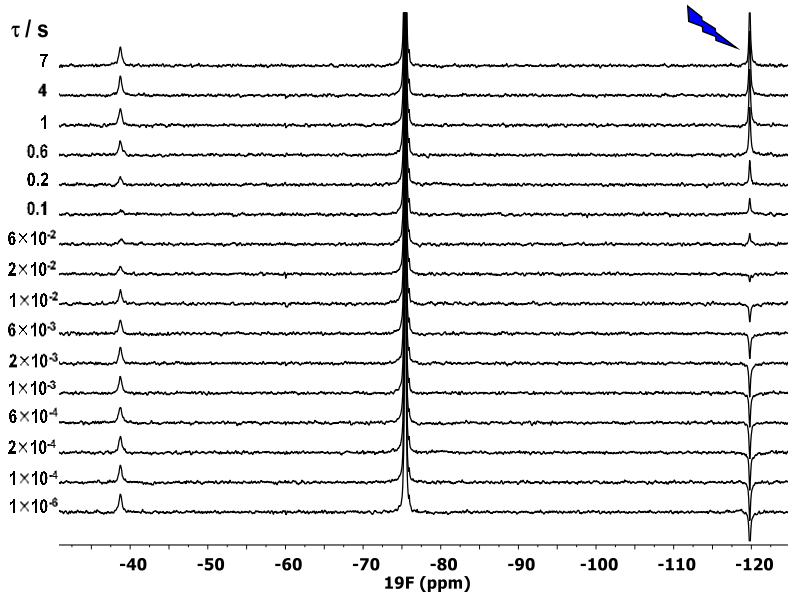

Figure 18. Selective magnetization transfer experiment by ^{19}F NMR. 5 mM $[Sc(OPC2A)]^{+}$ and 9 mM NaF, pH = 5.4, *T* = 298 K. The free F^{-} signal was inverted.

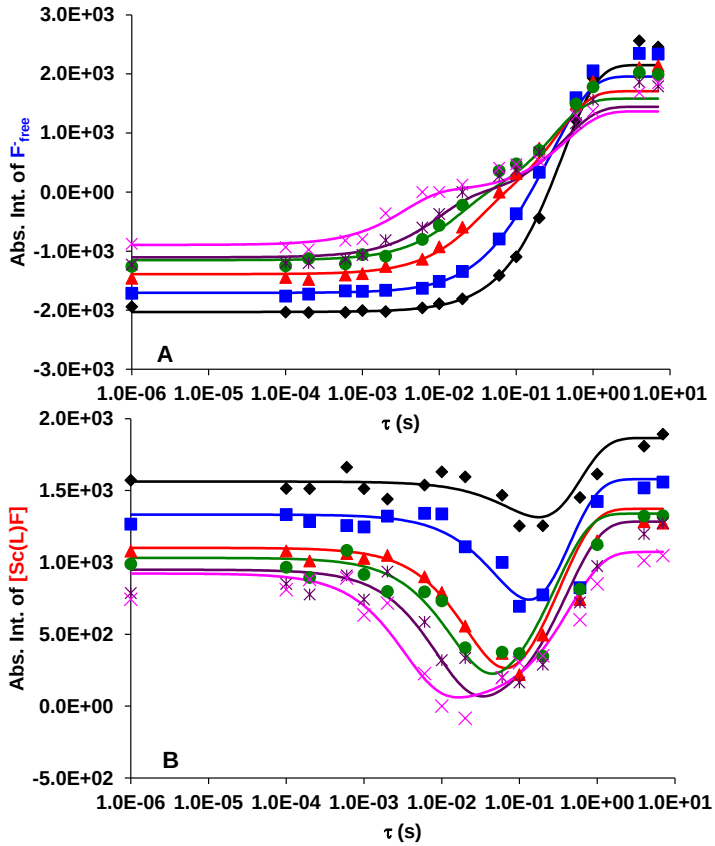

Figure 19. Abs. Int. values of $F^{-}_{\ free}$ (A) and [Sc(OPC2A)F] (B) signals vs. delay time (s) by the selective excitation of F^{-} signal at 273, 283, 293, 298, 303 and 313 K ($c_{[Sc(OPC2A)]}$ = 5.0 mM, c_F = 9.0 mM, pH = 5.4, 0.15 M NaCl). Fitting of the Abs. Int. values as a function of t were performed with eqs. (2) and (3). Symbols are the measured, curves show the fitted intensities.

Eyring and Arrhenius plots based on the k_d rate constants are shown in Figures 20. The activation parameters, corresponding to the rate-determining step of the ligand exchange reaction, namely the dissociation of the fluoride ligand from the [Sc(OPC2A)F] ternary complex, are summarized in Table 9.

Table 9. Activation Parameters of the [Sc(OPC2A)F] – F^- Exchange Reaction Calculated with Eyring and Arrhenius Equations.

	Eyring		Arrhenius
$\Delta H^{\ddagger}$ / kJ·mol^{-1}	**78 ± 1**	E_a / kJ·mol^{-1}	**81 ± 1**
$\Delta S^{\ddagger}$ / J·mol^{-1}K^{-1}	**42 ± 4**	lnA	**35.5 ± 0.5**
$\Delta G^{\ddagger}_{298}$ /kJ·mol^{-1}	**66 ± 1**		
k_d^{298} /s^{-1}	**16.5**	k_d^{298} /s^{-1}	**16.5**

Analysis of the kinetic parameters shows a large positive $\Delta S^{\ddagger}$ and a considerably large activation enthalpy. These findings are consistent with a dissociatively activated mechanism for the F^- exchange. This implies that the rate-determining step involves the dissociation of the Sc-F bond of the leaving ligand, followed by the coordination of the entering F^- ion and subsequent bond formation.

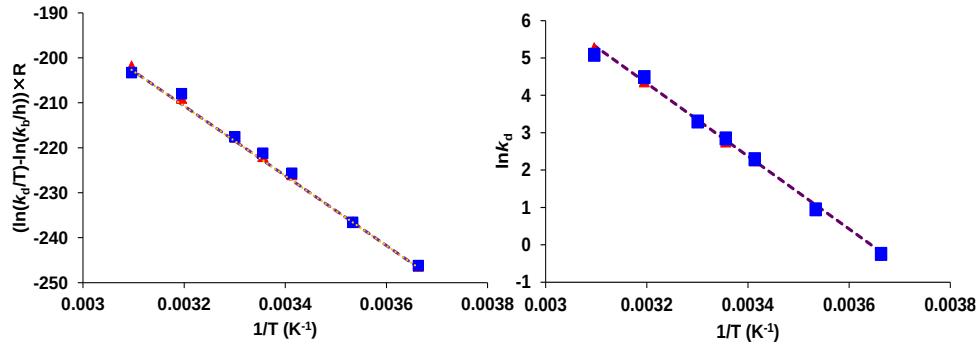

Figure 20. Eyring and Arrhenius plot for the [Sc(OPC2A)F] – F^- exchange reaction (k_d of $k_{[Sc(OPC2A)F]}$. ▲ and k_d of k_F: ■). $c_{[Sc(OPC2A)]}$ = 5.0 mM**,** c_F = 9.0 mM**,** pH = 5.4, I = 0.15 M NaCl.

4.2.3.2. F^-exchange of [Sc(PC2AAM^{nBu})(F)]

To check the inertness of the mixed [Sc(PC2AAM^{nBu})(F)] complex against F^- exchange using ^{19}F NMR, the signal of the mixed complex is somewhat broadened ($\nu_{1/2}$ = 150 Hz) due to the relaxation effect of the quadrupole ^{45}Sc (I = 7/2), while the free fluoride is narrow ($\nu_{1/2}$ = 4.5 Hz), indicating the absence of chemical exchange on the T_2-time scale. However, selective magnetization transfer experiment shows chemical exchange between [Sc(PC2AAM^{nBu})(F)] (site A) and F^- (site B); k+ and k- values obtained in [Sc(PC2AAM^{nBu})(F)] system are about 30 – 60 times lower than that of $[Sc(OPC2A)]^+$–F^- system.

The k_{obs}^{AB} value of 0.6 s^{-1} (14% uncertainty) indicates remarkable inertness of the monodentate fluoride. 3-4 order of magnitude larger fluoride exchange rate constants have been published for two Y(III) complexes formed with open-chain ligands, $Y(EDTA)F^{2-}$ and $Y(EGTA)F^{2-}$.[87]

In case of macrocyclic $Ln(DOTA\text{-tetramide})F^{2+}$ systems (Ln = Yb, Eu) the rate constants are k_{obs} = 61 s^{-1} and 0.41 s^{-1}, respectively.[105] These values are closer to the one determined by us in this current study and it might be rationalized by the more rigid structure around the M(III)-F entity in the macrocyclic complexes as compared to the linear chelates. However, the fluoride exchange rate of open-chain $[Al(EDTA)(F)]^{2-}$ much smaller, [92] reflecting the role of the individual metal centre and preventing us from further speculation to find simple structure-inertness correlation.

4.3. ^{44}Sc radiolabeling of OPC2A ligand

For radiochemical studies, the positron-emitting ^{44}Sc isotope was produced in a cyclotron by proton irradiation of a natural calcium target (30 min, 20 µA) via the ^{44}Ca(p, n)^{44}Sc reaction.[33] The separation of ^{44}Sc radionuclide from irradiated targets and other metal-based impurities was performed using DGA resin according to the methods described by Happel et al.[106] DGA resin is an extraction chromatographic resin based on *N,N,N',N'*-tetra-n-octyldiglycolamide. Radiolabeling of OPC2A was accomplished by mixing 200 µl of [^{44}Sc]$ScCl_3$ solution (150 MBq) with 700 µl of ammonium acetate buffer (pH = 4) and adding 100 µl of ligand solution (0.1 mM). This reaction mixture was incubated at 95 °C for 10 min, resulting in a radiolabeling yield of 85%, see Figure 21.

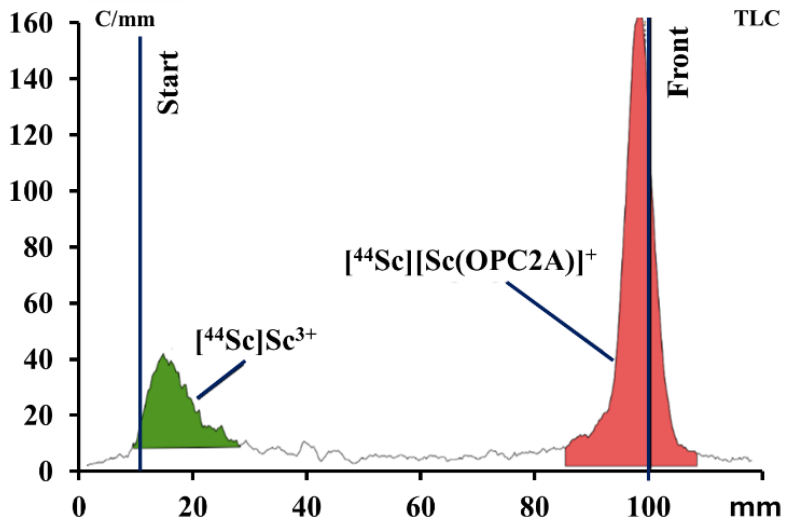

Figure 21. Radio-iTLC -SG paper chromatogram of the radiolabeling with ^{44}Sc isotope (stationary phase: iTLC -SG paper, mobile phase: 0.5 M Na_2CO_3 solution).

Subsequently, the radiolabeled complex was purified by solid-phase extraction using a Sep-Pak C18 Plus Light cartridge (Waters). The radiochemical purity (RCP) of the purified $[^{44}Sc][Sc(OPC2A)]^+$ complex was determined by instant-radioTLC and it was over 99%, see Figure 22. Radio-iTLC -SG paper chromatogram had only one peak at 95 mm, the $[^{44}Sc][Sc(OPC2A)]^+$ complex was moving together with the front, while the zero activity at the start point indicated the absence of the free Sc(III) after purification.

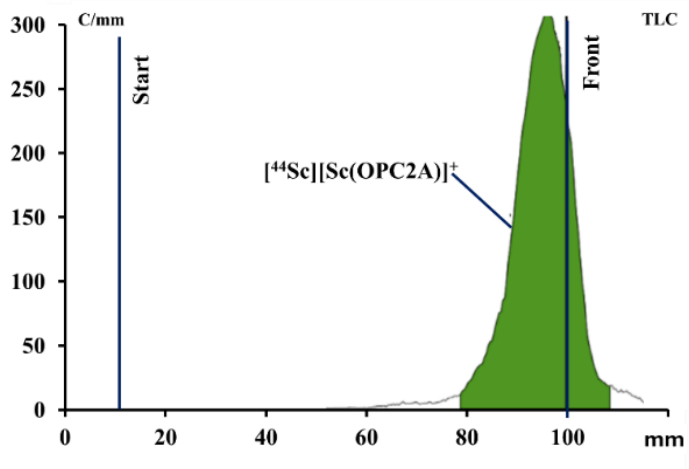

Figure 22. Radio-iTLC chromatogram of the purified $[^{44}Sc][Sc(OPC2A)]^+$ complex (Stationary phase: iTLC, mobile phase: 0.5 M Na_2CO_3 solution).

The inertness of the $[^{44}Sc][Sc(OPC2A)]^+$ was evaluated with serum stability test; transchelation by the EDTA ligand and transmetalation with endogenous metal ions (Zn(II), Cu(II), Mg(II) and Ca(II)). Aliquots from the incubated samples were taken at different time points (0, 30, 60, 120, 180 and 240 min) and analyzed with instant radio-TLC. After 240 min, the RCP of the samples was still above 99 % in all cases. These results showed that the radiocomplex possesses high stability under the conditions studied Table 10.

Table 10. Results of Stability Studies of the [^{44}Sc][Sc(OPC2A)]$^{+}$ Complex

	Radiochemical purity of the samples [%]					
	0 min	30 min	60 min	120 min	180 min	240 min
Trans chelation with EDTA	100	100	100	100	100	100
endogenous metal challenge	100	100	100	100	100	100
serum stability	100	100	100	100	100	100

The octanol/water partition coefficient of the [^{44}Sc][Sc(OPC2A)]$^{+}$ complex (log$P$ = –3.58) was determined. The low log$P$ values indicate the hydrophilic character of the radiotracer.

5. Investigation of Al(III), Ga (III), In(III) and Tl(III) - OPC2A systems

We used the same methodology applied for the [Sc(OPC2A)]$^{+}$ system to investigate the equilibrium of [Ga(OPC2A)]$^{+}$ and [In(OPC2A)]$^{+}$, including the determination of the stability constants of the parent complexes and their mixed hydroxo and fluoro ternary species. We also studied the dissociation kinetics of [Ga(OPC2A)]$^{+}$ and [In(OPC2A)]$^{+}$ parent complexes. (However, detailed kinetic data for the complex formation were not available, as was the case for the [Sc(OPC2A)]$^{+}$ system due to the limited time.) Consequently, we did not include all details in this part to avoid unnecessary repetition.

5.1. Equilibrium studies of M(III)-OPC2A^{2-}- H^{+}-X^{-} – systems

5.1.1. Determination of stability constants of [M(OPC2A)]$^{+}$ and ternary mixed hydroxo [M(OPC2A)OH] complexes

5.1.1.1. The stability constants of Al(III) complexes

We started our studies with Al(III), but our attempts to prepare [Al(OPC2A)]$^{+}$ complexes and record the ^{27}Al and ^{1}H-NMR spectra were unsuccessful. No formation of the [Al(OPC2A)]$^{+}$ complex could be detected under our experimental conditions; Figure 23 after 50 days of monitoring ^{1}H NMR and ^{27}Al-NMR spectra. The ^{1}H NMR spectrum of a expected Al(III) complex remained unchanged compared with free OPC2A. At the same time ^{27}Al-NMR spectrum showed only one signal at 0 ppm corresponding to free Al(III), and its intensity was comparable to that of a 3 mM standard sample of free Al(III), confirming that Al(III) did not form a complex with the OPC2A ligand. The reason could be the incompatibility of metal size. The ionic radius of Al(III) is too small to match the OPC2A cavity size. The lack of optimal interaction between the metal center and the donor atoms results in very weak chelation, which is sterically hindered by the pre-organized macrocyclic ring. Furthermore, Al(III) is known to hydrolyze strongly in aqueous solutions,[17] decreasing the apparent stability of the complex, and it likely prevents complexation with the OPC2A ligand.

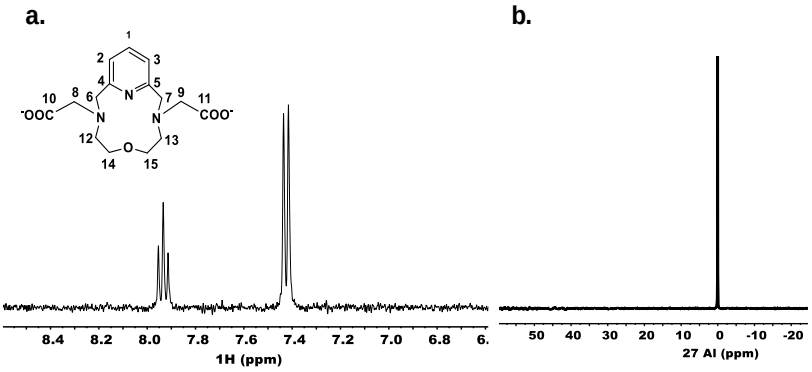

Figure 23 a) 400 MHz ^{1}H-NMR spectra at the aromatic region of OPC2A ligand (H in position 1, triplet; H in position 2,3, doublet). b) 104.3 MHz ^{27}Al NMR spectra of Al(III)-OPC2A^{2-} - H^{+} system (Al(III) free peak δ ≈ 0 ppm). $c_{Al(III)}$ = 3 mM, c_{OPC2A} = 3.15 mM, c_{H+} = 30 mM, I = 0.15 M NaCl, T= 298 K).

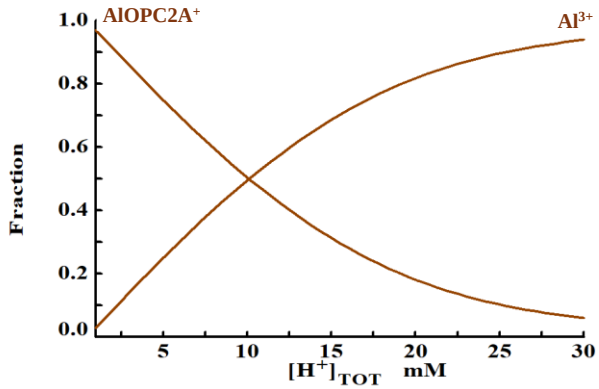

Figure 24 . Theoretical distribution curves of Al(III)-OPC2A^{2-}-H^{+} system assuming log$K$ = 15, $c_{Al(III)}$ = 2mM, c_{OPC2A} = 2.1 mM.

Figure 24 shows model calculation setting log$K_{[Al(OPC2A)]+}$ = 15 involving Al(III) hydroxo species.[17] The calculated [Al^{3+}] fits to the experimental findings, showing negligible complexation at 30 mM acid content. It means log$K_{[Al(OPC2A)]+}$ ≤ 15.

5.1.1.2. The stability constants of Ga(III) complexes

The out-of-cell ("batch") method was applied. The samples with different HNO_3 acid content were prepared in 5 mm NMR tubes and kept at room temperatures and monitored by ^{1}H and ^{71}Ga NMR, until the samples reached equilibrium. As was the case with Sc(III) the parent complex signal was very broad due to quadrupolar relaxation effect of Ga(III) nucleus.

The $K_{[Ga(OPC2A)]+}$ constants were calculated by using signal intensity of ^{71}Ga NMR spectra, see Figure 25. The data used for calculation were collected in Table 11. Employing ^{71}Ga NMR the equilibrium concentration of the free Ga(III) aqua ion was measured. The stability constant of $\log K_{[Ga(OPC2A)]+} = 17.2$ (2) was calculated using the mass balance equation.

The K^* values, see eq 46, have been calculated individually for all of the samples. The stability constant of the parent complex, $K_{[Ga(OPC2A)]+}$ is defined as follows:

$$Ga^{3+} + (H_2OPC2A) \rightleftharpoons [Ga(OPC2A)]^{+} + 2H^{+} \quad (45)$$

$$K^*_{[Ga(OPC2A)]} = \frac{[Ga(OPC2A)^{+}][H^{+}]^2}{[(H_2OPC2A)][\,Ga^{3+}]} \quad (46)$$

$K_{[Ga(OPC2A)]}$ can be calculated from K^* as follows:

$$\log K_{[Ga(OPC2A)]+} = \log K^* + \log \beta_2 \quad (47)$$

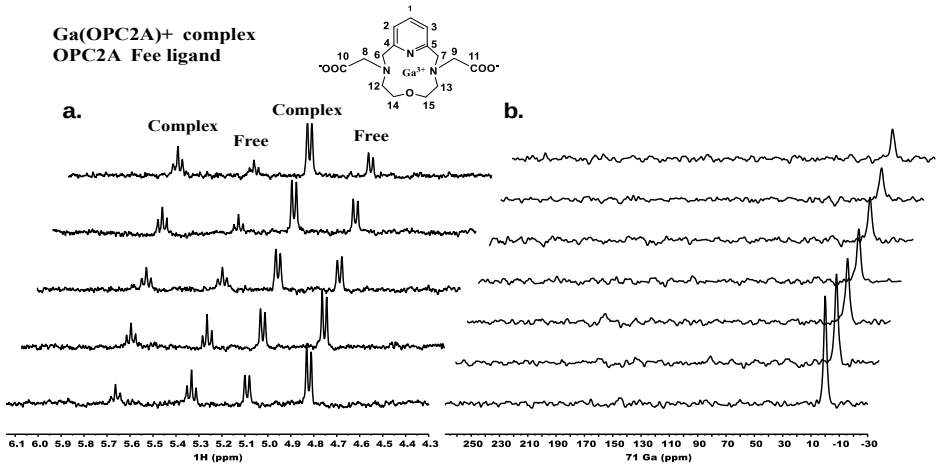

Figure 25 . a) 400 MHz ^{1}H-NMR spectra at the aromatic region (H in position 1, triplet; H in position 2,3 doublet) the acid concentrations are 10, 15, 20, 25, and 30 mM from top to bottom. **b)** 121.4 MHz ^{71}Ga NMR spectra of Ga(III)- $OPC2A^{2-}$ - H^{+} system; Ga(III) free peak at δ~0 ppm, the $c_{Ga(III)}$ = 3 mM, c_{OPC2A} = 3.15 mM, I = 0.15 M $NaNO_3$, T = 298 K, the acid concentrations are 10, 15, 20, 25, 30, 50 and 75 mM from top to bottom.

In terms of the differences in stability of metal complexes with various polyaminopolycarboxylate ligands, the stability constant of the $[Ga(OPC2A)]^{+}$ complex is lower than those of open chain $[Ga(EDTA)]^{-}$ [107] and the $[Ga(NOTA)]$[108] macrocyclic complex or $[Ga(AZZTA)]^{-}$,[109] even though the coordination number is the same (Table 12). The OPC2A ligand has three nitrogen and three oxygen donor atoms but has lower overall basicity than both EDTA and NOTA. On the other hand, the ionic radius of Ga^{3+} is likely not ideally matched with the cavity size of OPC2A, unlike NOTA, which provides a better preorganized and size-matched environment for Ga^{3+} coordination. All these combines to render the thermodynamic stability of the $[Ga(OPC2A)]^{+}$ complex lower than the

other complexes. The assignments of $[Ga(OPC2A)]^+$ and [Ga(OPC2A)F] complexes using 1D and 2D NMR are presented in Appendix, Figures A.12-A.19.

Table 11. Data used to calculate the stability constant, log$K_{[Ga(OPC2A)]+}$ with varying HNO_3 concentrations recorded by 121.4 MHz ^{71}Ga NMR (I = 0.15 M $NaNO_3$, $c_{Ga(III)}$ = 3 mM, c_{OPC2A} = 3.15 mM, T = 298 K).

$[H^+]_{tot.}$	$[Ga^{+3}]$	K^*	log K^*	logK^* + logβ_2
0.01	0.00055	0.18	-0.74	16.78
0.015	0.00060	0.74	-0.13	17.39
0.02	0.00117	0.49	-0.31	17.21
0.025	0.00153	0.55	-0.26	17.26
				17.2 (2)

Table 12. Stability constants of gallium(III) complexes with some amino polycarboxylate ligands at 25 °C

	I	log$K$	C.N
$[Ga(EDTA)]^-$ [107]	0.1M KNO_3	22.1	6
$[Ga(DTPA)]^{2-}$ [107]	0.1M KNO_3	27.8	8
$[Ga(AZZTA)]^-$ [109]	0.1M KCl	22.18	6
[Ga(NOTA)] [108]	0.1M $(NMe_4)Cl$	29.6	6
$[Ga(DOTA)]^-$ [110]	0.1M $(NMe_4)Cl$	26.05	8

The acid-base properties of $[Ga(OPC2A)]^+$ have been investigated by pH-potentiometry by titrating the previously prepared $[Ga(OPC2A)]^+$ ($c_{[Ga(OPC2A)]}$ = 2 mM) with standardized NaOH in the pH-range of 1.95-12, Figure 26. The results of Ga(III) titration do not give indication for the

formation of any protonated $[Ga(HOPC2A)]^{2+}$ or mixed hydroxo complexes. Also, the attempt to detect [Ga(OPC2A)OH] by ^{1}H and ^{71}Ga NMR was not successful, it was limited by hydrolysis of Ga(III) in basic region and formation of highly stable gallate $Ga(OH)_4^-$ or solid $Ga(OH)_3$.

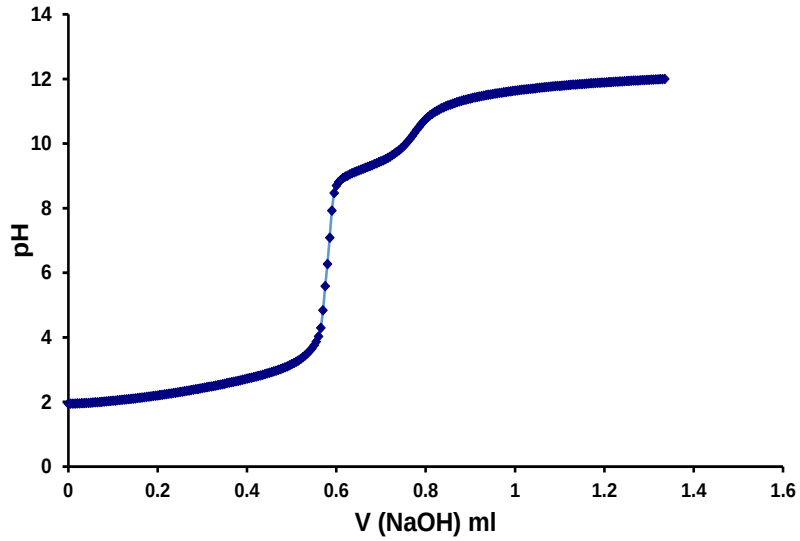

Figure 26 . The titration curve of $[Ga(OPC2A)]^+$ complex. $c_{[Ga(OPC2A)]+}$ = 2 mM, I = 0.15 M $NaNO_3$, T = 298 K.

5.1.1.3. Stability constant of In(III) complexes

The stability constant of In(III) complexes have also been determined by the out-of-cell ("batch") method. The $K_{[In(OPC2A)]+}$ constant has been calculated by using signal intensities of ^{115}In NMR spectra, Figure 27. The stability constant of $[In(OPC2A)]^+$ has been calculated using the mass balance equation.

$$In^{3+} + (H_2OPC2A) \rightleftharpoons [In(OPC2A)]^+ + 2H^+ \qquad (48)$$

$$K^*_{[In(OPC2A)]} = \frac{[In(OPC2A)^+][H^+]^2}{[(H_2OPC2A)][\,In^{3+}]} \qquad (49)$$

Table 13. Data used to calculate the stability constant, log$K_{[In(OPC2A)]^+}$ with varying HNO_3 concentrations recorded by 89.60 MHz ^{115}In NMR (I = 0.15 M $NaNO_3$, $c_{In(III)}$ = 3 mM, c_{OPC2A} = 3.15 mM, T = 298 K).

$[H^+]_{tot}$ mM	$[In^{+3}]$ mM	K^*	log K^*	log K^* + logβ_3
30	0.64	37.34	1.57	19.09*
50	1.24	3.83	0.58	18.10
75	1.46	1.75	0.24	17.76
100	2.28	1.39	0.14	17.66
150	2.66	40.05	1.60	19.12*
				17.8(1)

* By excluding the 30 mM and 150 mM samples (Table 13), the calculated stability constant becomes more reliable, as the first case involves a high complexation ratio, while in the other case the complexation ratio is low.

Table 14. Thermodynamic stability constants of $[In(OPC2A)]^+$, and [In(OPC2A)(OH)] complexes (I = 0.15 M NaCl and $NaNO_3$ T = 298 K).

	$[In(OPC2A)]^+$	Methods
log$K_{[In(OPC2A)]}$	17.8 (1)	^{115}In NMR spectrometry
log$K_{[In(HOPC2A)]}$	2.16 (3)	pH potentiometry (PSEQUAD)
log$K_{[In(OPC2A)OH]}$	-5.13 (2)	pH potentiometry (PSEQUAD)

As discussed above with $[Ga(OPC2A)]^+$, similarly in comparison to the stability constant of $[In(OPC2A)]^+$ with other amino polycarboxylate ligands (APCs), $[In(OPC2A)]^+$ has lower stability than In(APCs), likely for the same reason mentioned above, which relates to the characteristics of the OPC2A ligand itself, resulting in reducing the overall stability of the complex. At this point, the ion-size-fit factor becomes a critical

determinant of complex stability. NOTA and AAZTA form an exceptionally stable complex with In(III) due to preorganization and fitting of In(III) size with the cavity of those ligands, Table 15.

Table 15. Stability constants of indium (III) complexes with some amino polycarboxylate ligands at 25 °C.

	I	log*K*	C.N
$[In(EDTA)]^{-}$ [107]	0.1M KNO_3	25.1	6
$[In(DTPA)]^{2-}$ [107]	0.1M KNO_3	29.48	8
$[In(AZZTA)]^{-}$ [109]	0.1M KNO_3	29.58	6
[In(NOTA)] [111]	0.1M KCl	26.2	6

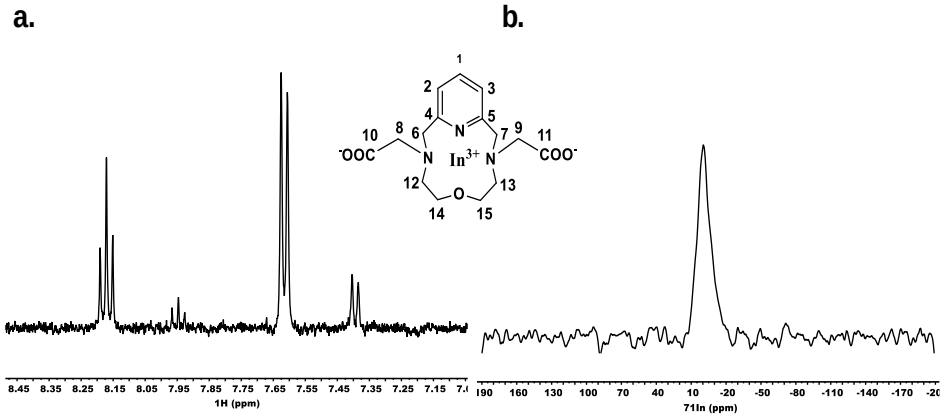

Figure 27. (a) Typical 400 MHz ^{1}H-NMR spectrum at the aromatic region (H at position 1, is triplet; and position 2,3, are doublet) of $[In(OPC2A)]^{+}$ with 10 mM acid concentration. (**b)** 89.60 MHz ^{115}In NMR spectrum of free In(III) peak at δ~0 ppm, $c_{In(III)}$ = 3 mM, c_{OPC2A} = 3.15 mM, *I* = 0.15 M $NaNO_3$, *T* = 298 K.

The pH potentiometric titration of $[In(OPC2A)]^{+}$ shows a base consuming process at pH > 5, see Figure 28 due to the formation of a mixed hydroxo [In(OPC2A)(OH)] complexes, which can be described by eqs 50 and 51:

$$[\mathrm{In(OPC2A)(H_2O)}]^{+} \rightleftharpoons [\mathrm{In(OPC2A)(OH)}] + \mathrm{H}^{+} \quad (50)$$

$$K_{[\mathrm{In(OPC2A)OH}]} = \frac{[\mathrm{In(OPC2A)(OH)}][\mathrm{H}^{+}]}{[\mathrm{In(OPC2A)(H_2O)}^{+}]} \quad (51)$$

Formation of a mixed hydroxo complex may indicate the presence of water molecule in the inner sphere. The log$K_{[\mathrm{In(OPC2A)OH}]}$ can be attributed to deprotonation of an inner sphere water molecule in the parent $[\mathrm{In(OPC2A)(H_2O)}]^{+}$ complex. Moreover, the formation of the protonated $[\mathrm{In(HOPC2A)}]^{2+}$ was detected, see Table 14. The stability of protonated species can be defined as follows:

$$[\mathrm{In(OPC2A)}]^{+} + \mathrm{H}^{+} \rightleftharpoons [\mathrm{In(HOPC2A)}]^{2+} \quad (52)$$

$$K_{[\mathrm{In(HOPC2A)}]^{2+}} = \frac{[\mathrm{In(HOPC2A)}^{2+}]}{[\mathrm{In(OPC2A)}^{+}][\mathrm{H}^{+}]} \quad (53)$$

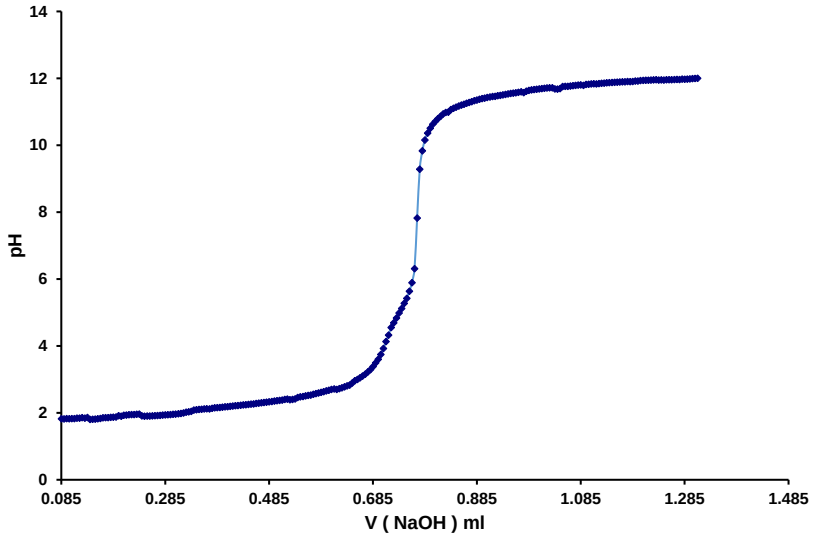

Figure 28 . The titration curve of $[\mathrm{In(OPC2A)}]^{+}$ complex, $c_{[\mathrm{Ga(OPC2A)}]^{+}}$ = 2 mM, I = 0.15 M $NaNO_3$, pH = 1.95 -12, T = 298 K.

5.1.1.4. Stability constant of Tl(III) complexes

Due to the high stability of the $[Tl(OPC2A)]^+$ complex, it was not possible to determine the stability constant of $[Tl(OPC2A)]^+$ under the experimental conditions used. The complexation was fast and went to completion. Adding a known amount of acid to lower the pH wasn't enough for a proper study of the equilibrium in the system. When we tried a different approach involving a double-competition experiment in the presence of a large excess of chloride ions where H^+ ions competed with the metal for the ligand, and Cl^- ions competed with the ligand for coordination to Tl(III), than solubility issues limited further analysis of the system. The ^{1}H-NMR and ^{205}Tl spectra confirmed complete complexation, showing no signals corresponding to free ligand or free Tl(III).

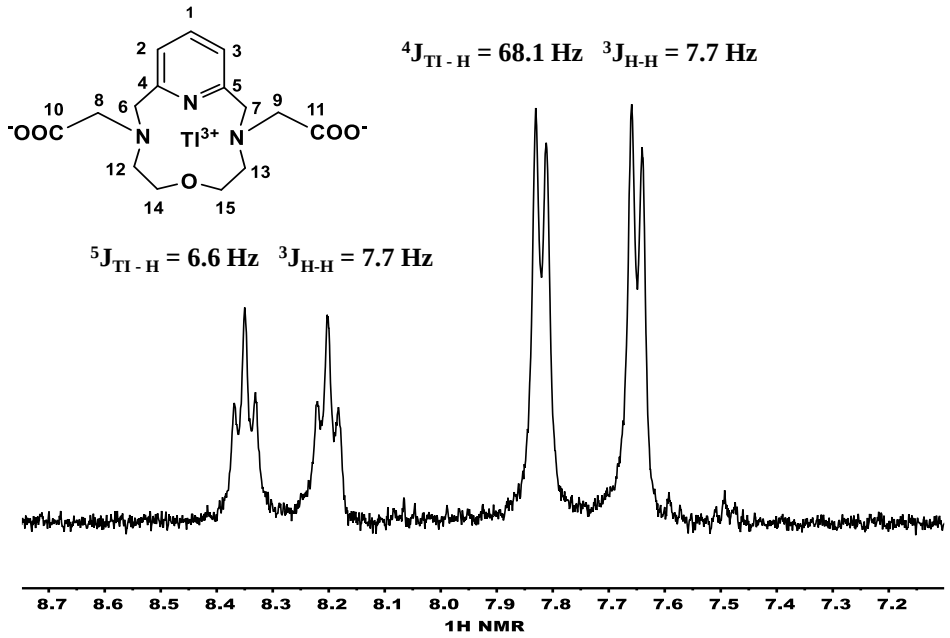

Figure 29. Typical 400 MHz ^{1}H-NMR spectrum at the aromatic region (H in position 1, triplet (dt); H in position 2,3 doublet (dd) ($c_{Tl} = c_L$ = 3 mM, c_{H^+} = 30 mM, 0.15 M $NaNO_3$, 298 K).

The ^{1}H NMR spectrum of the [Tl(OPC2A)]$^{+}$ complex shows one sets of signals. Although the ^{205}Tl atom is far from the ^{1}H atoms of the aromatic ring (protons 1, 2 and 3; see Figure 29), but still, it shows changes in spectra, that confirms the spin-spin coupling between ^{205}Tl and ^{1}H coupling through 4 and 5 bonds. The ^{1}H-NMR spectrum of [Tl(OPC2A)]$^{+}$ shows the signals assigned to the free ligand; than the signals observed previously at δ 7.48 and 8.08 ppm disappear upon complexation after adding Tl(III). The chemical shifts change after complexation, and new signals appear showing ^{205}Tl - ^{1}H to coupling, at δ = 8.2, 8.35 ppm (dt, $^{5}J_{\text{Tl-H}}$ = 60.6 Hz and $^{3}J_{\text{H-H}}$ = 7.7 Hz), and δ = 7.65, 7.82 ppm, (dd, $^{4}J_{\text{Tl-H}}$ = 68.1 Hz and $^{3}J_{\text{H-H}}$ = 7.7 Hz); which confirms the complex formation. The complex formation is also confirmed by ^{205}Tl NMR spectrum. A signal that belongs to the [TI(OPC2A)]$^{+}$ complex (Figure 30) is recorded at a chemical shift of δ = 2245 ppm, half width ($\nu_{1/2}$ = 1800Hz, proton coupled) which is close to [Tl(DOTA)]$^{-}$ signal at δ = 2218 ppm and [Tl(EDTA)]$^{-}$ δ = 2301 ppm. The positions of these signals are within the expected range for a Tl(III)-APCs compound. The absence of a signal due to Tl(III) aqua at δ = 2039 ppm confirms the full complexation of the metal ion by the OPC2A ligand.[68,70]

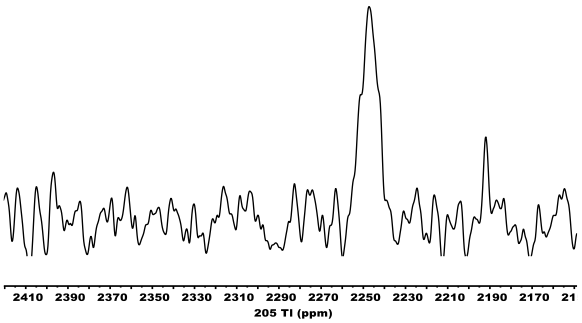

Figure 30. 75.1 MHz ^{1}H coupled ^{205}Tl-NMR spectrum of [Tl(OPC2A)]$^{+}$ complex ($c_{Tl} = c_L$ = 3 mM, c_H = 30 mM, I = 0.15 M $NaNO_3$, T = 298 K).

pH-potentiometric titration was performed on pre-equilibrated sample, which revealed the presence of $[Tl(HOPC2A)]^{2+}$, $[Tl(OPC2A)]^{+}$, and [Tl(OPC2A)OH] species, see Figure 31. The stability constant of different species is summarized in Table 16. The presence of a hydroxo complex points to the possibility of Tl(III) forming a ternary mixed complex, [Tl(OPC2A)X] (X = I^- or Cl^-).

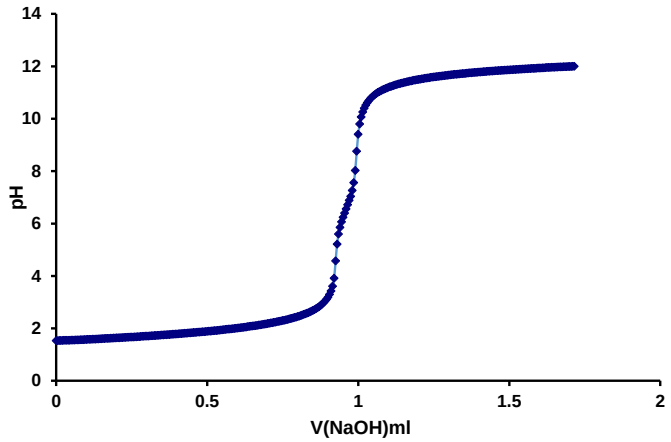

Figure 31 . The titration curve of $[Tl(OPC2A)]^{+}$ complex. ($c_{[Tl(OPC2A)]+}$ = 2 mM, I = 0.15 M $NaNO_3$, pH = 1.8 -11.85, T = 298 K.)

Table 16. Thermodynamic stability constants of $[Tl(OPC2A)]^{+}$, $[Tl(HOPC2A)]^{2+}$ and [Tl(OPC2A)(OH)] complexes (I = 0.15 M $NaNO_3$, T = 298 K).

	$[Tl(OPC2A)]^{+}$	Methods
$\log K_{[Tl(OPC2A)]+}$	≥ 34	Estimated*
$\log K_{[Tl(HOPC2A)]2+}$	3.62(5)	pH potentiometry
$\log K_{[Tl(OPC2A)OH]}$	-6.66 (2)	pH potentiometry

* $\log K_{[Tl(OPC2A)]}$ is estimated from model calculation ($c_{Tl} = c_{OPC2A}$ = 3 mM, c_{NaCl} = 0.15 M, c_{HNO3} = 1 M) involving Tl(III)-chloride complexes, i.e.

both chloride and proton competition. $\log K_{[Tl(OPC2A)]}$ = 34 and $\log \beta_{[Tl(OPC2A)I]}$= 36.3 were needed to return the experimental finding, thus the 100% complexation at the above-mentioned sample composition.

5.1.2. Investigation of [M(OPC2A)X] ternary complexes (M = Ga, In; X = F^- and Tl; X = I^- and Cl^-)

5.1.2.1. Determination of the stability constant of [Ga(OPC2A)F] complex

The stability constant of the ternary complex was measured by ^{19}F-NMR by considering the signal intensities of free and bound fluoride. In the ^{19}F-NMR spectra, a free fluoride signal was observed at –120 ppm, and a second signal was observed corresponding to the bound fluoride present in [Ga(OPC2A)F] at around –155 ppm.

The formation of [Ga(OPC2A)F] is described by the eqs 54 and 55:

$$[Ga(OPC2A)]^+ + F^- \rightleftharpoons [Ga(OPC2A)F] \qquad (54)$$

$$K_{[Ga(OPC2A)F]} = \frac{[Ga(OPC2A)F]}{[Ga(OPC2A)^+][F^-]} \qquad (55)$$

The stability constant was calculated from $[F^-]_{free}$ / [Ga(OPC2A)F] ratio at different total c_{F^-} concentration, see Figure 32 and Table 17. The $\log K_{Ga(OPC2A)F}$ = 3.32(2) which indicates quite high stability of this complex. The reported stability constants, $\log K_{GaLF}$ = 3.37, 3.15, 2.3 and 2.1 with NTA^{3-}, $HEDTA^{3-}$, $EDTA^{4-}$ and $CDTA^{4-}$ ligands, respectively.[91] Ga(III) forms a weaker bond than Al(III) with fluoride. For instance, the reported stability constant $\log K_{[Al(EDTA)F]}$ = 4.8, which is higher than $\log K_{[Ga(EDTA)F]}$ = 1.9 [67] The ^{1}H NMR spectra show a well-resolved signal on the aromatic region, corresponding to free ligand OPC2A, parent complex $[Ga(OPC2A)]^+$, and ternary complex [Ga(OPC2A)F, see Figure 33.

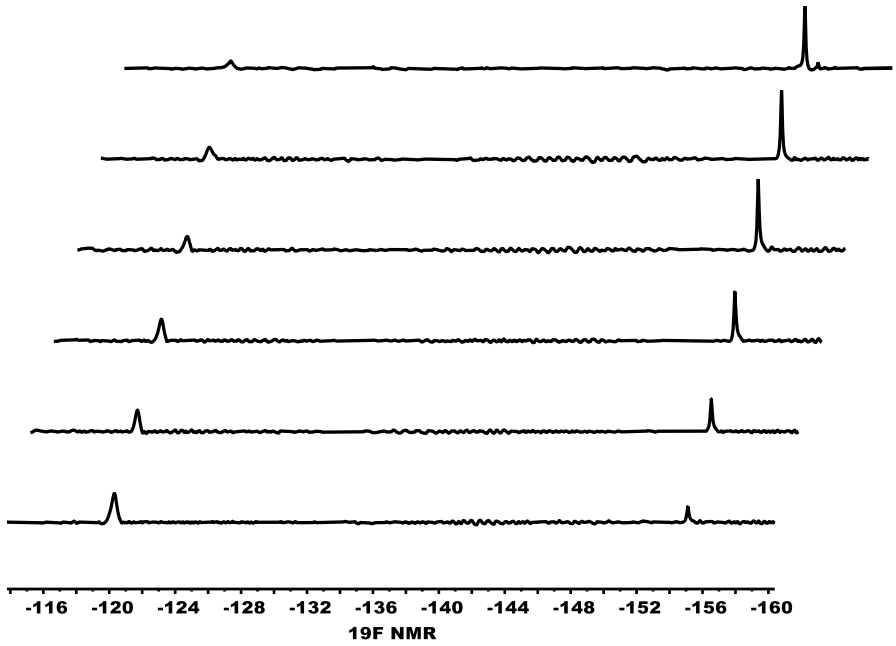

Figure 32. 376.4 MHz ^{19}F NMR spectra of 5 mM [Ga(OPC2A)]$^{+}$ at different concentrations of NaF (c_{NaF} = 8, 7, 6, 5, 4 and 3 mM from top to bottom).

Table 17. Data used to calculate the stability constant, log $K_{[Ga(OPC2A)F]}$ by titration of 5 mM [Ga(OPC2A)]$^{+}$ parent complex with NaF (3-8 mM) using 376.4 MHz ^{19}F NMR (I = 0.15 M $NaNO_3$, pH = 4.9, T = 298 K).

	F^-	F^- bound ratio	F^- free ratio	K	log$K_{[Ga(OPC2A)F]}$
Conc ScL 5mM	Conc of F^- add in mM	Integration ratio of bound F^-	Integration ratio of free F^-	[GaF]/[Ga]*[F^-]	
5	3	4.1	0.9	1793.5	3.25
5	4	4.36	0.64	4543.5	3.66
5	5	4.54	0.46	21455.6	3.83
5	6	3.29	1.71	1828.9	3.26
5	7	2.46	2.01	794.3	2.9
5	8	2.52	2.48	1049.7	3.02
					3.32 (2)

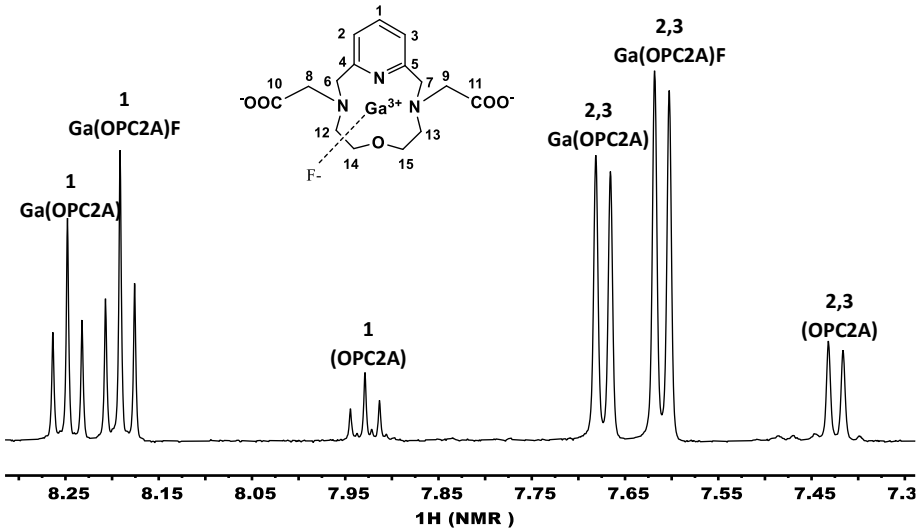

Figure 33. Typical 500 MHz ^{1}H NMR spectrum of [Ga(OPC2A)F] complex, c_{Ga} = 8.3 mM, c_{OPC2A} = 10 mM, c_{F-} = 5 mM, pH= 4.8 in D_2O, *T* = 298 K.

5.1.2.2. Determination of stability constant of [In(OPC2A)F] complex

From pH potentiometric titration, we observed the formation of a mixed hydroxo complex with indium, indicating the presence of inner sphere water molecule. This water molecule can be replaced by F^- to form a mixed fluoro complex, as shown in the equation below:

$$[In(OPC2A)H_2O]^+ + F^- \rightleftharpoons [In(OPC2A)F] + H_2O \qquad (56)$$

$$K_{[In(OPC2A)F]} = \frac{[In(OPC2A)F]}{[In(OPC2A)(H_2O)^+][F^-]} \qquad (57)$$

Uncertain data regarding the stability constant of the ternary complex [In(OPC2A)F] are currently unavailable. But it can be roughly estimated at pH = 7, the $\log K_{[In(OPC2A)F]} \approx 2.9$ (0.15), Figure 34. Based on the HSAB theory, the softer acid In(III) tends to form weaker bonds with fluoride,

which is a hard base, while hard acids like Ga(III) and Al(III) make stronger bonds with fluoride.[18] The reported stability of InLF with NTA^{3-}, $HEDTA^{3-}$, $EDTA^{4-}$ and $CDTA^{4-}$ ligands are log K_{InLF} = 2.0, 2.0, 1.6 and 2.1, respectively.[91]

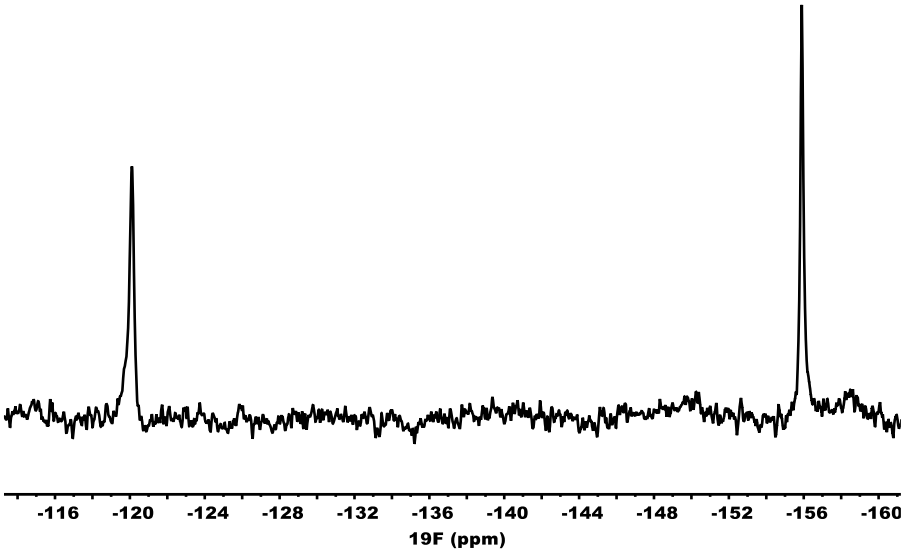

Figure 34. Typical 376.4 MHz ^{19}F NMR spectrum of 5 mM $[In(OPC2A)]^+$ with 5 mM NaF at pH = 7, I = 0.15 M $NaNO_3$, T = 298 K.

The reason behind the challenge to determine the stability constant of [In(OPC2A)F] is the presence of multiple species containing fluoride which makes the system more complicated. During the titration of the $[In(OPC2A)]^+$ parent complex with F^-, several signals were observed in the ^{19}F NMR, each likely corresponding to a distinct coordinated fluoride with a different environment. Specifically, when the concentration of the parent complex is higher than the concentration of the fluoride, two signals appear at –155.5 ppm and –156.2 ppm. The intensity of the signal at –156.2 ppm decreased and disappeared when fluoride was present in excess. See Figure 35. The signal at –155.5 ppm corresponds to the [In(OPC2A)F] ternary complex, while the signal at –156.2 ppm is

tentatively assigned to a bridging fluoride species, possibly $[(In(OPC2A))_2F]^+$. In both titration experiments of 5 mM $[In(OPC2A)]^+$ with NaF and 2mM NaF with $[In(OPC2A)]^+$ the two signals were present, when the concentration of the parent complex was higher than F^- concentration. Selective magnetization transfer (DANTE) experiments confirmed that these two signals are in a quite slow exchange regime Figure 34. Note: this exchange takes place between [In(OPC2A)F] and $[(In(OPC2A))_2F]^+$, i.e. between two coordinated fluorides with k_{obs}^{AB} = 2.99 s^{-1} and k_{obs}^{BA} = 2.43 s^{-1}, respectively as will be discussed in the section 5.2.3.2. This means remarkable extra inertness of the bridging fluoride against exchange compared to the inertness of [In(OPC2A)F] with free fluoride (k_{obs} = 55 s^{-1}).

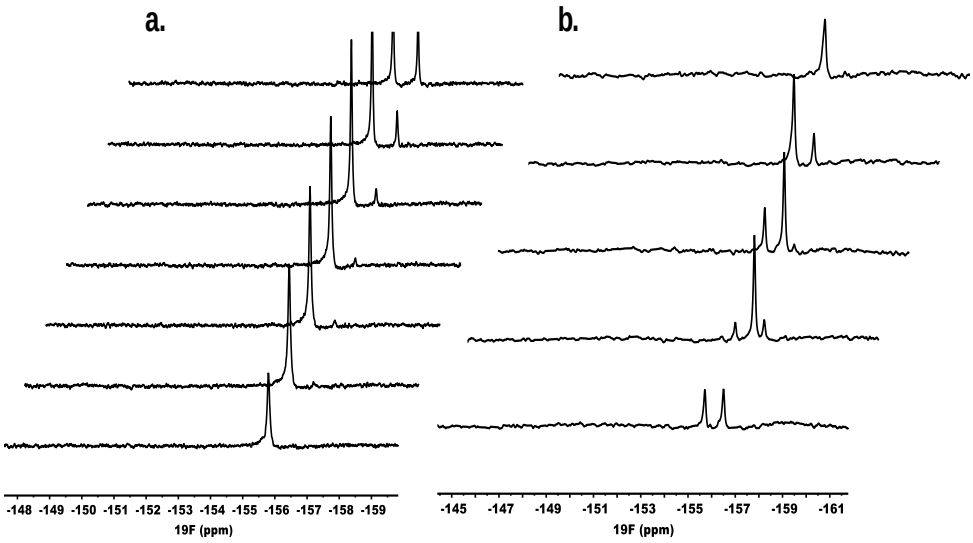

Figure 35. 470.45 MHz ^{19}F NMR spectra: **a.** Titration of 5 mM $[In(OPC2A)]^+$ with 3, 4, 5, 6, 7, and 8 mM of F^- from top to bottom. **b.** Titration of 2 mM of NaF with 1, 2, 3, 4, and 6 mM $[In(OPC2A)]^+$ parent complex from top to bottom.

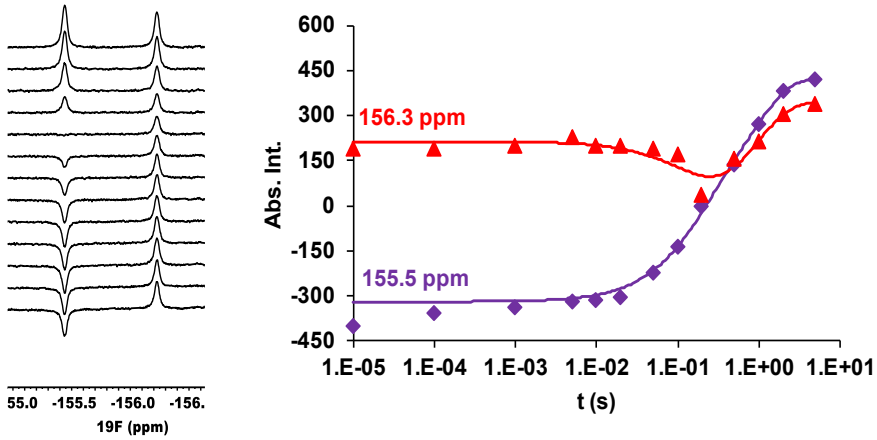

Figure 36. Abs. Int. values of signal 1 (-155.5 ppm) and signal 2 (-156.2 ppm) Absolute intensity vs. delay time (s) by the selective excitation of F^- signal at -155.5 ppm ($c_{[In(OPC2A)]}$ = 5.0 mM, c_F = 3 mM, pH = 4.9, I = 0.15 M $NaNO_3$, T = 298 K).

5.1.2.3. Investigation of Tl(OPC2A)X ternary complexes

5.1.2.3.1. Determination of stability constant of [Tl(OPC2A)I] complex.

Tl(III) forms a stable complex with APCs ligands, the $[Tl(EDTA)]^-$ complex was studied by our group. The $[Tl(EDTA)]^-$ complex has the ability to form a stable mixed ligand complex with halide as $[Tl(EDTA)X]^{2-}$, where X can be Cl^-, Br^- or I^-. The stability constants are log$K$ = 2.3, 3.5 and 5.9 for $[Tl(EDTA)Cl]^{2-}$, $[Tl(EDTA)Br]^{2-}$ and $[Tl(EDTA)I]^{2-}$, respectively.[67]

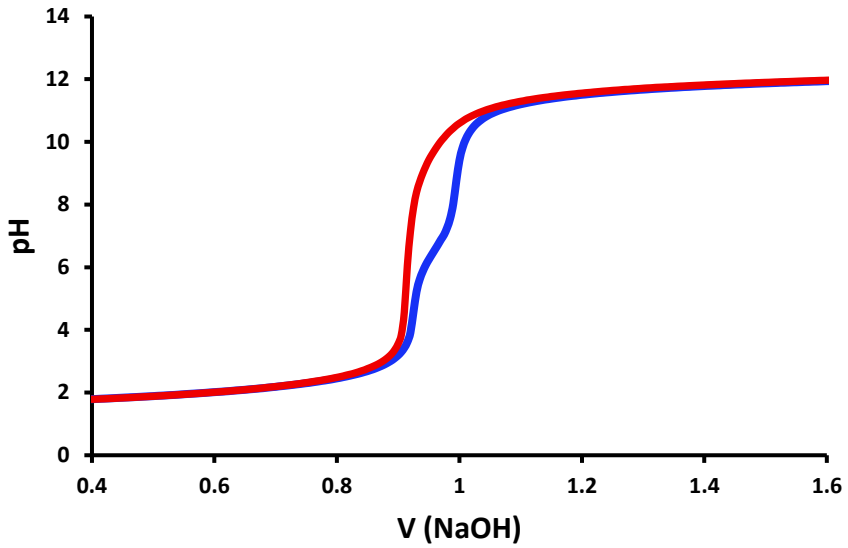

Figure 37 . Titration curves of $[Tl(OPC2A)]^+$ and its mixed [Tl(OPC2A)I] complex ($c_{Tl} = c_{OPC2A} = c_I = 2$ mM, 0.15 M $NaNO_3$, 298 K). Blue curve shows the titration of $[Tl(OPC2A)]^+$ in the absence of iodide and red curve shows it in the presence of iodide.

After mapping the acid-base properties of the $[Tl(OPC2A)]^+$ complexes, we performed pH-potentiometric titration to explore the equilibrium properties of the mixed complexes formed with iodide ion. The redox properties of iodide had to be considered; therefore, iodide was transferred to the solutions as the last step before starting titration. The samples were cooled and purged with nitrogen (N_2) to eliminate any dissolved oxygen before starting the titration. Using pH-potentiometric data, we estimated the stability constants of the [Tl(OPC2A)I] mixed complex by the PSEQUAD program.[80] Figure 37 shows the titration curves, confirming the distinct differences between the two systems. When sample contains iodide, the titration curve does not show a base consumption process as in the pH range 5-8 as in the case of iodide-free system, which suggests that

the [Tl(OPC2A)I] mixed complex is forming.The log$K_{[Tl(OPC2A)I]}$ = 6.0(1) which is comparable to the stability constant of reported [Tl(EDTA)I] with log$K$ = 5.9,[67] and higher than the stability constants of [Tl(CDTA)I], the log$K_{[Tl(CDTA)I]}$ = 5.02 and log$K_{[Tl(CDO2A)I]}$ = 4.39, and lower than log$K_{[Tl(CDTABBA)I]}$ = 6.9.[70]

5.1.2.3.2. Structural study of [Tl(OPC2A)Cl] complex by X-ray diffraction

In order to have more detailed insight into the coordination environment and geometry of the $[Tl(OPC2A)]^+$ complex in the solid state, single-crystal X-ray diffraction studies were performed.

During the equilibrium study, a white precipitate was observed in the bottom of NMR tube, upon preparing a 3 mM solution of $[Tl(OPC2A)]^+$ after mixing 3 mM of Tl(III) , 3.15 mM of OPC2A , 0.1 M HCl and 0.15 M NaCl to maintain constant ionic strength, the precipitate formed within 10 minutes. Single-crystal X-ray diffraction analysis of the precipitate revealed the structure to be $[Tl_2H(OPC2A)_2Cl_2]$ $[TlCl_4]$. In this complex, Tl(III) and Cl^- are present in the coordination sphere of the mixed complex as well as in the counter anion. The "twin" cation, $[Tl_2H(OPC2A)_2Cl_2]^+$, consists of two mixed ligand complex entity partially protonated at one of the carboxylate arms. The ratio of the protonation between the two ligands is about 1/3 to 2/3, as estimated from X-ray data; and the 1 equivalent proton on the two carboxylate groups together counts +1 charge. With the $TlCl_4^-$ anion it gives compound with overall charge zero, eq 58. The molecular structure is shown in Figure 38. In fact this stoichiometry equivalent with the $[C_{15}H_{19.33}ClN_3O_5Tl \cdot C_{15}H_{19.67}ClN_3O_5Tl \cdot Cl_4Tl]$ molecular formula.

$$3[TlCl_4]^- + 2\ H_3OPC2A^+ \longrightarrow [Tl_2H(OPC2A)_2Cl_2]\ [TlCl_4] + 5H^+ + 6\ Cl^- \quad (58)$$

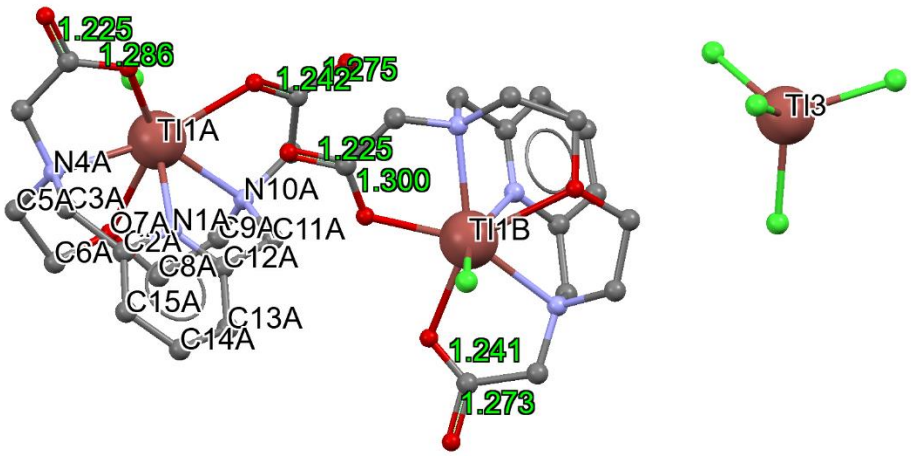

Figure 38 . Structure of $[Tl_2H(OPC2A)_2Cl_2]\ [TlCl_4]$ determined by single-crystal X-ray diffraction.

To prepare single crystals of [Tl(OPC2A)Cl], we employed a slow diffusion method. The parent complex was first prepared in the absence of chloride ions and without the addition of acid (HCl), preparing a sample with $c_{Tl} = c_{OPC2A} = 3$ mM, $c_H \sim 6$ mM. The solution was left for 24 hours to ensure complete complexation. For crystallization, 0.5 ml of the 3 mM $[Tl(OPC2A)]^+$ solution was carefully transferred into a crystallization tube. Then, 0.2 ml of water was gently layered on top as the second layer. Finally, 0.5 ml 3 mM NaCl solution (i.e.1 equivalent) was added as the third layer. Within less than an hour, a white precipitate formed.

This method allowed the formation of [Tl(OPC2A)Cl] through the slow and controlled diffusion of chloride ions into the $[Tl(OPC2A)]^+$ solution,

eq 59, essentially letting the chloride ions gradually interact with the parent complex, leading to crystallization, see Figure 39.

$$[Tl(OPC2A)]^{+} + Cl^{-} \rightleftharpoons [Tl(OPC2A)Cl] \qquad (59)$$

Here both pendant side arms of the OPC2A ligand, which are carboxylic acid groups, are deprotonated, and one water molecule is present in the lattice. The overall charge of the complex is zero, resulting in a neutral complex with formula $C_{15}H_{17}ClN_3O_5Tl \cdot H_2O$. The geometry of [Tl(OPC2A)Cl] is pentagonal bipyramidal.

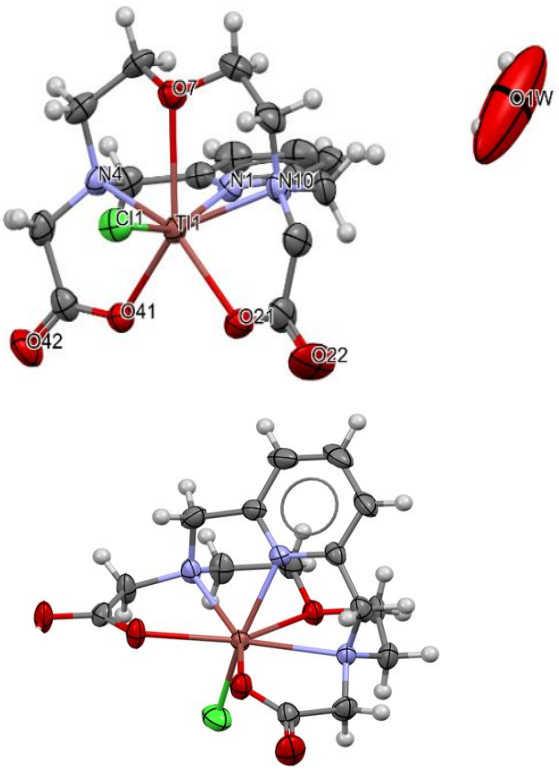

Figure 39. Structure of $[Tl(OPC2A)Cl] \cdot H_2O$ determined by single-crystal X-ray diffraction.

Attempts to obtain similar single crystals using iodide instead of chloride were unsuccessful, there are many rational reasons. We used to play with the composition of complex using different solvents with different ratio, but still none of the methods tested, such as slow evaporation, diffusion-controlled crystallization, changing the iodide concentration, resulted in good quality crystals. The structure of crystals obtained by X-ray confirmed decomplexation of $[Tl(OPC2A)]^+$ with I^- to TlI_4^- and free ligand $(H_3OPC2A)^+$: using different ratios of $[Tl(OPC2A)]^+$ to iodide yielded the same result, Figure 40.

$$TlI_4^- + H_3OPC2A^+ \rightleftharpoons (H_3OPC2A)^+.TlI_4^- \qquad (60)$$

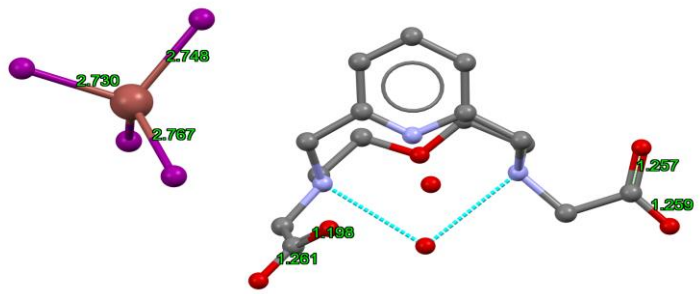

Figure 40. Structure of $[(H_3OPC2A)][TlI_4]$ determined by single-crystal X-ray diffraction.

At the same time, the ^1H NMR spectrum recorded on the mother liquid indicated the presence of $[Tl(OPC2A)]^+$, showing a pattern similar to that presented in Figure 29. Even after precipitation occurred, strong signals corresponding to the complex were still observed, with no detectable signals for the free ligand. It may indicate that the reaction described by Eq 60 was a minor reaction, the driving force could be the very low solubility.

5.2. Kinetic study

5.2.1. Formation of $[M(OPC2A)]^+$ complexes M = Ga(III) and In(III)

Detailed kinetic study of formation reactions was not planned in the time frame of my Ph.D. term, the following two sub-chapters just gave conditional rate constants, k_{obs} for formation and help the planning NMR experiments.

5.2.1.1. Formation of $[Ga(OPC2A)]^+$

Since the substantial spectral changes in UV-vis absorption (attributed to the pyridine ring of the macrocyclic OPC2A ligand), the complex formation can effectively be monitored by UV-Vis spectrophotometry. One can assume that the complexation reactions follow the well-established mechanism for M(III)–macrocycle systems (such as DOTA), which involves the rapid formation of a protonated intermediate in a fast pre-equilibrium step, followed by a slow, base-catalyzed deprotonation and structural rearrangement, that serves as the rate-determining step.[93,94] This intermediate is often referred to as an "out-of-cage complex". In a similar way to the formation of the $[Sc(OPC2A)]^+$ complex, the formation of Ga(III) complexes can also be followed at 275 nm. The results indicate the formation $[Ga(OPC2A)]^+$, see Figure 41 and Figure 43. At pH = 2.42 and 25 °C it takes about 2.5 hours to reach the equilibrium. However, at lower pH values (1.7–1.9), the rate of formation is significantly slower, with equilibrium being reached only after approximately three days. In addition to UV-vis spectroscopy, ^{1}H NMR was also used to monitor the formation of the complex. The presence of two sets of signals in ^{1}H NMR indicates the coexistence of free ligand and complex. The change in their

relative intensities over time reflects the progression of the complex reaction: signals corresponding to the complex gradually increase, while those of the free ligand decrease. ^{71}Ga NMR was also employed to follow complex formation during equilibrium study by quantifying the concentration of free metal ions. The decrease of the signal intensity of the free M(III) ion was monitored as a function of time.

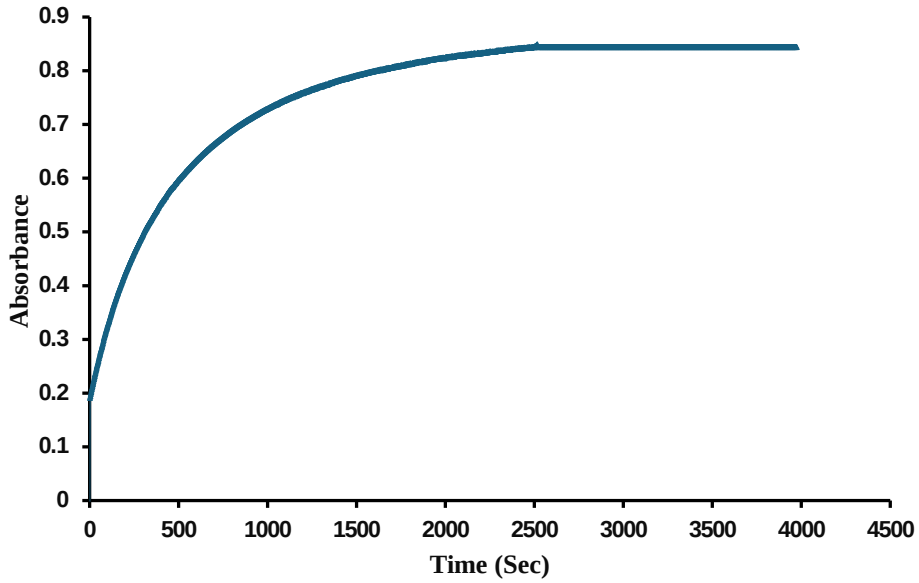

Figure 41. Absorbance vs. time for $[Ga(OPC2A)]^+$ complex formation spectrum at λ = 275 nm, $c_{OPC2A} = c_{Ga}$ = 0.25 mM, I = 1 M $NaNO_3$, pH = 2.42, l = 1cm, T = 298 K.

5.2.1.2. Formation of $[In(OPC2A)]^+$

To investigate the time course of $[In(OPC2A)]^+$ complex formation, similar experiments were performed with In(III) under the same conditions as those used for Sc(III) and Ga(III) complexation with OPC2A. The complexation for the $[In(OPCTA)]^+$ complex at pH = 2.45 and 25 °C takes 1.5 hours to reach the equilibrium; at lower pH values (less than pH 1.7), the rate of formation is slower, with equilibrium being

reached after approximately 36 hours. The spectral changes at wavelength 275 nm over time are shown at Figure 42 and Figure 43. Moreover, we used ^{1}H and ^{71}Ga multinuclear NMR in addition to UV-vis spectroscopy, to monitor the formation of the complex during the equilibrium study, by quantifying the concentration of free metal ions.

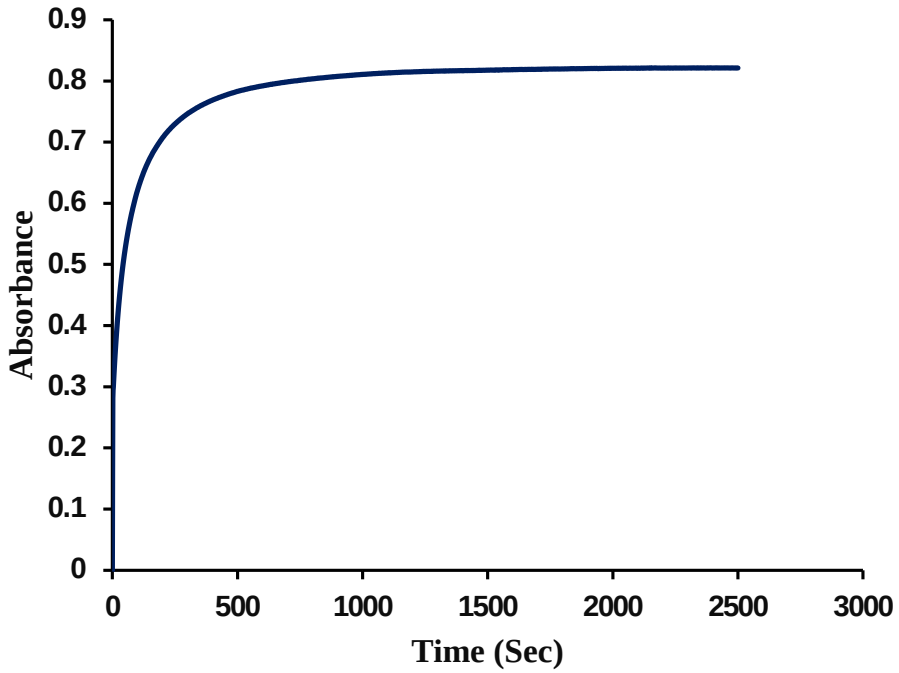

Figure 42. Absorbance vs. time for $[In(OPC2A)]^{+}$ complex formation spectrum at λ = 275 nm, $c_{OPC2A} = c_{In}$ = 0.25 mM, I = 1 M $NaNO_3$, pH = 2.42, l = 1cm, T = 298 K.

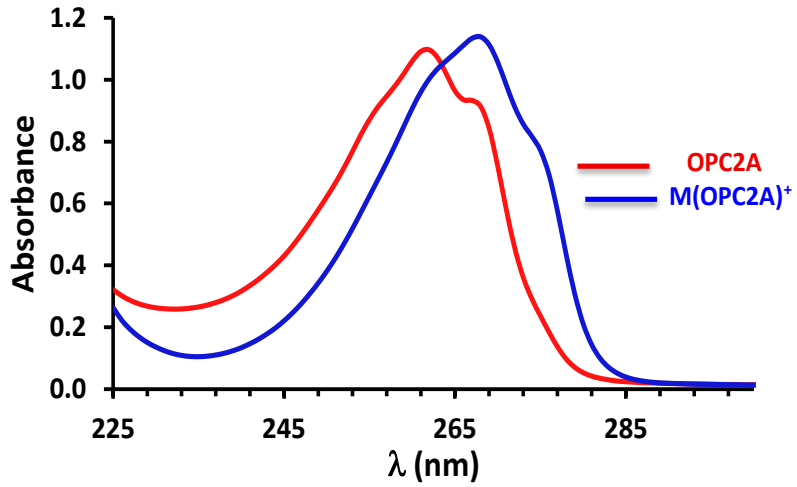

Figure 43. Typical absorption spectra of OPC2A ligands and $[In(OPC2A)]^+$ complex ($c_{OPC2A} = c_{In} = 0.25$ mM, I = 1M $NaNO_3$, pH = 2-3, l = 1cm, T= 298 K.

5.2.2. Acid assisted dissociation of $[M(OPC2A)]^+$ complexes

5.2.2.1. Dissociation of $[Ga(OPC2A)]^+$

To assess the behavior of this complex, the decomplexation of $[Ga(OPC2A)]^+$ was studied in strong acidic solutions. The concentration of added acid to previously prepared complex was in the range of 0.1 -1 M HNO_3. As mentioned above, significant difference is observed in the UV-vis spectra at 275 nm, see Figure 44. The primary absorbance vs. time curves have been fitted by monoexponential function (parameters: k_{obs}, A_o, A_∞, $A_T = A_\infty + (A_o - A_\infty)*Exp^{(-kobs*t)}$ returning k_{obs} (s^{-1}) values. The symbol t represents time, A_o initial absorbance, A_t absorbance at time t and $A\infty$ final absorbance (at $t \rightarrow \infty$) . The k_{obs} vs. $[H^+]$ graph is shown in Figure 45 for $[Ga(OPC2A)]^+$ complex. Evaluation resulted in k_1 = 2.08(6) x 10^{-4} $M^{-1}s^{-1}$ and k_2 = 2.5(1) x 10^{-4} $M^{-2}s^{-1}$ for $[Ga(OPC2A)]^+$ and calculated half-life at 1 M acid concentration, is k_{obs} = 4.58 x10^{-4} s^{-1} , $t_{1/2}$ = 0.42 hr, Table 18.

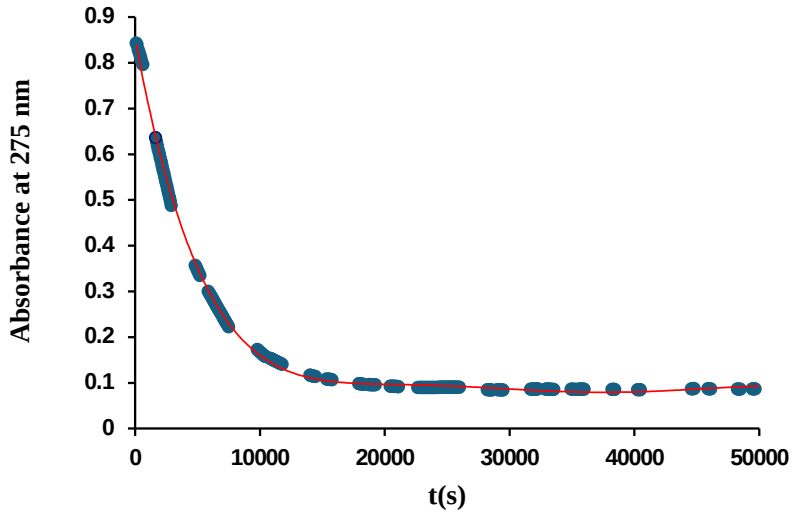

Figure 44 . Absorbance values of $[Ga(OPC2A)]^+$ as a function of time in 0.5 M HNO_3 solution (c_H = 0.5 M, c_{OPC2A} = 0.25 mM c_{Ga} = 0.25 mM, I = 1 M $NaNO_3$, l = 1cm, T = 298 K. (● symbol represents the experimental value while, the solid line — corresponds to the fitted data, 4.58 x10^{-4} s^{-1}

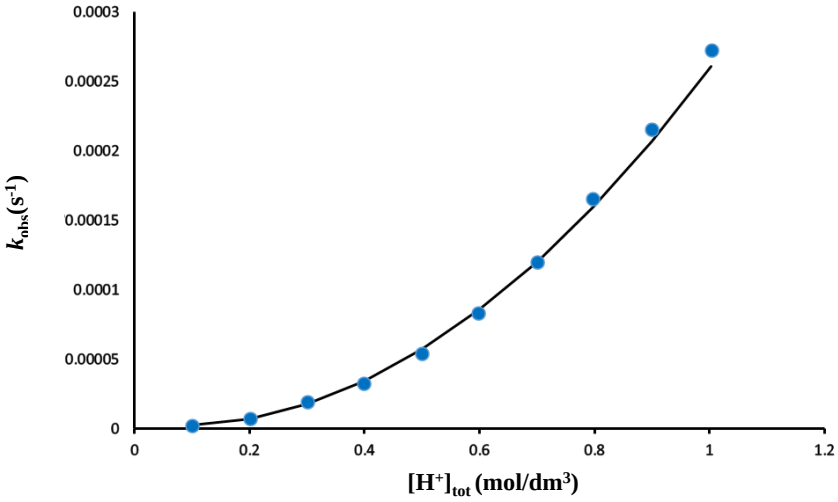

Figure 45 . Pseudo-first-order rate constants (k_{obs}) plotted as a function of $[H^+]_{tot}$ for the dissociation of $[Ga(OPC2A)]^+$ (I = 1.5 M $HNO_3/NaNO_3$, $c_{[Ga(OPC2A)]}$ = 0.25 mM, T = 298 K).

The plots of the rate constants as a function of acid concentration yielded exponential relationships for $[Ga(OPC2A)]^+$ complex, see Figure 45. The k_{obs} values increase with the first- and second-order function of $[H^+]$, which can be expressed as follows:

$$k_{obs} = k_0 + k_1[H^+] + k_2[H^+]^2 \qquad (61)$$

where $k_0 = 0\ s^{-1}$, the intercept characterizes the acid independent part often referred to the spontaneous or the water assisted dissociation, its contribution is negligible. The slopes of corresponding first-order acid catalysis, the rate coefficients characteristic for acid-assisted dissociation ($k_1[H^+]$) the proton-assisted reaction pathway is characterized by a situation where one proton is engaged in the rate-determining step, while $k_2[H^+]^2$ represent second-order acid catalysis, when two steps of protonation of the complex, or formation of a highly reactive diprotonated intermediate occur. $[Ga(OPC2A)]^+$ possess high inertness which is higher than the observed inertness for $[Sc(OPC2A)]^+$. The rate coefficients obtained during the fitting are summarized in Table 18, along with the half-lives calculated from the rate coefficients by using 1 M acid concentration ($t_{½} = \ln 2/k_{obs}$).

Table 18. The rate constants and calculated half-lives for $[Ga(OPC2A)]^+$ and $[Ga(DOTA)]^-$ and $[Ga(DO3AM^{Bu})]^-$ complexes for comparison.

	$[Ga(OPC2A)]^+$	$[Ga(DOTA)]^-$[110]	$[Ga(DO3AM^{Bu})]^-$ [110]
k_1 ($M^{-1}\ s^{-1}$)	**2.08(6) x 10^{-4}**	-	-
k_2 ($M^{-2}\ s^{-1}$)	**2.5(1) x 10^{-4}**	6.0 x 10^{-7}	1.0 x 10^{-6}
$t_{1/2}$ (h) (1 M H^+)	**0.42**	12.2	2.7

5.2.2.2. Dissociation of $[In(OPC2A)]^+$

The experiment's extension to In(III) in order to determine the kinetic parameters has been made by using the same methodology, concentration and acid range. The rate constant of dissociation of $[In(OPC2A)]^+$ complex, see Figure 46 and Figure 47, the k_0 = 0 which means no contribution of water assisted dissociation, first order k_1 ($M^{-1}s^{-1}$) = 2.4(2) x 10^{-4} and second order, k_2 ($M^{-2}s^{-1}$) = 1.3(1) x 10^{-4} and calculated half-life at 1M $[H^+]$ acid, k_{obs} = 3.7 x 10^{-4} s^{-1}, $t_{1/2}$ = 0.52 hr.

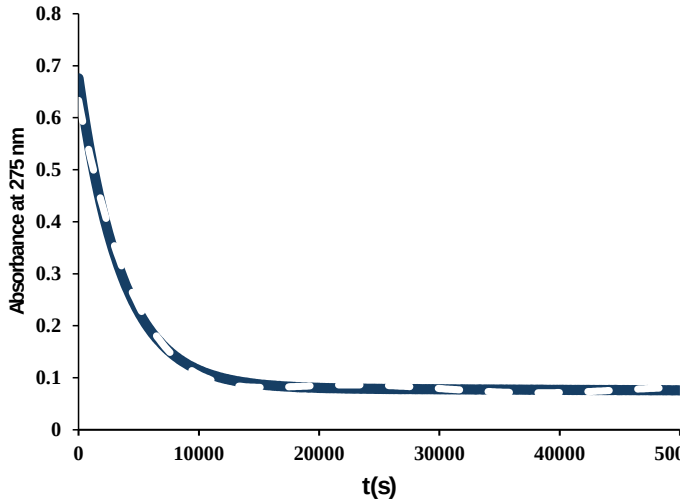

Figure 46 . Absorbance values of $[In(OPC2A)]^+$ as a function of time in 0.5 M HNO_3 solution (c_{H+} = 0.5 M, c_{OPC2A} = 0.25 mM c_{In} = 0.25 mM, I = 1 M $NaNO_3$, l = 1cm, T = 298 K. (Dashed line represents the experimental value while, the solid line —— corresponds to the fitted data, k_{obs} = 3.7 x 10^{-4} s^{-1}).

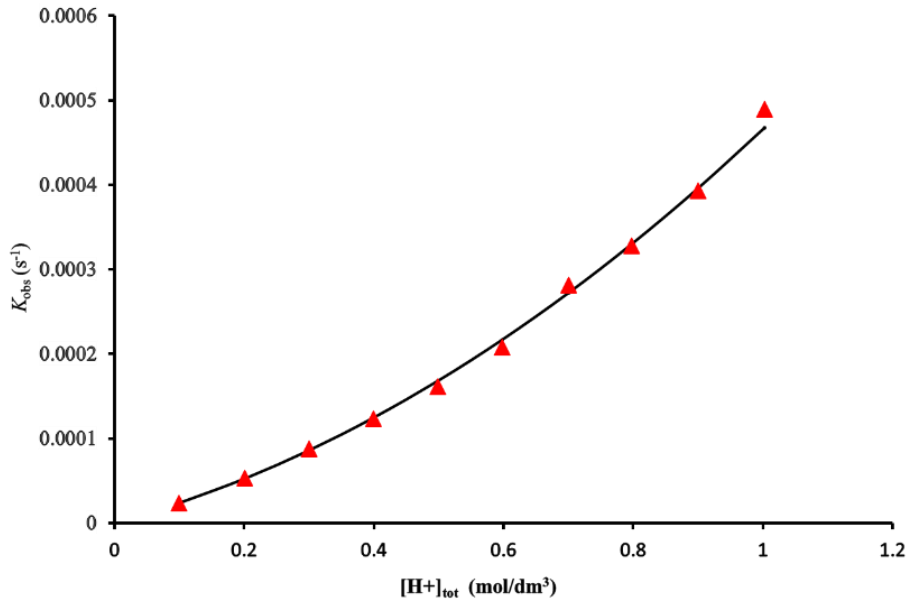

Figure 47. Pseudo-first-order rate constants (k_{obs}) plotted as a function of $[H^+]_{tot}$ for the dissociation of $[In(OPC2A)]^+$ (I = 1.5 M $HNO_3/NaNO_3$, $c_{In(OPC2A)}$ = 0.25 mM, T = 298 K).

The rate of acid-assisted dissociation of the $[Ga(OPC2A)]^+$ complex is in the same order of magnitude as that of the $[In(OPC2A)]^+$ complex, whereas the $[Sc(OPC2A)]^+$ complex dissociate faster with more than one order of magnitude under highly acidic conditions. Altogether all the $[Sc(OPC2A)]^+$, $[Ga(OPC2A)]^+$ and $[In(OPC2A)]^+$ show outstanding inertness required for the *in vivo* studies.

5.2.3. F- exchange of [M(OPC2A)F] complexes

5.2.3.1. [Ga(OPC2A)F] ternary complex

The (DANTE) selective magnetization transfer experiment was performed to investigate the kinetic inertness of the mixed fluoro complex and determine the rate of exchange between the two sites. ^{19}F NMR is able to detect the following mutual chemical exchange process:

$$[Ga(OPC2A)F] + *F^- \rightleftharpoons [Ga(OPC2A)*F] + F^- \qquad (62)$$

The result shows that the chemical exchange between [Ga(OPC2A)F] (site A) and F^- (site B), described by $k+$ and k^-, is slower than the [Sc(OPC2A)F] analogue. The line broadening for bound F^- is less than for [Sc(OPC2A)F] too, which indicates that the exchange is quite slow, see in Appendix Figure A. 20 and Figure A. 21, for the exchange rate of the [Ga(OPC2A) $]^+ - F^-$ system. The k_{obs}^{AB} or $k^+ = 15\ s^{-1}$ (15.9% uncertainty) and k_{obs}^{BA} $k^- = 16\ s^{-1}$.

5.2.3.2. [In(OPC2A)F] ternary complex

The [In(OPC2A)F] system gives the exchange rate with k_{obs}^{AB} or $k^+ = 54.7\ s^{-1}$ and k_{obs}^{BA} $k^- = 53.5$ (4.87 % uncertainty), which is faster than the rate of exchange in Sc(III) and Ga(III) systems, see Appendix Figure A. 22 and Figure A.23. The chemical exchange process in [In(OPC2A)F] system can be expressed by eq 63:

$$[In(OPC2A)F] + *F^- \rightleftharpoons In(OPC2A)*F + F^- \qquad (63)$$

In order to understand these exchange processes, one has to clarify the equilibria in this complicated system, and it requires further experiments.

6. Summary

This thesis discusses coordination chemistry study of M(III) cations of Group 13 elements (Al, Ga, In and Tl) and a lanthanide, Sc(III) with a macrocyclic ligand, OPC2A. The OPC2A is a newly designed macrocyclic ligand derived from the 12 membered DOTA: one nitrogen is incorporated within a pyridine ring to make it more rigid; one carboxylate arm is removed followed by replacing NH with non-protonable ether-oxygen to improve the kinetic inertness, as shown in Scheme 4.

Scheme 4. Structure of 6-Oxa-3,9,15-triazabicyclo (9.3.1) pentadeca-1(15),11,13-triene-3,9-diacetic acid (3,9-OPC2A) ligand.

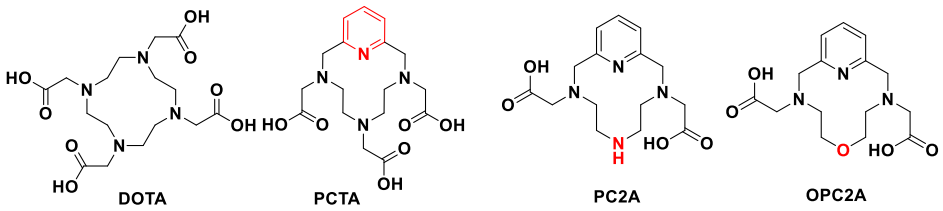

The work includes equilibrium and kinetics studies of the formation and dissociation for the parent complexes, $M(OPC2A)^{+}$, and their mixed complexes, M(OPC2A)X, where M represents Sc(III), Ga(III), In(III) and Tl(III), while X = OH^{-} for Sc(III), In(III) and Tl(III)); X = F^{-} for Sc(III), Ga(III) and In(III)); X = I^{-} and Cl^{-} for Tl(III). These complexes may have potential applications in the medical field, including diagnosis, therapy and/or theranostics with selected radioisotopes (for example based on ^{18}F and ^{44}Sc PET, and $^{44}Sc/^{47}Sc$ matched isotopic pair, respectively). Multinuclear NMR spectroscopy (^{1}H, ^{13}C, ^{19}F and ^{27}Al, ^{45}Sc, ^{71}Ga, ^{111}In, ^{205}Tl), pH-potentiometry, UV-Vis spectroscopy, ESI-MS and single crystal X-ray diffraction methods have been employed for chemical

characterization, followed by a radiolabeling study in case of ^{44}[Sc(OPC2A)]$^{+}$.

The new scientific achievements can be summarized as follows:

I. Scandium (III)

I.1. Equilibrium studies confirmed the formation of a stable [Sc(OPC2A)]$^{+}$ complex ($\log K_{[Sc(OPC2A)]+}$ = 16.72(4) in a reaction which proceeds through the formation and rearrangement of an "out of cage" intermediate.

I.2. The decomplexation reaction follows a $k_{obs} = k_1[H^+] + k_2[H^+]^2$ rate law returning a $t_{1/2}$ = 0.37 h in 1 M HCl, and an unmeasurable long $t_{1/2}$ at pH = 7.4.

I.3. The acid-base properties of [Sc(OPC2A)]$^{+}$ have also been investigated by pH-potentiometry. The titration curve of [Sc(OPC2A)]$^{+}$ indicates formation of the mixed hydroxo [Sc(OPC2A)(OH)] complex. The $\log K_{[Sc(OPC2A)(OH)]}$ = –7.00(4) can likely be associated with the deprotonation of an inner sphere water in the parent [Sc(OPC2A)(H_2O)]$^{+}$ complex.

I.4. The [Sc(OPC2A)F] mixed complex is remarkably stable; $\log K_{[Sc(OPC2A)F]}$ = 4.54(4) and moderately inert against F^--exchange, with k_d^{298} = 16.5 s^{-1} and activation parameters $\Delta H^{\ddagger}$ = 78.1 kJ·mol^{-1}, $\Delta S^{\ddagger}$ = 42.4 J·mol^{-1}K^{-1}, $\Delta G^{\ddagger}298$ = 66 kJ·mol^{-1}.

I.5. The [^{44}Sc] Sc(III)-labelled [Sc(OPC2A)]$^{+}$ forms at 95 °C within 10 minutes but requires purification. The complex remains stable in rat

blood serum for at least 4 hours and exhibits high resistance toward transmetalation and transchelation processes.

I.6. Potentiometric titration data in the pH range of 1.52 to 12.0 showed no evidence of mixed hydroxo species such as [Sc(PC2AAM^{nBu})(OH)]. Attempts to detect [HSc(PC2AAM^{nBu})]$^{2+}$ were also unsuccessful.

I.7. The stability constant log$K_{[Sc(PC2AAM^{nBu})F]}$ = 2.5(1) indicates substantial strong interaction between the Sc(III) macrocyclic complex cation and the fluoride anion.

I.8. The [Sc(PC2AAM^{nBu})(F)] complex is remarkably inert, selective magnetization transfer experiment shows chemical exchange between [Sc(PC2AAM^{nBu})(F)] and F^- or k^+ and k^- values obtained in [Sc(PC2AAM^{nBu})(F)] system are about 30 – 60 times lower than that of [Sc(OPC2A)]$^+$–F^- system. The k_{obs}^{AB} = 0.6 s^{-1} (14% uncertainty).

II. Group 13 M(III) cations

II.1. Al(III) does not form [Al(OPC2A)]$^+$ parent complex under our experimental conditions due to the small size of the cation compared to the cavity of the MC ligand and because of the hydrolytic behavior of Al(III).

II.2. log$K_{[M(OPC2A)]^+}$= 17.2(2) and 17.8(1) for [Ga(OPC2A)]$^+$ and [In(OPC2A)]$^+$ have been measured, respectively. These species are forming slowly in acidic medium, similarly to the corresponding Sc-complex. The formation of [Tl(OPC2A)]$^+$ is likely much faster and complete even under very acidic conditions. Based on model calculations, the estimated stability constant of log$K_{[Tl(OPC2A)]^+} \geq 34$.

II.3. The pH potentiometric titrations may indicate the presence of inner-sphere water molecules in $[In(OPC2A)(H_2O)]^+$ and $[Tl(OPC2A)(H_2O)]^+$ complexes, as these complexes easily form [M(OPC2A)OH] ternary complexes via deprotonation of the inner sphere water, $\log K_{[M(OPC2A)OH]}$ = -5.13(2) and -6.66(2) for M = In and Tl, respectively. However, [Ga(OPC2A)OH] could be detected neither by pH potentiometry nor by ^{1}H-NMR, likely $Ga(OH)_3$ was precipitated out.

II.4. The decomplexation reactions follow a $k_{obs} = k_1[H^+] + k_2[H^+]^2$ rate law. The complexes are outstandingly inert under acidic conditions with rate constants k_1 = 2.08(6) x10^{-4} $M^{-1}s^{-1}$ and k_2 = 2.5(1) x10^{-4} M^{-2} s^{-1} and k_1 = 2.4(2) x 10^{-4} $M^{-1}s^{-1}$, k_2 = 1.3(1) x 10^{-4} $M^{-2}s^{-1}$for $[Ga(OPC2A)]^+$ and $[In(OPC2A)]^+$, respectively. The decomplexation half-time in 1 M HCl is 0.42, and 0.52 hours for $[Ga(OPC2A)]^+$, and $[In(OPC2A)]^+$, respectively, i.e. somewhat better than the relevant time for the Sc(III)-complex.

II.5. [M(OPC2A)F] mixed complexes are formed with $\log K_{[M(OPC2A)F]}$ ~ 3.5(1) and 2.9(2) for M = Ga and In, respectively. In both systems additional F-containing species are detected by ^{19}F NMR, including a tentatively assigned F-bridged dimer, $[In(OPC2A)_2]F^+$.

II.6. [Tl(OPC2A)I] mixed complex with $\log K_{[Tl(OPC2A)I]}$ ~ 6 is detected by pH-potentiometry in solution, while molecular structures using single crystal X-ray analysis were determined for the following solid compounds: [Tl(OPC2A)Cl], $[Tl_2H(OPC2A)_2Cl_2][TlCl_4]$ and $[(H_3OPC2A)][TlI_4]$.

These findings support our conclusions: OPC2A is an excellent ligand platform for the selected M(III) complexation. The parent complexes are able to carry halide anions. These complexes are strongly recommended for further in vivo studies.

7. References

(1) Tircsó, G.; Molnár, E.; Csupász, T.; Garda, Z.; Botár, R.; Kálmán, F. K.; Kovács, Z.; Brücher, E.; Tóth, I. Gadolinium(III)-Based Contrast Agents for Magnetic Resonance Imaging. A Re-Appraisal. In *Metal Ions in Bio-Imaging Techniques*; Walter de Gruyter GmbH, 2021; pp 39–70. https://doi.org/10.1515/9783110685701-008.

(2) Tripier, R.; Tircsó, G.; Platas-Iglesias, C.; Harriswangler, C. Importance of Ligand Design in Lanthanide Azamacrocyclic Complexes Relevant to Biomedical Applications. *Handb. Phys. Chem. Rare Earths* **2022**, *61*, 129–220. https://doi.org/10.1016/BS.HPCRE.2022.05.001.

(3) Thaddeus J. Wadas, E. H. W., Gary R. Weisman, and Carolyn J. Anderson. Coordinating Radiometals of Copper, Gallium, Indium, Yttrium, and Zirconium for PET and SPECT Imaging of Disease. *Chem. Rev.* **2010**, *110* (5), 2858–2902. https://doi.org/10.1021/cr900325h.

(4) Stöcklin, G.; Qaim, S. M.; Rösch, F. The Impact of Radioactivity on Medicine Metallic. *ract* **1995**, *70–71* (Supplement), 249–272. https://doi.org/10.1524/ract.1995.7071.special-issue.249.

(5) Lewis, J. S.; Windhorst, A. D.; Zeglis, B. M. *Radiopharmaceutical Chemistry*, 1st ed.; Springer Cham, 2019. https://doi.org/10.1007/978-3-319-98947-1.

(6) Gold, V.; McNaught, A. *The IUPAC Compendium of Chemical Terminology: The Gold Book*, 5th ed.; International Union of Pure and Applied Chemistry (IUPAC): Research Triangle Park, NC, 2025.

(7) Müller, C.; Bunka, M.; Haller, S.; Köster, U.; Groehn, V.; Bernhardt, P.; van der Meulen, N.; Türler, A.; Schibli, R. Promising Prospects for ^{44}Sc-/^{47}Sc-Based Theragnostics: Application of ^{47}Sc for Radionuclide Tumor Therapy in Mice. *J Nucl Med* **2014**, *55* (10), 1658–1664. https://doi.org/10.2967/jnumed.114.141614.

(8) Pniok, M.; Kubíček, V.; Havlíčková, J.; Kotek, J.; Sabatie-Gogová, A.; Plutnar, J.; Huclier-Markai, S.; Hermann, P. Thermodynamic and Kinetic Study of Scandium(III) Complexes of DTPA and DOTA: A Step Toward Scandium Radiopharmaceuticals. *Chem. – Eur. J.* **2014**, *20* (26), 7944–7955. https://doi.org/10.1002/chem.201402041.

(9) McBride, W. J.; Sharkey, R. M.; Karacay, H.; D'Souza, C. A.; Rossi, E. A.; Laverman, P.; Chang, C.-H.; Boerman, O. C.; Goldenberg, D. M. A Novel Method of 18F Radiolabeling for PET. *J. Nucl. Med.* **2009**, *50* (6), 991–998. https://doi.org/10.2967/jnumed.108.060418.

(10) Whetter, J. N.; Vaughn, B. A.; Koller, A. J.; Boros, E. An Unusual Pair: Facile Formation and In Vivo Validation of Robust Sc–18F Ternary Complexes for Molecular Imaging. *Angew. Chem. Int. Ed.* **2021**, *61* (7), e202114203. https://doi.org/10.1002/anie.202114203.

(11) Archibald, S. J.; Allott, L. Correction to: The Aluminium-[^{18}F]Fuoride Revolution: Simple Radiochemistry with a Big Impact for Radiolabelled Biomolecules. *EJNMMI Radiopharm. Chem.* **2021**, *6* (1), 32. https://doi.org/10.1186/s41181-021-00148-7.

(12) Monica, H.; Nordstrom, B. *Transition Metals*, Second Edition.; Infobase Publishing: New York, 2019.

(13) Giunta, C. J.; Mainz, V. V.; Girolami, G. S. *150 Years of the Periodic Table: A Commemorative Symposium*; Perspectives on the history of chemistry; Springer: Cham, 2021.

(14) Koumarianou, E.; Pawlak, D.; Korsak, A.; Mikolajczak, R. Comparison of Receptor Affinity of natSc-DOTA-TATE versus natGa-DOTA-TATE. *Nucl. Med. Rev. Cent. East. Eur.* **2011**, *14* (2), 85–89. https://doi.org/10.5603/NMR.2011.00021.

(15) Paul L. Brown; Christian Ekberg. *Hydrolysis of Metal Ions*; Wiley-VCH Verlag GmbH & Co. KGaA, 2016. https://doi.org/10.1002/9783527656189.

(16) Wood, S. A.; Samson, I. M. The Aqueous Geochemistry of Gallium, Germanium, Indium and Scandium. *Ore Geol. Rev.* **2006**, *28* (1), 57–102. https://doi.org/10.1016/j.oregeorev.2003.06.002.

(17) Baes, C. F.; Mesmer, R. E. *In The Hydrolysis of Cations*; Wiley, New York, 1976.

(18) Pearson, R. G. Hard and Soft Acids and Bases, HSAB, Part 1: Fundamental Principles. *J. Chem. Educ.* **1968**, *45* (9), 581. https://doi.org/10.1021/ed045p581.

(19) Meehan, P. R.; Aris, D. R.; Willey, G. R. Structural Chemistry of Sc(III): An Overview. *Coord. Chem. Rev.* **1999**, *181* (1), 121–145. https://doi.org/10.1016/s0010-8545(98)00214-8.

(20) Lindqvist-Reis, P.; Persson, I.; Sandström, M. Structure of Solvated Metal Ions: Solution and Crystal Structure of Ga^{3+}, In^{3+}, Sc^{3+}, Y^{3+}, La^{3+} and Ca^{2+} Ions with Water and Non-Aqueous Oxygen Donor Solvents. *Dalton Trans* **2006**, No. 32, 3868–3878. https://doi.org/10.1039/b604267h.

(21) Stotz, R. W.; Melson, G. A. Preparation and Mechanism of Formation of Anhydrous Scandium(III) Chloride and Bromide. *Inorg. Chem.* **1972**, *11* (7), 1720–1721. https://doi.org/10.1021/ic50113a058.

(22) Alliot, C.; Kerdjoudj, R.; Michel, N.; Haddad, F.; Huclier-Markai, S. Cyclotron Production of High Purity 44m,44Sc with Deuterons from $^{44}CaCO_3$ Targets. *Nucl. Med. Biol.* **2015**, *42* (6), 524–529. https://doi.org/10.1016/j.nucmedbio.2015.03.002.

(23) Huclier-Markai, S.; Sabatie, A.; Ribet, S.; Kubícek, V.; Paris, M.; Vidaud, C.; Hermann, P.; Cutler, C. S. Chemical and Biological Evaluation of Scandium(III) -Poly amino poly carboxylate Complexes as Potential PET Agents and Radiopharmaceuticals. *Radiochim. Acta* **2011**, *99* (10), 653–662. https://doi.org/10.1524/ract.2011.1869.

(24) Byegård, J.; Skarnemark, G.; Skålberg, M. The Stability of Some Metal EDTA, DTPA and DOTA Complexes: Application as Tracers in Groundwater Studies. *J. Radioanal. Nucl. Chem.* **1999**, *241* (2), 281–290. https://doi.org/10.1007/bf02347463.

(25) Majkowska, A.; Neves, M.; Antunes, I.; Bilewicz, A. Complexes of Low Energy Beta Emitters ^{47}Sc and ^{177}Lu with Zoledronic Acid for Bone Pain Therapy. *Appl. Radiat. Isot.* **2009**, *67* (1), 11–13. https://doi.org/10.1016/j.apradiso.2008.08.014.

(26) Majkowska-Pilip, A.; Bilewicz, A. Macrocyclic Complexes of Scandium Radionuclides as Precursors for Diagnostic and Therapeutic Radiopharmaceuticals. *J. Inorg. Biochem.* **2011**, *105* (2), 313–320. https://doi.org/10.1016/j.jinorgbio.2010.11.003.

(27) Edelmann, F. T. 2 - Scandium, Yttrium, and the Lanthanide and Actinide Elements, Excluding Their Zero Oxidation State Complexes. In *Comprehensive Organometallic Chemistry II*; Elsevier Ltd, 1995; pp 11–212. https://doi.org/10.1016/B978-008046519-7.00026-5.

(28) Xue, Z.-L.; Cook, T. M. Solution NMR of Transition Metal Complexes. In *Reference Module in Chemistry, Molecular Sciences and Chemical Engineering*; Elsevier Inc, 2013. https://doi.org/10.1016/B978-0-12-823144-9.00051-0.

(29) Mikolajczak, R.; Huclier-Markai, S.; Alliot, C.; Haddad, F.; Szikra, D.; Forgacs, V.; Garnuszek, P. Production of Scandium Radionuclides for Theranostic Applications: Towards Standardization of Quality Requirements. *EJNMMI Radiopharm. Chem.* **2021**, *6* (1), 19–19. https://doi.org/10.1186/s41181-021-00131-2.

(30) Nagy, G.; Szikra, D.; Trencsényi, G.; Fekete, A.; Garai, I.; Giani, A. M.; Negri, R.; Masciocchi, N.; Maiocchi, A.; Uggeri, F.; Tóth, I.; Aime, S.; Giovenzana, G. B.; Baranyai, Z. AAZTA: An Ideal Chelating Agent for the Development of ^{44}Sc PET Imaging Agents. *Angew. Chem. Int. Ed.* **2017**, *56* (8), 2118–2122. https://doi.org/10.1002/anie.201611207.

(31) Kury, J. W.; Paul, A. D.; Hepler, L. G.; Connick, R. E. The Fluoride Complexing of Scandium(III) in Aqueous Solution: Free Energies, Heats and Entropies. *J. Am. Chem. Soc.* **1959**, *81* (16), 4185–4189. https://doi.org/10.1021/ja01525a018.

(32) Mattoni, S.; Paccagnella, A.; Fanti, S. The Role of Fluorine-18-Fluorodeoxyglucose-Positron Emission Tomography/Computed Tomography (^{18}F-FDG-PET/CT) in Staging and Restaging of Patients with Uterine Sarcomas: A Systematic Review. *Gynecol. Pelvic Med.* **2022**, *5*, 7–7. https://doi.org/10.21037/gpm-20-76.

(33) van der Meulen, N. P.; Bunka, M.; Domnanich, K. A.; Müller, C.; Haller, S.; Vermeulen, C.; Türler, A.; Schibli, R. Cyclotron Production of 44Sc: From Bench to Bedside. *Nucl. Med. Biol.* **2015**, *42* (9), 745–751. https://doi.org/10.1016/j.nucmedbio.2015.05.005.

(34) Zhernosekov, K. P.; Filosofov, D. V.; Baum, R. P.; Aschoff, P.; Bihl, H.; Razbash, A. A.; Jahn, M.; Jennewein, M.; Rosch, F. Processing of Generator-Produced 68Ga for Medical Application. *J. Nucl. Med.* **2007**, *48* (10), 1741–1748. https://doi.org/10.2967/jnumed.107.040378.

(35) Schmidt, C. E.; Gajecki, L.; Deri, M. A.; Sanders, V. A. Current State of ^{44}Ti/^{44}Sc Radionuclide Generator Systems and Separation Chemistry. *Curr. Radiopharm.* **2023**, *16* (2), 95–106. https://doi.org/10.2174/1874471016666221111154424.

(36) Chakravarty, R.; Goel, S.; Valdovinos, H. F.; Hernandez, R.; Hong, H.; Nickles, R. J.; Cai, W. Matching the Decay Half-Life with the Biological Half-Life: ImmunoPET Imaging with ^{44}Sc-Labeled Cetuximab Fab Fragment. *Bioconjug. Chem.* **2014**, *25* (12), 2197–2204. https://doi.org/10.1021/bc500415x.

(37) Kostelnik, T. I.; Orvig, C. Radioactive Main Group and Rare Earth Metals for Imaging and Therapy. *Chem. Rev.* **2019**, *119* (2), 902–956. https://doi.org/10.1021/acs.chemrev.8b00294.

(38) Martell, A. E.; Hancock, R. D. *Metal Complexes in Aqueous Solutions*, 1996th ed.; Modern Inorganic Chemistry; Springer, 2013.

(39) Green, M. A.; Welch, M. J. Gallium Radiopharmaceutical Chemistry. *Int. J. Rad. Appl. Instrum. B* **1989**, *16* (5), 435,445-443,448. https://doi.org/10.1016/0883-2897(89)90053-6.
(40) Greenwood, N. N. The Chemistry of Gallium. In *Advances in Inorganic Chemistry and Radiochemistry*; Elsevier Science & Technology: United States, 1963; Vol. 5, pp 91–134. https://doi.org/10.1016/S0065-2792(08)60153-3.
(41) Richens, D. T. *The Chemistry of Aqua Ions: Synthesis, Structure and Reactivity; a Tour through the Periodic Table of the Elements*; Wiley: Chichester, 1997.
(42) Kulprathipanja, S.; Hnatowich, D. J. A Method for Determining the pH Stability Range of Gallium Radiopharmaceuticals. *Int. J. Appl. Radiat. Isot.* **1977**, *28* (1), 229–233. https://doi.org/10.1016/0020-708X(77)90176-4.
(43) Davidovich, R.; Fedorov, P.; Popov, A. Structural Chemistry of Fluoride and Mixed-Ligand Fluoride Complexes of Gallium(III). *Rev. Inorg. Chem.* **2017**, *37* (3–4), 147–184. https://doi.org/10.1515/revic-2017-0010.
(44) Wadas, T. J.; Wong, E. H.; Weisman, G. R.; Anderson, C. J. Coordinating Radiometals of Copper, Gallium, Indium, Yttrium, and Zirconium for PET and SPECT Imaging of Disease. *Chem. Rev.* **2010**, *110* (5), 2858–2902. https://doi.org/10.1021/cr900325h.
(45) Anderegg, G.; Arnaud-Neu, F.; Delgado, R.; Felcman, J.; Popov, K. Critical Evaluation of Stability Constants of Metal Complexes of Complexones for Biomedical and Environmental Applications* (IUPAC Technical Report). *Pure Appl. Chem.* **2005**, *77* (8), 1445–1495. https://doi.org/10.1351/pac200577081445.
(46) Jung, W.-S.; Chung, Y. K.; Shin, D. M.; Kim, S.-D. Crystal- and Solution-Structure Characteristics of Ethylenediaminetetraacetato aluminate(III) and Gallate(III). *Bull. Chem. Soc. Jpn.* **2002**, *75* (6), 1263–1267. https://doi.org/10.1246/bcsj.75.1263.
(47) Jószai, R.; Purgel, M.; Pápai, I.; Wakita, H.; Tóth, I. Multinuclear NMR and DFT Studies of the Structure and Fluxionality for MIII–Ethylenediamine-Tetraacetate Complexes (M(EDTA)−, M=Al, Ga and In) in Solution. *J. Mol. Liq.* **2007**, *131–132*, 72–80. https://doi.org/10.1016/j.molliq.2006.08.030.
(48) Davey, P. R. W. J.; Paterson, B. M. Modern Developments in Bifunctional Chelator Design for Gallium Radiopharmaceuticals. *Molecules* **2022**, *28* (1), 203. https://doi.org/10.3390/molecules28010203.

(49) Kato, C.; Moynier, F.; Foriel, J.; Teng, F.-Z.; Puchtel, I. S. The Gallium Isotopic Composition of the Bulk Silicate Earth. *Chem. Geol.* **2017**, *448*, 164–172. https://doi.org/10.1016/j.chemgeo.2016.11.020.

(50) Zhou, Q.; Henoumont, C.; Vander Elst, L.; Laurent, S.; Muller, R. N. NMR Determination of Free Gallium(III) Ions in Aqueous Solutions of Ga Complexes, "Cold" Analogs of PET/SPECT Tracers. *Contrast Media Mol. Imaging* **2011**, *6* (3), 165–167. https://doi.org/10.1002/cmmi.441.

(51) Roesch, F. Scandium-44: Benefits of a Long-Lived PET Radionuclide Available from the ^{44}Ti/^{44}Sc Generator System. *Curr. Radiopharm.* **2012**, *5* (3), 187–201. https://doi.org/10.2174/1874471011205030187.

(52) Pneumaticos, S. G.; Chatziioannou, S. N.; Moore, W. H.; Johnson, M. The Role of Radionuclides in Primary Musculoskeletal Tumors beyond the 'Bone Scan.' *Crit. Rev. Oncol. Hematol.* **2001**, *37* (3), 217–226. https://doi.org/10.1016/s1040-8428(00)00106-2.

(53) Haynes, W. M.; Lide, D. R.; Bruno, T. J., Eds. *CRC Handbook of Chemistry and Physics,* 97th ed.; CRC Press: Boca Raton London New York, 2016.

(54) Caminiti, R.; Johansson, G.; Tóth, I.; Pohjola, S.; Niinistö, L.; Volden, H. V.; Weidlein, J.; Zingaro, R. A. On the Structures of Polynuclear Hydrolysis Complexes of Indium(III) in Aqueous Solution. *Acta Chem. Scand.* **1986**, *40a*, 435–440. https://doi.org/10.3891/acta.chem.scand.40a-0435.

(55) Benjamin, S. L.; Levason, W.; Reid, G. Medium and High Oxidation State Metal/Non-Metal Fluoride and Oxide–Fluoride Complexes with Neutral Donor Ligands. *Chem Soc Rev* **2013**, *42* (4), 1460–1499. https://doi.org/10.1039/c2cs35263j.

(56) Petrosyants, S. P.; Ilyukhin, A. B. Organometallic Polymers MF_3(4,4′-Bipy) with M = Ga and In. *Russ. J. Inorg. Chem.* **2010**, *55* (1), 30–33. https://doi.org/10.1134/s0036023610010079.

(57) Sevastianova, T. N.; Davydova, E. I.; Kazakov, I. V.; Timoshkin, A. Yu. Crystal Structures and Thermal Behavior of Complexes of Group 13 Metal Halides with Pyridine-Type Ligands. *Russ. Chem. Bull.* **2015**, *64* (11), 2523–2535. https://doi.org/10.1007/s11172-015-1188-8.

(58) Davidovich, R. L.; Logvinova, V. B.; Tkachev, V. V.; Shilov, G. V. Mixed-Ligand Fluorooxalate Complex Compounds of Indium(III) M2[$InF_3(C_2O_4)H_2O$] (M = K, Rb): Synthesis and Crystal Structure.

J. Struct. Chem. **2017**, *58* (1), 207–210. https://doi.org/10.1134/s0022476617010309.

(59) Subramanian, K. M.; Wolf, W. A New Radiochemical Method to Determine the Stability Constants of Metal Chelates Attached to a Protein. *J. Nucl. Med. Off. Publ. Soc. Nucl. Med.* **1990**, *31* (4), 480–488.

(60) Baranyai, Z.; Tircsó, G.; Rösch, F. The Use of the Macrocyclic Chelator DOTA in Radiochemical Separations. *Eur. J. Inorg. Chem.* **2020**, *2020* (1), 36–56. https://doi.org/10.1002/ejic.201900706.

(61) Gunn Gus. Indium. In *Critical Metals Handbook*; John Wiley & Sons: United Kingdom, 2014; p 1. https://doi.org/10.1002/9781118755341.ch9.

(62) Lawerence, R. E.; Westbrook, L. R. INDIUM OCCURRENCE, RECOVERY, AND USES. *Ind. Eng. Chem.* **1938**, *30* (6), 611–621. https://doi.org/10.1021/ie50342a003.

(63) McKillop, A.; Smith, J. D.; Worrall, I. J. *Organometallic Compounds of Aluminum, Gallium, Indium, and Thallium*; Chapman and Hall: London, 1985.

(64) Ma, T.; Yang, P.; Parris, J. M.; Csupász, T.; Li, M.-X.; Bányai, I.; Tóth, I.; Lin, Z.; Kortz, U. Indium in Polyoxopalladate(II) Chemistry: Synthesis of All-Acetate-Capped $[InPd_{12}O_8(OAc)_{16}]^{5-}$ and Controlled Transformation to Phosphate-Capped Double-Cube and Monocube. *Inorg. Chem.* **2019**, *58* (23), 15864–15871. https://doi.org/10.1021/acs.inorgchem.9b02282.

(65) Chatalic, K. L. S.; Veldhoven-Zweistra, J.; Bolkestein, M.; Hoeben, S.; Koning, G. A.; Boerman, O. C.; de Jong, M.; van Weerden, W. M. A Novel 111In-Labeled Anti–Prostate-Specific Membrane Antigen Nanobody for Targeted SPECT/CT Imaging of Prostate Cancer. *J. Nucl. Med.* **2015**, *56* (7), 1094–1099. https://doi.org/10.2967/jnumed.115.156729.

(66) Tóth, I.; Győri, B. *Thallium: Inorganic Chemistry*; John Wiley & Sons, Ltd: Chichester, UK, 2011. https://doi.org/10.1002/9781119951438.eibc0224.

(67) Tóth, I.; Brücher, E.; Zékány, L.; Veksin, V. Equilibrium Studies on the AlIII-, GaIII-, InIII- and TlIII-Ethylenediaminetetraacetate-Halide and -Sulphide Systems. *Polyhedron* **1989**, *8* (16), 2057–2064. https://doi.org/10.1016/S0277-5387(00)80504-5.

(68) Fodor, T.; Bányai, I.; Bényei, A.; Platas-Iglesias, C.; Purgel, M.; Horváth, G. L.; Zékány, L.; Tircsó, G.; Tóth, I. $[Tl^{III}(Dota)]^-$: An Extraordinarily Robust Macrocyclic Complex. *Inorg. Chem.* **2015**,

54 (11), 5426–5437. https://doi.org/10.1021/acs.inorgchem.5b00458.
(69) Fodor, T. Robust Thallium(III) Complexes with Inorganic and Organic Multidentate Ligands, University of Debrecen, Debercen, 2016.
(70) Farkas, E. Equilibrium and kinetic studies of Al(III)-, Ga(III)- and Tl(III)-aminopolycarboxylate complexes with hydroxo- and halogeno-mixed ligands, University of debercen, Debrecen, 2019.
(71) Cvjetko, P.; Cvjetko, I.; Pavlica, M. Thallium Toxicity in Humans. *Arch. Ind. Hyg. Toxicol.* **2010**, *61* (1), 111–119. https://doi.org/10.2478/10004-1254-61-2010-1976.
(72) Firth, G.; Blower, J. E.; Bartnicka, J. J.; Mishra, A.; Michaels, A. M.; Rigby, A.; Darwesh, A.; Al-Salemee, F.; Blower, P. J. Non-Invasive Radionuclide Imaging of Trace Metal Trafficking in Health and Disease: "PET Metallomics." *RSC Chem. Biol.* **2022**, *3* (5), 495–518. https://doi.org/10.1039/d2cb00033d.
(73) Hijnen, N. M.; De Vries, A.; Blange, R.; Burdinski, D.; Grüll, H. Synthesis and in Vivo Evaluation of ^{201}Tl(III)–DOTA Complexes for Applications in SPECT Imaging. *Nucl. Med. Biol.* **2011**, *38* (4), 585–592. https://doi.org/10.1016/j.nucmedbio.2010.10.009.
(74) Rigby, A.; Firth, G.; Rivas, C.; Pham, T.; Kim, J.; Phanopoulos, A.; Wharton, L.; Ingham, A.; Li, L.; Ma, M. T.; Orvig, C.; Blower, P. J.; Terry, S. Y. A.; Abbate, V. Toward Bifunctional Chelators for Thallium-201 for Use in Nuclear Medicine. *Bioconjug. Chem.* **2022**, *33* (7), 1422–1436. https://doi.org/10.1021/acs.bioconjchem.2c00284.
(75) Pagnanelli, R. A.; Basso, D. A. Myocardial Perfusion Imaging with 201Tl. *J. Nucl. Med. Technol.* **2010**, *38* (1), 1–3. https://doi.org/10.2967/jnmt.109.068593.
(76) Csupász, T.; Szücs, D.; Kálmán, F. K.; Hollóczki, O.; Fekete, A.; Szikra, D.; Tóth, É.; Tóth, I.; Tircsó, G. A New Oxygen Containing Pyclen-Type Ligand as a Manganese(II) Binder for MRI and 52Mn PET Applications: Equilibrium, Kinetic, Relaxometric, Structural and Radiochemical Studies. *Molecules* **2022**, *27* (2), 371–398. https://doi.org/10.3390/molecules27020371.
(77) Sajó, I. *komplexometria*; Műszaki Könyvkiadó: Budapest, 1962.
(78) Morris, G. A.; Freeman, R. Selective Excitation in Fourier Transform Nuclear Magnetic Resonance. *J. Magn. Reson.* **1978**, *29* (3), 433–462. https://doi.org/10.1016/0022-2364(78)90003-3.
(79) Irving, H. M.; Miles, M. G.; Pettit, L. D. A Study of Some Problems in Determining the Stoicheiometric Proton Dissociation Constants

of Complexes by Potentiometric Titrations Using a Glass Electrode. *Anal. Chim. Acta* **1967**, *38*, 475–488. https://doi.org/10.1016/s0003-2670(01)80616-4.

(80) L. Zekany; I. Nagypal. PSEQUAD. *Comput. Methods Determ. Form. Constants* **1985**, No. Journal Article, 291–353. https://doi.org/10.1007/978-1-4684-4934-1_8.

(81) Krause, L.; Herbst-Irmer, R.; Sheldrick, G. M.; Stalke, D. Comparison of Silver and Molybdenum Microfocus X-Ray Sources for Single-Crystal Structure Determination. *J. Appl. Crystallogr.* **2015**, *48* (1), 3–10. https://doi.org/10.1107/S1600576714022985.

(82) Garda, Z.; Molnár, E.; Hamon, N.; Barriada, J. L.; Esteban-Gómez, D.; Váradi, B.; Nagy, V.; Pota, K.; Kálmán, F. K.; Tóth, I.; Lihi, N.; Platas-Iglesias, C.; Tóth, É.; Tripier, R.; Tircsó, G. Complexation of Mn(II) by Rigid Pyclen Diacetates: Equilibrium, Kinetic, Relaxometric, Density Functional Theory, and Superoxide Dismutase Activity Studies. *Inorg. Chem.* **2021**, *60* (2), 1133–1148. https://doi.org/10.1021/acs.inorgchem.0c03276.

(83) Söylemez, Z.; Özer, U. Y. Mixed Ligand Chelates of Scandium(III) in Aqueous Solution. *J. Inorg. Nucl. Chem.* **1973**, *35* (2), 545–553. https://doi.org/10.1016/0022-1902(73)80568-8.

(84) Kálmán, F. K.; Tircsó, G. Kinetic Inertness of the Mn 2+ Complexes Formed with AAZTA and Some Open-Chain EDTA Derivatives. *Inorg. Chem.* **2012**, *51* (19), 10065–10067. https://doi.org/10.1021/ic300832e.

(85) Aldrich, K. E.; Popov, I. A.; Root, H. D.; Batista, E. R.; Greer, S. M.; Kozimor, S. A.; Lilley, L. M.; Livshits, M. Y.; Mocko, V.; Janicke, M. T.; Scott, B. L.; Stein, B. W.; Yang, P. Synthesis, Solid-State, Solution, and Theoretical Characterization of an “in-Cage” Scandium-NOTA Complex. *Dalton Trans. Int. J. Inorg. Chem.* **2022**, *51* (26), 9994–15. https://doi.org/10.1039/d1dt03887g.

(86) Király, R.; Tóth, I.; Brücher, E. Aminopolycarboxylates of Rare Earths—VI: Determination of Stability Constants and Formation Enthalpies of Rare Earth(III)—Ethylenediamine Tetraacetate—Fluoride Mixed Ligand Complexes. *J. Inorg. Nucl. Chem.* **1981**, *43* (2), 345–349. https://doi.org/10.1016/0022-1902(81)90021-X.

(87) Risolo, L.; Ricci, M.; Lalli, D.; Platas-Iglesias, C.; Botta, M. Fluoride Binding in Unlikely Partners: The Formation of Anion–Anion Complexes with [M(EGTA)] − and [M(OBETA)] − (M = Gd^{3+} , Y^{3+}). *Inorg. Chem. Front.* **2025**, *12* (3), 1187–1199. https://doi.org/10.1039/D4QI02908A.

(88) Vaughn, B. A.; Ahn, S. H.; Aluicio-Sarduy, E.; Devaraj, J.; Olson, A. P.; Engle, J.; Boros, E. Chelation with a Twist: A Bifunctional Chelator to Enable Room Temperature Radiolabeling and Targeted PET Imaging with Scandium-44. *Chem. Sci. Camb.* **2020**, *11* (2), 333–342. https://doi.org/10.1039/c9sc04655k.

(89) Dioury, F.; San, C.; Gnanalingam, G.; Henoumont, C.; Rousselin, Y.; Haouz, A.; Shepard, W.; Hosten, B.; Vijayakumar, K.; Laurent, S.; Port, M. Bifunctional Hexadentate Pyclen–Based Chelating Agent for Mild Radiofluorination in Aqueous Solution at Room Temperature with a Ga-18F Ternary Complex. *Chem. Eur. J.* **2024**, *30* (68), e202403358. https://doi.org/10.1002/chem.202403358.

(90) Callegari, E.; Martinelli, J.; Guidolin, N.; Boccalon, M.; Baranyai, Z.; Tei, L. Thermodynamic and Kinetic Stabilities of Al(III) Complexes with N2O3 Pentadentate Ligands. *Mol. Basel Switz.* **2023**, *28* (9), 3764. https://doi.org/10.3390/molecules28093764.

(91) Yuchi, A.; Hotta, H.; Wada, H.; Nakagawa, G. Mixed Ligand Complexes of Trivalent Metal Ions with an Amine-N-Polycarboxylate and Fluoride. *Bull. Chem. Soc. Jpn.* **1987**, *60* (4), 1379–1382. https://doi.org/10.1246/bcsj.60.1379.

(92) Nemes, J.; Tóth, I.; Zékány, L. Formation Kinetics of an Aluminum(III)-Ethylenedinitrilotetraacetate-Fluoride Mixed Ligand Complex. *Dalton Trans.* **1998**, No. 16, 277–2714. https://doi.org/10.1039/a802603c.

(93) Toth, E.; Brucher, E.; Lazar, I.; Toth, I. Kinetics of Formation and Dissociation of Lanthanide(III)-DOTA Complexes. *Inorg. Chem.* **1994**, *33* (18), 4070–4076. https://doi.org/10.1021/ic00096a036.

(94) Pérez-Malo, M.; Szabó, G.; Eppard, E.; Vagner, A.; Brücher, E.; Tóth, I.; Maiocchi, A.; Suh, E. H.; Kovács, Z.; Baranyai, Z.; Rösch, F. Improved Efficacy of Synthesizing MIII-Labeled DOTA Complexes in Binary Mixtures of Water and Organic Solvents. A Combined Radio- and Physicochemical Study. *Inorg. Chem.* **2018**, *57* (10), 6107–6117. https://doi.org/10.1021/acs.inorgchem.8b00669.

(95) Burai, L.; Fábián, I.; Király, R.; Szilágyi, E.; Brücher, E. Equilibrium and Kinetic Studies on the Formation of the Lanthanide(III) Complexes, $[Ce(Dota)]^-$ and $[Yb(Dota)]^-$ (H4dota = 1,4,7,10-Tetraazacyclododecane-1,4,7,10-Tetraacetic Acid). *Dalton Trans.* **1998**, No. 2, 243–248. https://doi.org/10.1039/a705158a.

(96) Szilágyi, E.; Tóth, É.; Kovács, Z.; Platzek, J.; Radüchel, B.; Brücher, E. Equilibria and Formation Kinetics of Some Cyclen

Derivative Complexes of Lanthanides. *Inorganica Chim. Acta* **2000**, *298* (2), 226–234. https://doi.org/10.1016/S0020-1693(99)00467-3.

(97) Anderegg, G. Critical Survey of Stability Constants of NTA Complexes. *Pure Appl. Chem.* **1982**, *54* (12), 2693–2758. https://doi.org/10.1351/pac198254122693.

(98) Bodor, A.; Tóth, I.; Bányai, I.; Szabó, Z.; Hefter, G. T. 19F NMR Study of the Equilibria and Dynamics of the Al^{3+}/F^{-} System. *Inorg. Chem.* **2000**, *39* (12), 2530–2537. https://doi.org/10.1021/ ic991248w.

(99) Bond, A. M.; Hefter, G. T. *Critical Survey of Stability Constants and Related Thermodynamic Data of Fluoride Complexes in Aqueous Solution*; Oxford : Pergamon Press, 1980.

(100) Tarasov, V. P.; Buslaev, Yu. A. ^{19}F and ^{45}Sc Nuclear Spin Relaxation for the Hexafluoroscandate, Hexafluorotitanate, and Hexafluorogermanate Ions in Aqueous Solution. *J. Magn. Reson. 1969* **1977**, *25* (1), 197–203. https://doi.org/10.1016/0022-2364(77)90132-9.

(101) Pfadenhauer, E. H.; McCain, D. C. Nuclear Magnetic Resonance of Fluoroscandate Anion, ScF_6^{3-}, in Aqueous Solution. *J. Phys. Chem.* **1970**, *74* (17), 3291–3293. https://doi.org/10.1021/ j100711a025.

(102) Brucher, E.; Glaser, J.; Toth, I. Carbonate Exchange for the Complex Tris(Carbonato)Dioxouranate(4-) in Aqueous Solution as Studied by Carbon-13-NMR Spectroscopy. *Inorg. Chem.* **1991**, *30* (9), 2239–2241. https://doi.org/10.1021/ic00009a055.

(103) Lente, G. *Deterministic Kinetics in Chemistry and Systems Biology : The Dynamics of Complex Reaction Networks*, 1st ed.; SpringerBriefs in Molecular Science; Springer International Publishing: Cham, 2015. https://doi.org/10.1007/978-3-319-15482-4.

(104) Bányai, I. Dynamic NMR for Coordination Chemistry. *New J. Chem.* **2018**, *42* (10), 7569–7581. https://doi.org/10.1039/ C8NJ00 233A.

(105) Blackburn, O. A.; Routledge, J. D.; Jennings, L. B.; Rees, N. H.; Kenwright, A. M.; Beer, P. D.; Faulkner, S. Substituent Effects on Fluoride Binding by Lanthanide Complexes of DOTA-Tetraamides. *Dalton Trans.* **2016**, *45* (7), 3070–3077. https://doi.org/10.1039/c5dt04349b.

(106) Happel, S.; Dirks, C. Application of Extraction Chromatography to the Separation of Sc and Zr Isotopes from Target Materials. *Int. J Pharmacol Pharm Sci.* **2014**, *1* (3).

(107) Delgado, R. Redox Method for the Determination of Stability Constants of Some Trivalent Metal Complexes. *Talanta* **1997**, *45* (2), 451–462. https://doi.org/10.1016/S0039-9140(97)00157-4.
(108) Šimeček, J.; Schulz, M.; Notni, J.; Plutnar, J.; Kubíček, V.; Havlíčková, J.; Hermann, P. Complexation of Metal Ions with TRAP (1,4,7-Triazacyclononane Phosphinic Acid) Ligands and 1,4,7-Triazacyclononane-1,4,7-Triacetic Acid: Phosphinate-Containing Ligands as Unique Chelators for Trivalent Gallium. *Inorg. Chem.* **2012**, *51* (1), 577–590. https://doi.org/10.1021/ic202103v.
(109) Baranyai, Z.; Uggeri, F.; Maiocchi, A.; Giovenzana, G. B.; Cavallotti, C.; Takács, A.; Tóth, I.; Bányai, I.; Bényei, A.; Brucher, E.; Aime, S. Equilibrium, Kinetic and Structural Studies of AAZTA Complexes with Ga^{3+}, In^{3+} and Cu^{2}. *Eur. J. Inorg. Chem.* **2013**, *2013* (1), 147–162. https://doi.org/10.1002/ejic.201201108.
(110) Kubíček, V.; Havlíčková, J.; Kotek, J.; Tircsó, G.; Hermann, P.; Tóth, É.; Lukeš, I. Gallium(III) Complexes of DOTA and DOTA−Monoamide: Kinetic and Thermodynamic Studies. *Inorg. Chem.* **2010**, *49* (23), 10960–10969. https://doi.org/10.1021/ic101378s.
(111) Clarke, E. T.; Martell, A. E. Stabilities of the Fe(III), Ga(III) and In(III) Chelates of N,N′,N″-Triazacyclononanetriacetic Acid. *Inorganica Chim. Acta* **1991**, *181* (2), 273–280. https://doi.org/10.1016/s0020-1693(00)86821-8.

8. Appendix

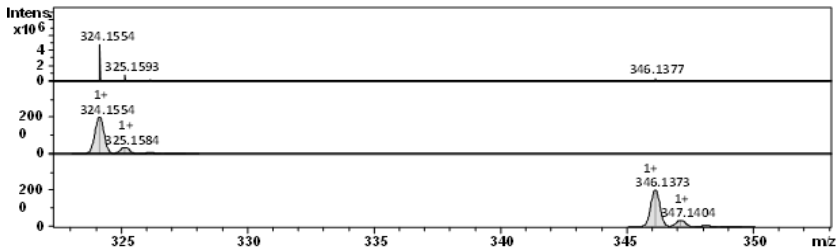

Figure A.1. ESI-MS spectrum of (H_2OPC2A) as $[H_2OPC2A+H]^+$ and $[H_2OPC2A+Na]^+$ calculated and measured sample in positive ionization mode.

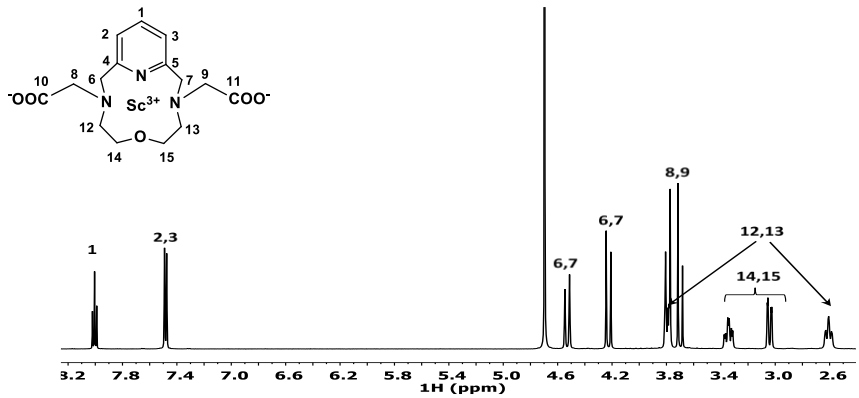

Figure A.2. 500 MHz ^{1}H NMR spectrum of $[Sc(OPC2A)]^+$ complex. c_{OPC2A} = 8.3 mM c_{Sc} = 8.3 mM, I = 150 mM NaCl, pH = 4.75 in D_2O, T = 298 K.

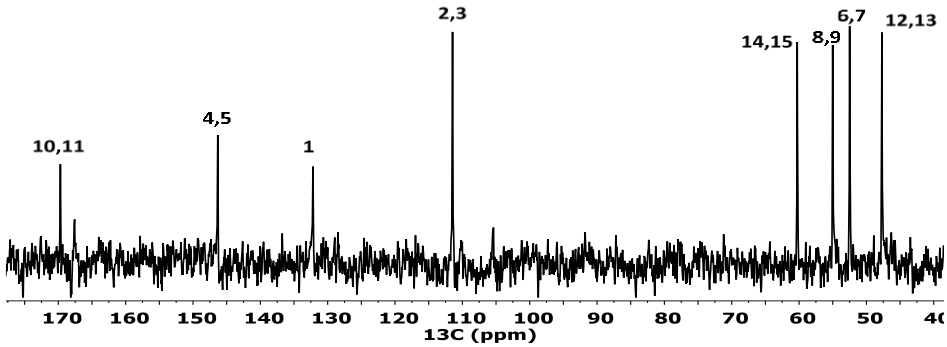

Figure A.3. 126 MHz ^{13}C-NMR spectrum of $[Sc(OPC2A)]^+$ complex. $c_{[Sc(OPC2A)]}$ = 8.3 mM, I = 150 mM NaCl, pH = 4.75 in D_2O, T = 298 K.

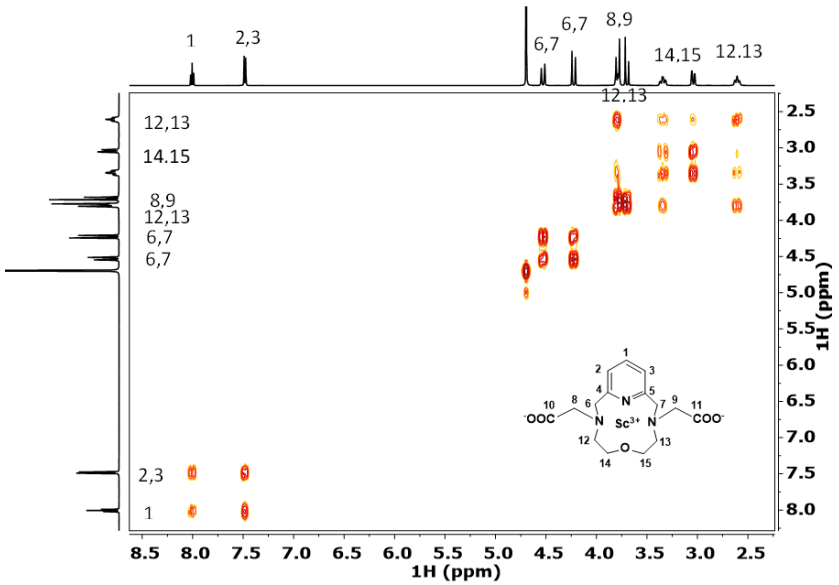

Figure A.4. 500 MHz 2D ^{1}H–^{1}H COSY NMR spectra of $[Sc(OPC2A)]^{+}$ complex. c_{OPC2A} = 8.3 mM, c_{Sc} = 8.3 mM, I = 150 mM NaCl, pH = 4.75 in D_2O, T = 298 K.

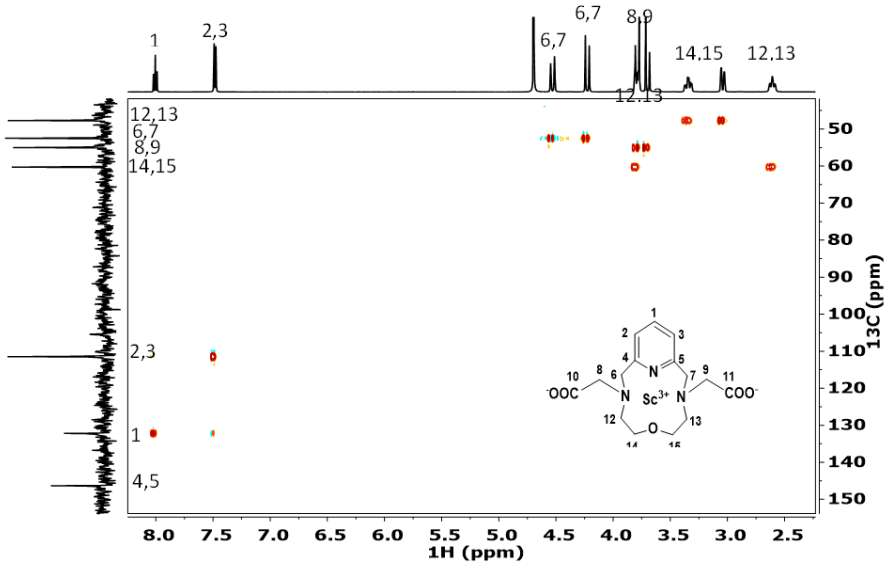

Figure A.5. 2D ^{1}H-^{13}C HSQC spectra (11.75 T) of $[Sc(OPC2A)]^{+}$ complex. c_{OPC2A} = 8.3 mM, c_{Sc} = 8.3 mM, I = 150 mM NaCl, pH = 4.75 in D_2O, T = 298 K.

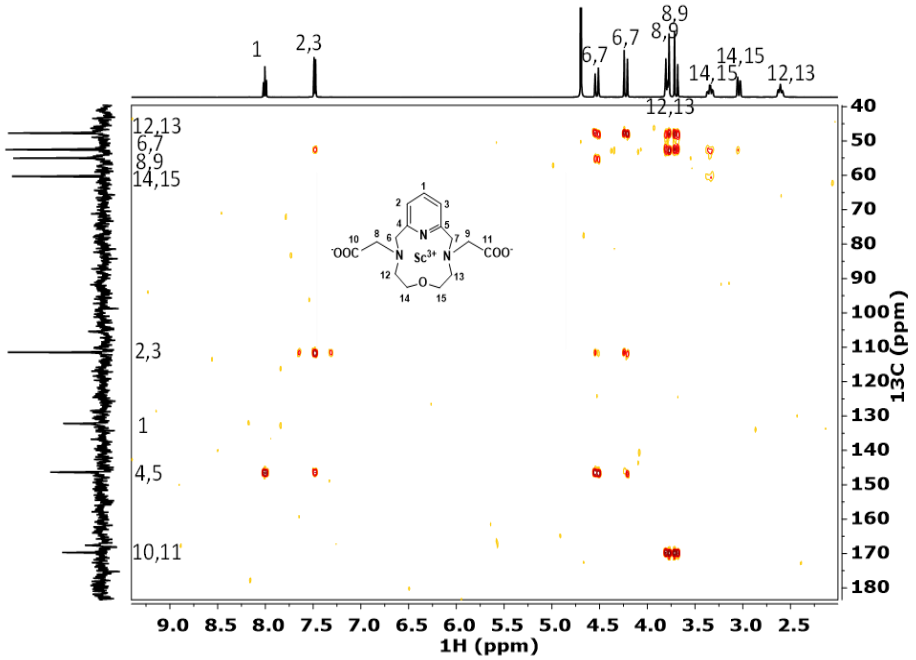

Figure A.6. 2D ^{1}H-^{13}C HMBC spectra (11.75 T) of $[Sc(OPC2A)]^{+}$ complex. c_{OPC2A} = 8.3 mM, c_{Sc} = 8.3 mM, I = 150 mM NaCl, pH = 4.75 in D_2O, T = 298 K.

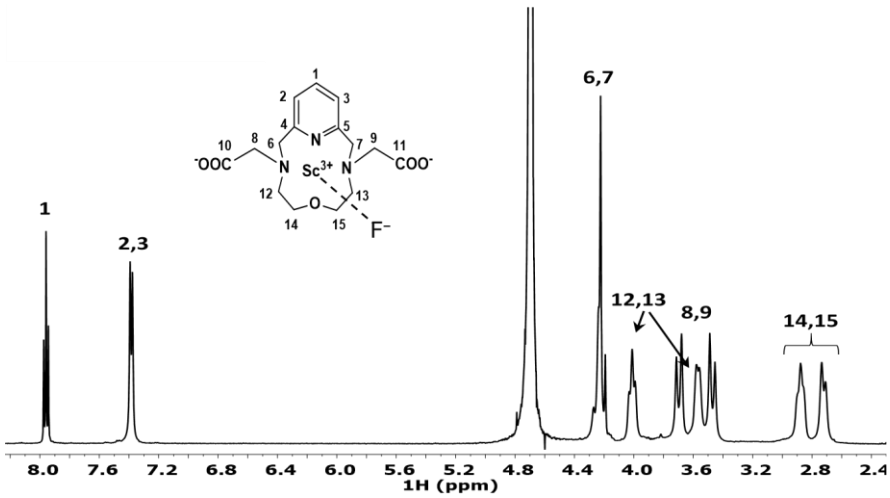

Figure A.7. 500 MHz ^{1}H NMR spectrum of [Sc(OPC2A)F] complex. $c_{[Sc(OPC2A)F]}$ = 8.3 mM, I = 150 mM NaCl, pH = 4.86 in D_2O, T = 298 K.

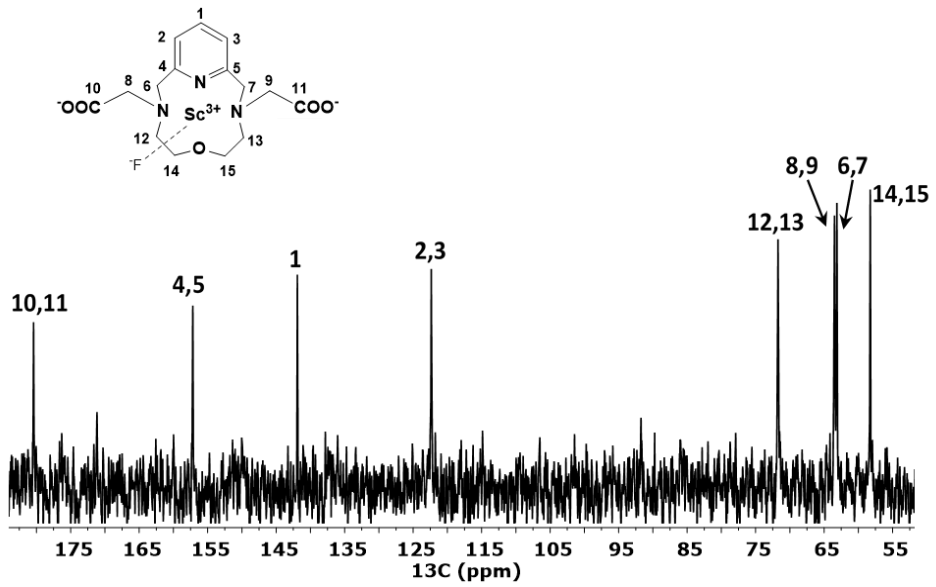

Figure A.8. 126 MHz ^{13}C-NMR spectrum of [Sc(OPC2A)F] complex. $c_{[Sc(OPC2A)F]}$ = 8.3 mM, I = 150 mM NaCl, pH = 4.86 in D_2O, T = 298 K.

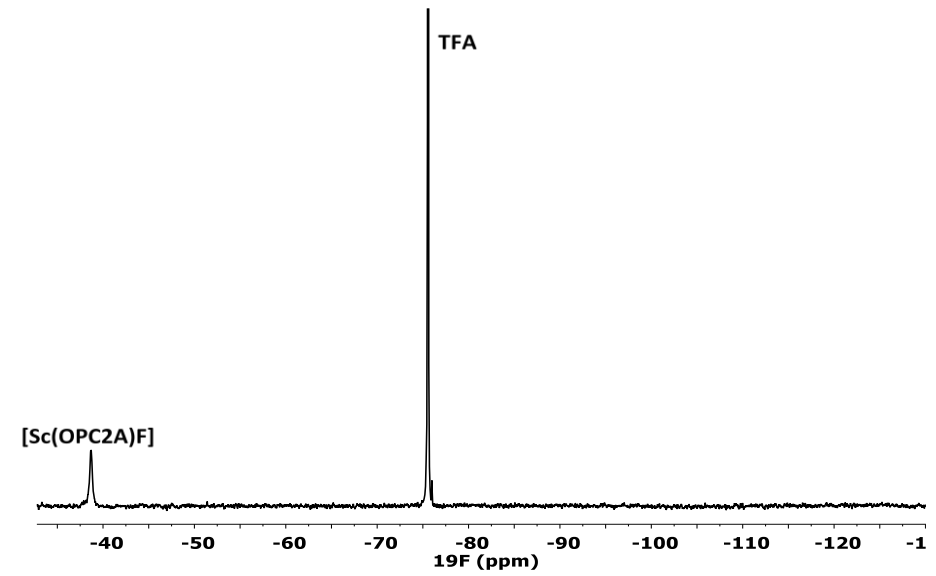

Figure A. 9. 470.45 MHz ^{19}F NMR spectrum of [Sc(OPC2A)F] complex. $c_{[Sc(OPC2A)]}$ = 5 mM = c_F = 5mM, I = 150 mM NaCl, δ = –76 ppm for TFA and δ = –39 ppm for [Sc(OPC2A)F], pH = 4.9, T = 298 K.

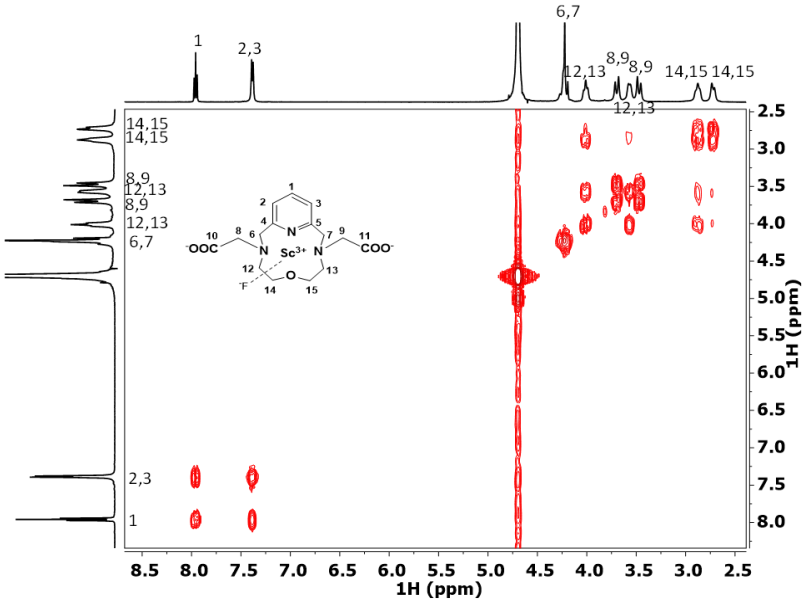

Figure A.10. 500 MHz 2D ^{1}H–^{1}H COSY spectra of [Sc(OPC2A)F]. $c_{[Sc(OPC2A)]}$ = 8.3 mM = c_F = 8.3 mM, I = 150 mM NaCl, pH = 4.86, T = 298 K.

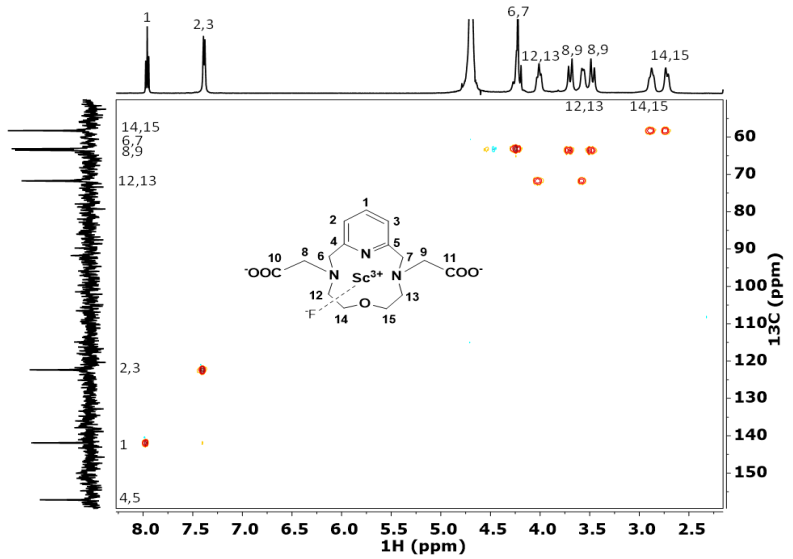

Figure A.11. 2D ^{1}H-^{13}C HSQC spectra (11.75 T) of [Sc(OPC2A)F] complex. $c_{Sc(OPC2A)}$ = 8.3 mM = c_F = 8.3 mM, I = 150 mM NaCl, pH = 4.86, T = 298 K.

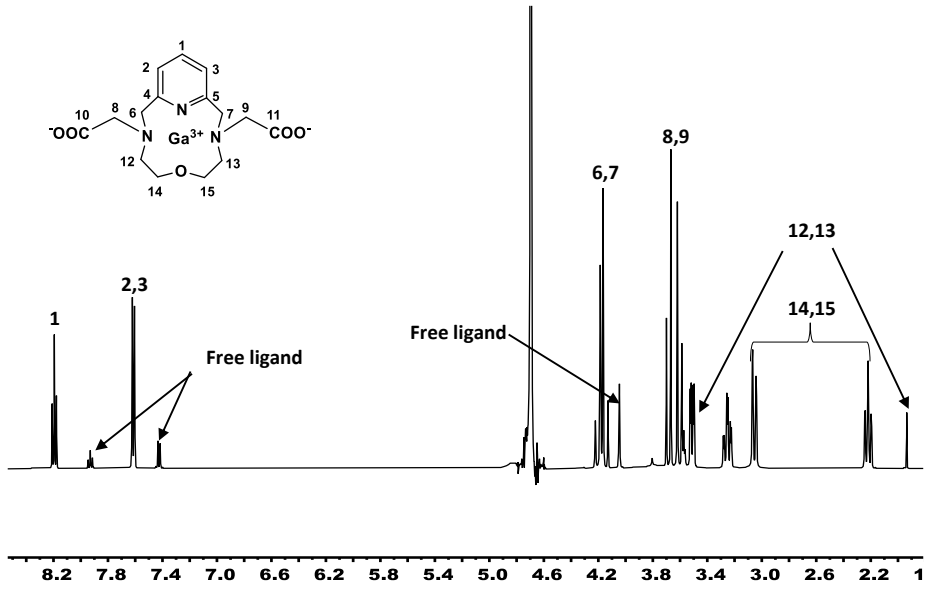

Figure A.12. 500 MHz ^{1}H NMR spectrum of $[Ga(OPC2A)]^{+}$ complex. c_{OPC2A} = 8.3 mM, c_{Ga} = 8.3 mM, pH = 4.8 in D_2O, T = 298 K.

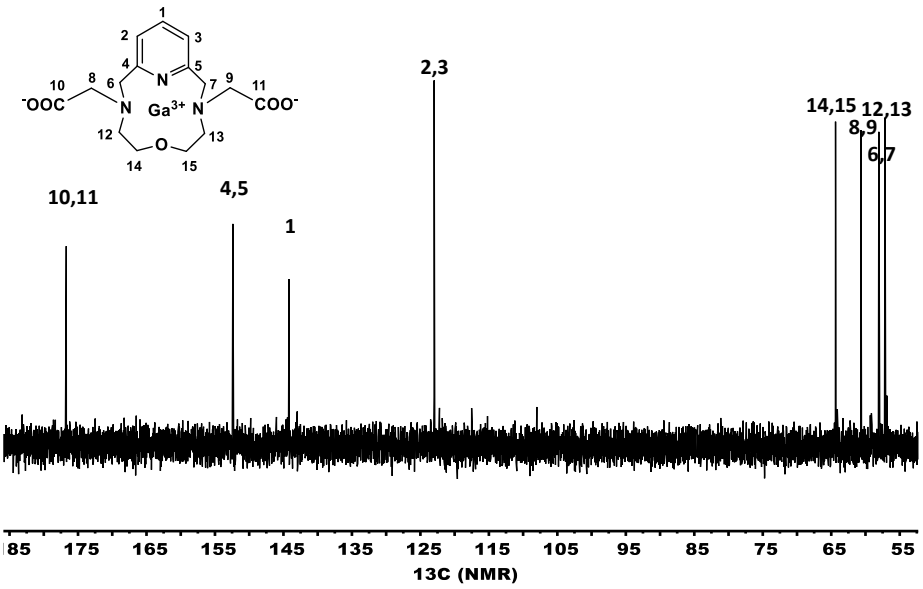

Figure A.13. 126 MHz ^{13}C NMR spectrum of $[Ga(OPC2A)]^{+}$ complex. $c_{[Ga(OPC2A)]}$ = 8.3 mM, pH = 4.75 in D_2O, T = 298 K.

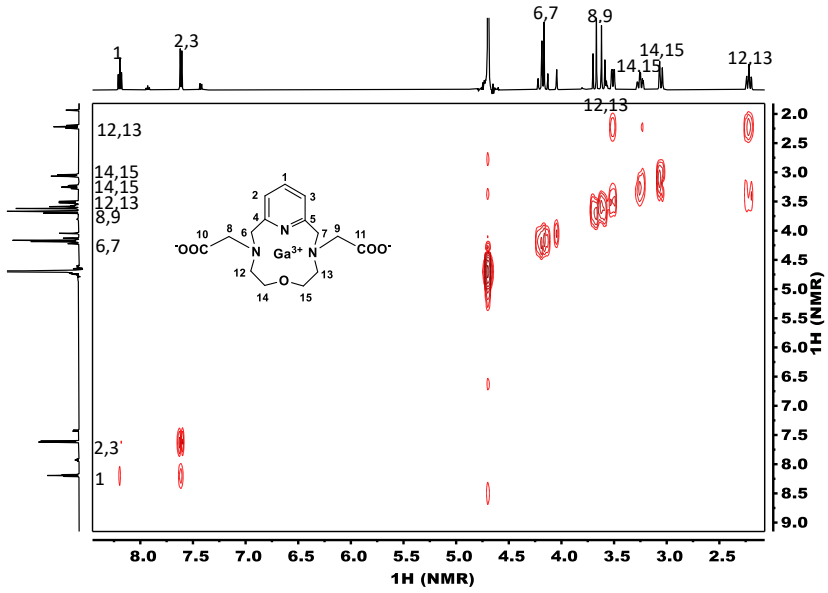

Figure A.14. 500 MHz 2D ^{1}H–^{1}H COSY ^{1}H NMR spectra of $[Ga(OPC2A)]^{+}$ complex. c_{OPC2A} = 8.3 mM, c_{Ga} = 8.3 mM, pH = 4.8 in D_2O, T = 298K.

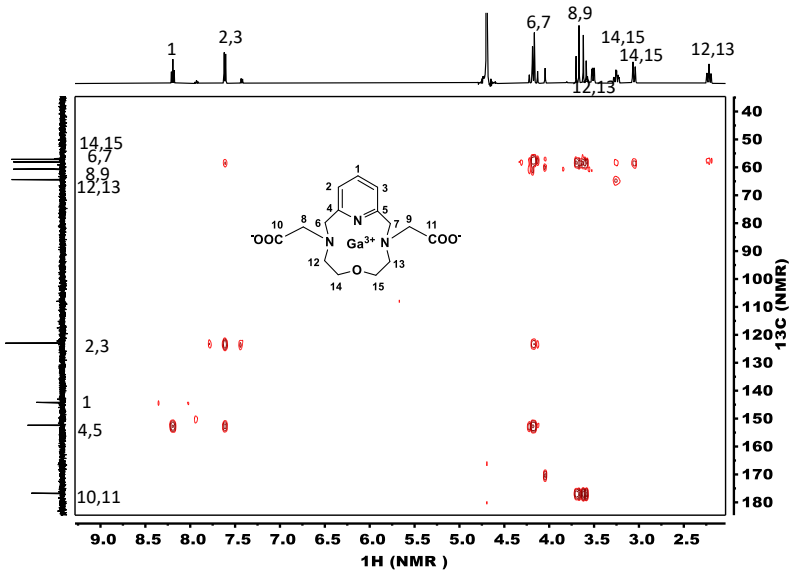

Figure A.15. 2D ^{1}H-^{13}C HSQC spectra (11.75 T) of $[Ga(OPC2A)]^{+}$ complex. c_{OPC2A} = 8.3 mM, c_{Ga} = 8.3 mM, pH = 4.8 in D_2O, T = 298 K.

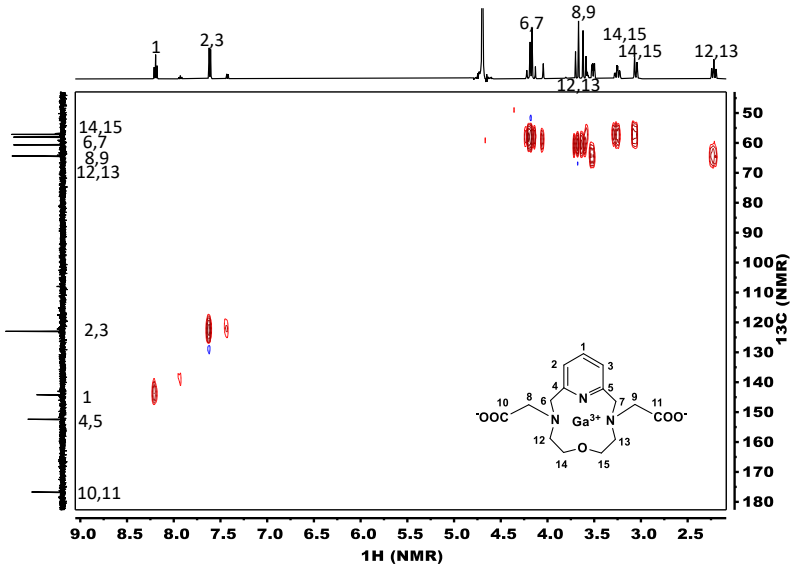

Figure A.16. 2D ^{1}H-^{13}C HMBC spectra (11.75 T) of $[Ga(OPC2A)]^{+}$ complex. c_{OPC2A} = 8.3 mM, c_{Ga} = 8.3 mM, I = 150 mM NaCl, pH = 4.75 in D_2O, T = 298 K.

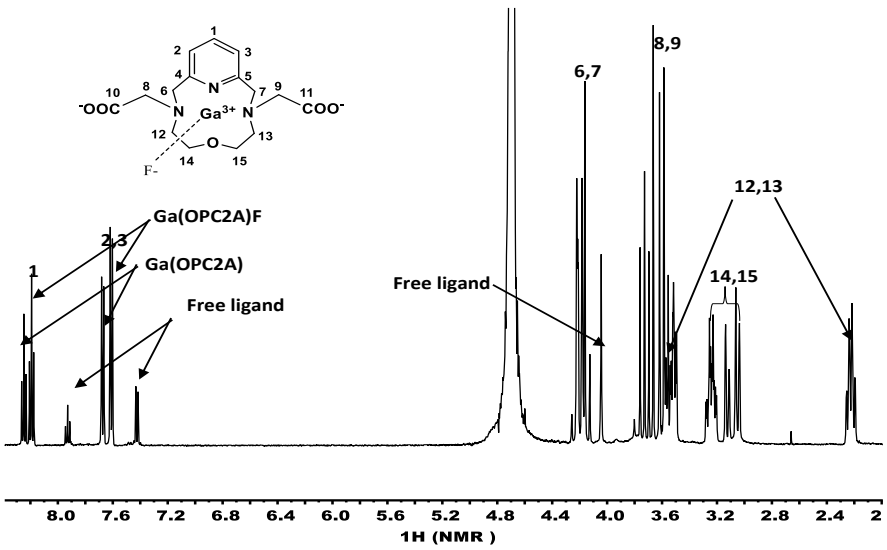

Figure A.17. 500 MHz ^{1}H NMR spectrum of [Ga(OPC2A)F] complex. $c_{[Ga(OPC2A)]}$ = 8.3 mM, c_F = 8.3 mM, pH = 4.8 in D_2O, T = 298 K.

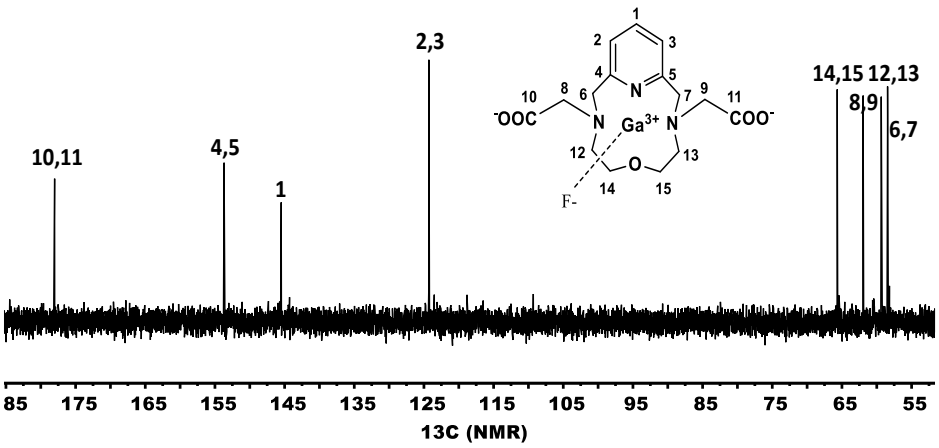

Figure A. 18. 126 MHz ^{13}C NMR spectrum of [Ga(OPC2A)F] complex. $c_{[Ga(OPC2A)]}$ = 8.3 mM, c_F = 8.3 mM, pH = 4.8 in D_2O, *T* = 298 K.

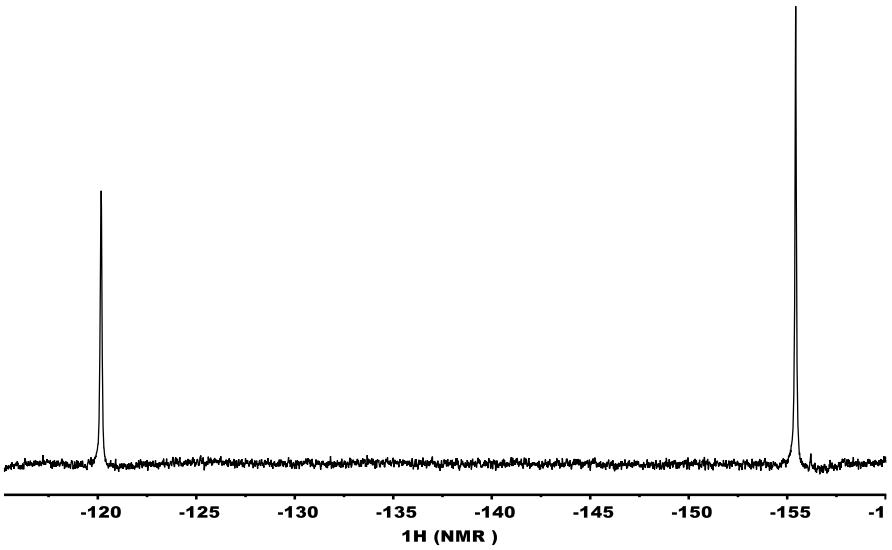

Figure A. 19. 470.45 MHz, ^{19}F NMR spectrum of [Ga(OPC2A)F] complex. $c_{[Ga(OPC2A)]}$ = 5 mM = c_F = 5 mM, chemical shift (δ) of free F = –122 ppm and [Ga(OPC2A)F] = –155 ppm at pH = 4.8 and *T* = 298 K.

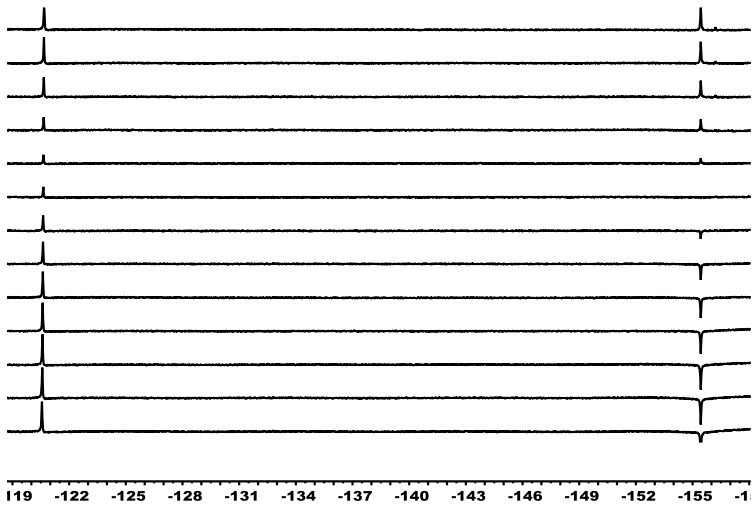

Figure A.20. Selective magnetization transfer experiments by ^{19}F NMR. 5 mM $[Ga(OPC2A)]^+$ and 10 mM NaF at pH = 6 and T = 298 K, the bound F signal was selectively inverted.

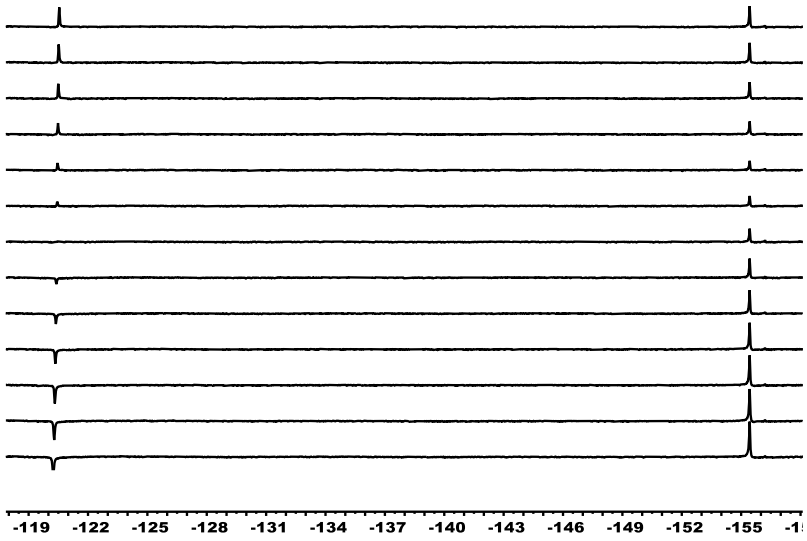

Figure A.21. Selective magnetization transfer experiments by ^{19}F NMR. 5 mM $[Ga(OPC2A)]^+$ and 10 mM NaF at pH = 6 and T = 298 K, the free F signal was selectively inverted.

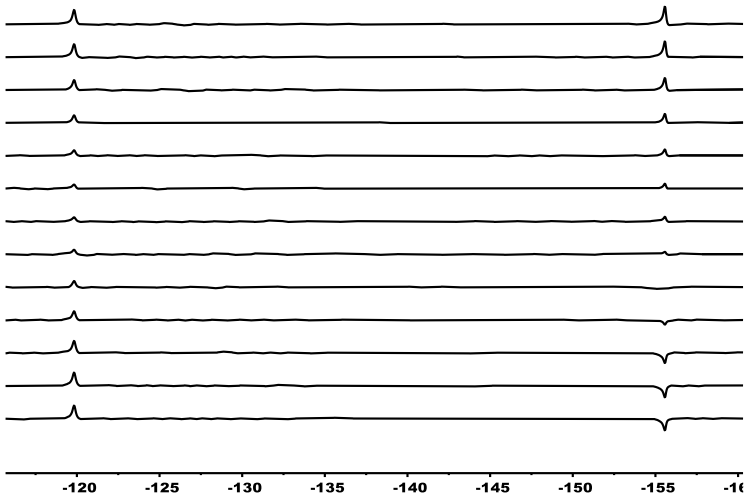

Figure A.22. Selective magnetization transfer experiments by ^{19}F NMR. 5 mM $[In(OPC2A)]^+$ and 10 mM NaF at pH = 7.2 and T = 298 K, the bound F signal was selectively inverted.

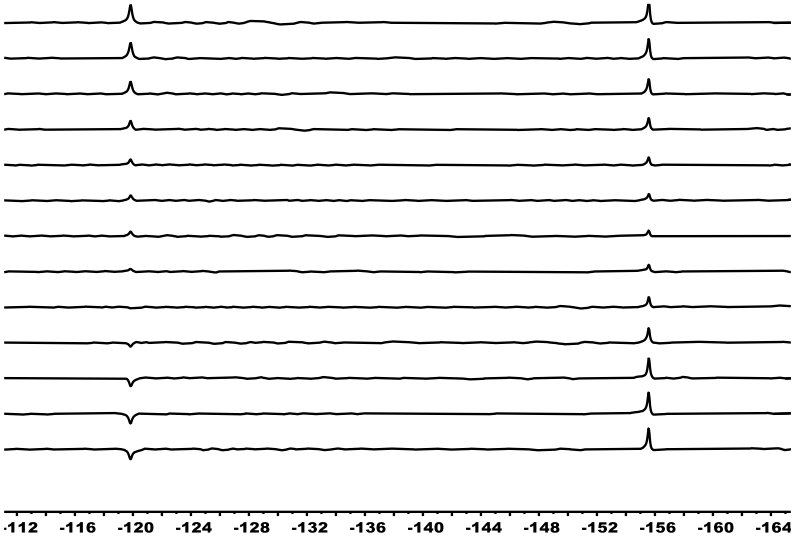

Figure A.23. Selective magnetization transfer experiments by ^{19}F NMR. 5 mM $[In(OPC2A)]^+$ and 10 mM NaF at pH = 7.2 and T = 298 K, the free F signal was selectively inverted.

Table A.1. The integrated ratios are determined by titrating 2 mM NaF with 5 mM $[In(OPC2A)]^+$, while monitoring the chemical shifts of the various F signals using 376.5 MHz ^{19}F NMR.

[In(OPC2A)F]	Peak 1	Peak 2	Peak 3
δ (ppm)	155.7	156.5	156.9
1mM	-	-	-
2mM	3.92	1.08	-
3mM	0.88	2.12	-
4mM	1	6.07	1.03
5mM	0.97	1.03	-